

Abstract:

A tutorial intended to assist with the understanding of the basic parameters of a single-loop, phase-feedback frequency locked oscillator. Since the uses of phase-locked loops are many and varied, only a sample of their uses and design equations have been given here. Some mathematical ability is necessary to deal with the ideas expressed. To assist, all working has been shown for the derivation of the formulae. The aim of this note is to encourage manipulation of the variables and build confidence with phase-locked loop parameters in general. It is recommended that all formulae derivations are followed through with pencil and paper to gain a full understanding of their function. The NJ88C33 has been used as the particular example.

Introduction

The NJ88C33 is a single chip solution for VHF PLL Synthesis, capable of lower levels of phase-noise than earlier PLL ICs since it uses current source outputs from the phase detector to charge pump a passive loop filter, rather than the active types favoured previously. The simplest type of practical loop using this phase detector is of "the third order, type two". An analysis of these loops is not generally available from control theory books, prompting the generation of this Tutorial Note.

In Part A we introduce the NJ88C33. The implementation of a third order charge pumped phase-locked loop is examined in Part B where the loop equations are developed using standard control theory to predict the time and frequency responses for the basic loop. Part C is devoted to bench measurements of the parameters involved to prove the equations of Part B and explains the use of the evaluation card and a simple programming board to gain an insight into how the device works with its programming sequences. This section also covers a discussion of commonly encountered problems when designing circuits using synthesiser ICs, along with an examination of the sensitive areas of the NJ88C33. Last, but not least, is a series of Appendices which deal with the derivation of the basic concepts behind the formulae used in the loop analysis.

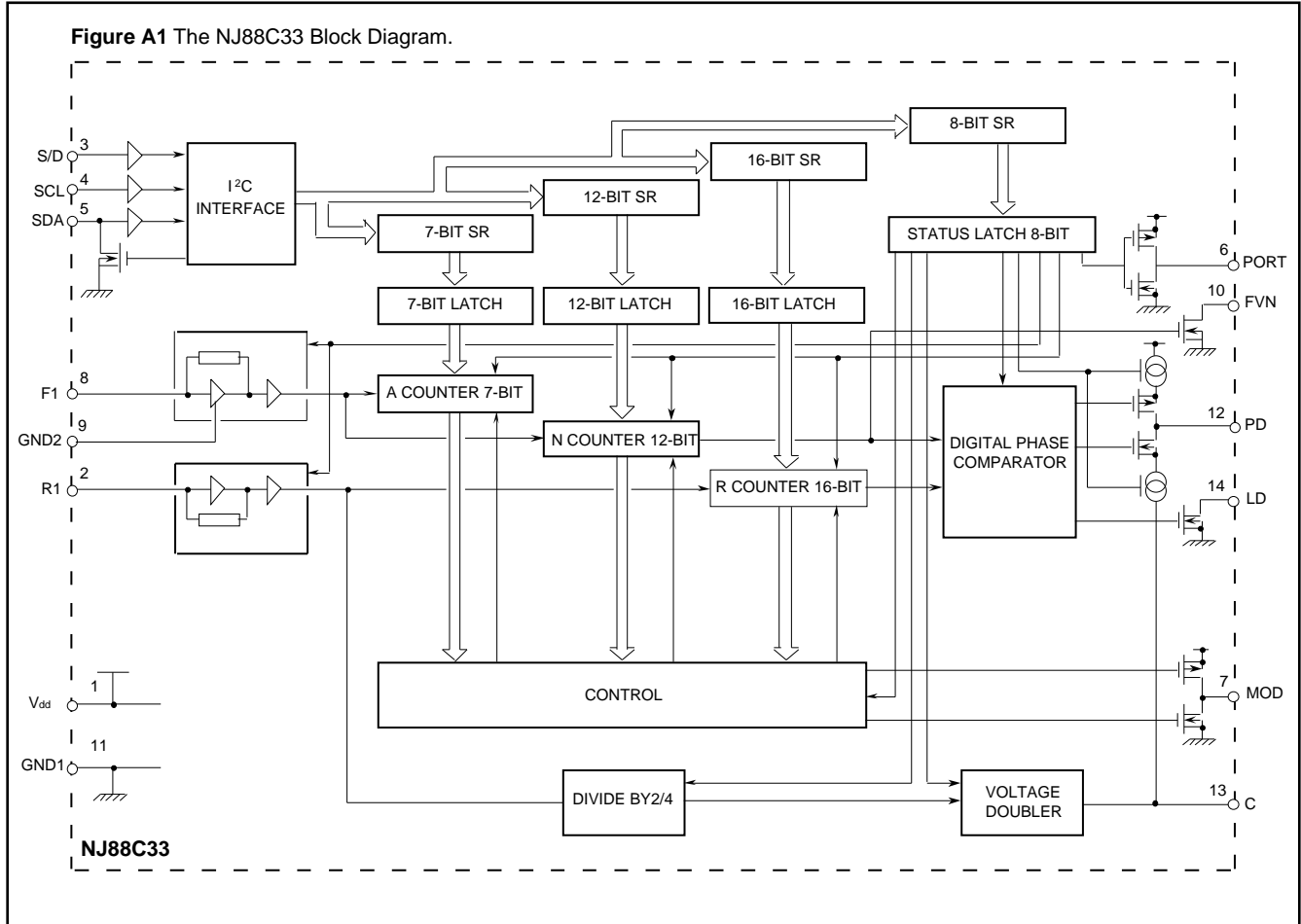
Contents:**Page**

Part A: A Description of the NJ88C33: Its Demonstration Boards and the Loop's Analysis	2
Part B: Analysis of the Basic Phase Locked Loop:	
a) The Derivation of the Loop Filter	7
b) The Derivation of the Loop Equation	9
c) Loop Dynamics	11
d) The Characteristic Equation and its Root Loci	11
e) The Time Domain Responses	15
f) Natural Loop Frequency, Damping and Settle Time	20
g) Bode Plots of the Magnitude and Phase Response	24
Part C: Using the NJ88C33 and its Demonstrator Cards:	
a) Measuring Buffer Sensitivity, Phase Detector Gain and Dead-band	28
b) Generating the Loop Component Values	34
c) The Practical Implementation of the Loop	37
d) Measurement of Transients/ Damped Frequency of Oscillation	44
e) Measurement of Noise Bandwidth and Sidebands	45
f) Programming the NJ88C33	50
Appendix A: The Derivation of the Second Order Response and Some Useful Formulae	53
Appendix B: Implementing the Root Finding Procedure for the Characteristic Equation	75
References	77

AN-94

Part A: A Description of the NJ88C33, its Demonstration Boards and the Loop's Analysis.

The NJ88C33 is a dual-modulus frequency synthesiser IC capable of accepting an input frequency (FI) of up to 150MHz and a reference input (RI) up to 50MHz. As shown in Figure A1 it contains the R, A and N counters necessary to drive a digital phase comparator with switched current-source outputs. These "tri-state" type outputs allow a "sample-and-hold" type of loop filter to be implemented. The compliance of the phase detector output (PD) is to within 0.4Volt of +V_{dd} to -V_{dd} by virtue of the negative output "voltage doubler" (C), doubling the range of control available for the (external) VCO. A lock detect (LD) and the N-counter output (FVN) are provided for test purposes but are not normally used.



An output (PORT) is provided to allow one external function to be toggled. It can be looped to the single/dual modulus control line (S/D) to allow software selection of the modulus mode via the I²C Bus, or to toggle the ratio select line of a prescaler IC (e.g: the 64/65 or 128/129 of the SP8704/5). A modulus control output pin (MOD) has been provided to control the modulus of an external dual ratio prescaler (P or P + 1). This can be programmed to function as a push-pull output or an open-drain output. The MOD pin goes low during the A-counter's active period, it then goes high (open) until both the A and N-counters are reset at the beginning of each comparison frequency period as determined by the R-counter. Typically the prescaler will divide by its higher ratio (P + 1) during the MOD low period, making the output frequency for the dual modulus mode:

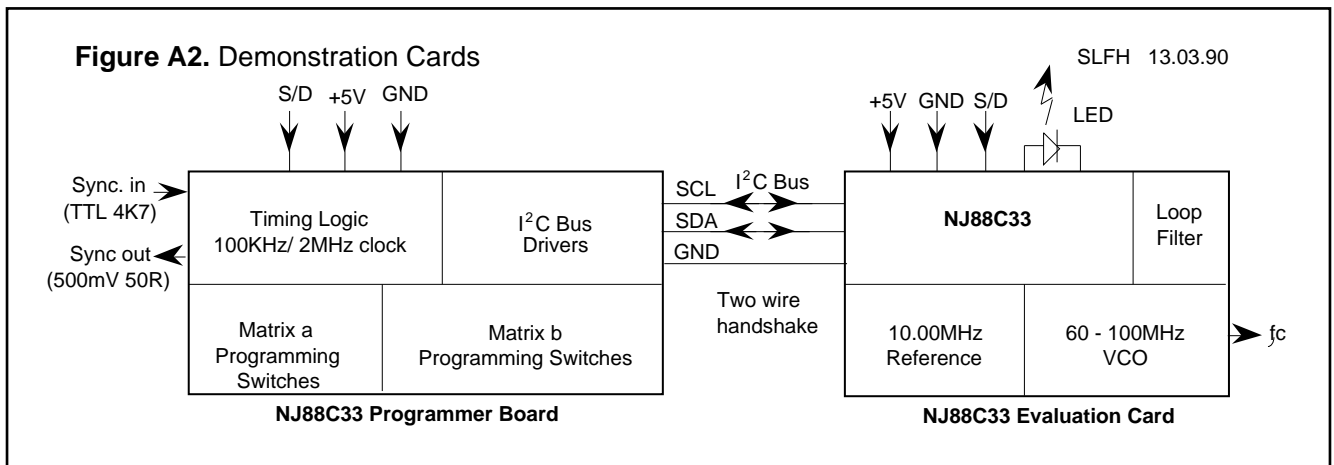
$$F_{VCO} = F_{ref} (P \cdot N + A) / R \quad (FI = F_{VCO} / P < 50 \text{ MHz})$$

For the single modulus mode and no prescaler the output frequency will be:

$$F_{VCO} = F_{ref} N / R \quad (FI = F_{VCO} < 120 \text{ MHz})$$

Programming of the NJ88C33's internal functions can be achieved via the I²C Bus using a two wire handshake, making the device ideal for direct connection to standard TTL/HCMOS logic as well as any I²C Bus compatible microprocessors. The ability of the I²C bus to drive a high capacitance load (400pF maximum as per the I²C standard) and the use of Schmitt Triggers ensures that the transfer of data on the bus is jitter free. These features allow both the power supply lines and the data lines to be fitted with "feed-through" type line filters, ensuring the integrity of any shielding used in EMI critical applications requiring a "complete" screen.

To encourage familiarity with the NJ88C33 and to assist with its practical circuit implementation, two demonstration boards are available. Their main features are outlined in Part C along with the operation of the boards. The basic equations required to analyse the phase-locked loop's dynamics being derived in Part B. Figure A2 shows the interconnections between the two boards as well as their block functions.

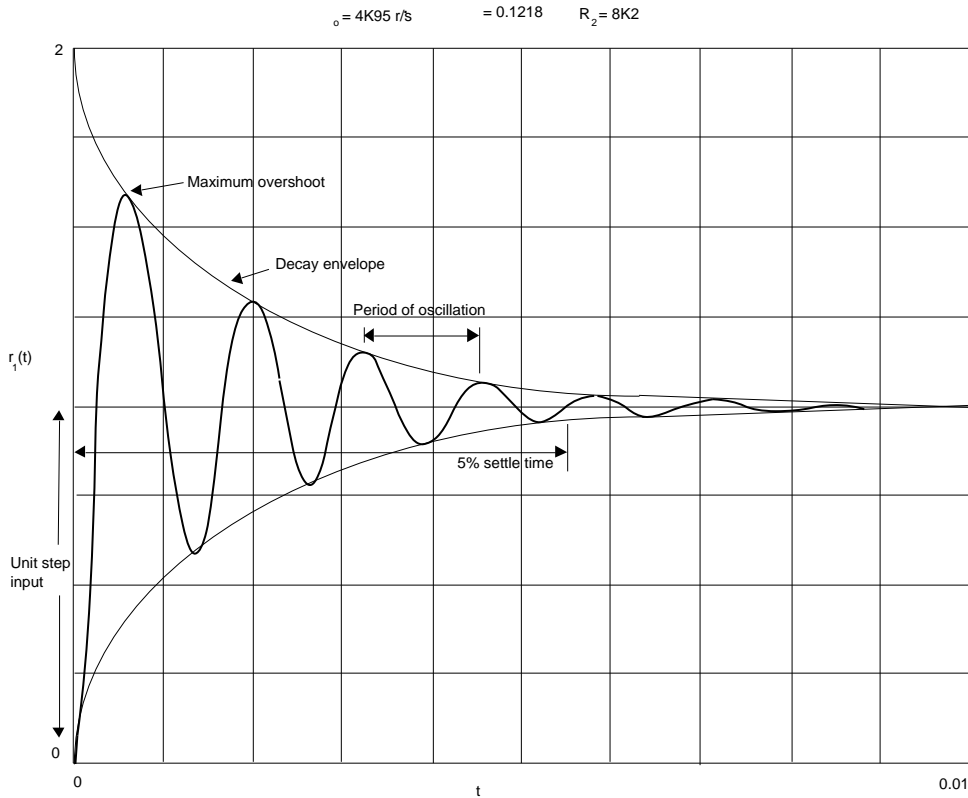


As system design becomes more complex it is desirable to be able to produce a rigorous design path from concept through to finished product. Compliance to particular standards such as BS5750 requires the documentation path from inception to finished product to be traceable. The mathematical rigour used in this document should allow prospective users to simply quote AN-94 as a reference then use the annotated equations in their design process without any further work; so allowing a shorter design cycle. To assist, this application note is intended to give some justification to the basic ideas from which these design paths can be selected.

For a deceptively simple circuit configuration, the passive filter used in a charge pumped phase detector has a complicated operation. In fact it is so complex that one is tempted to resort to “tweak and measure” methods, until a satisfactory result can be obtained; negating any attempt at a formalised approach to the design method to be used. Despite this complexity, the analysis is quite straight forward once a few basic formulae have been derived and a “feel” for how the dynamic operation of the loop behaves with changes to each parameter or component. Part C, the empirical section, will use these equations to look at the practical results from the evaluation cards.

To gain an idea of our goal, we make a forward reference to Figure B2 and Equation B3 to see the form of the “phase-locked loop” (or more accurately the “phase feedback frequency locked oscillator”). Equation B3 will be seen to contain an impedance transfer function $Z(s)$ relating to the loop filter. $Z(s)$ appears in both the numerator and the denominator of the closed loop transfer function $B(s)$ for the completed phase-locked loop and will therefore dominate the equation for $B(s)$. An analysis of a phase-locked loop is really an analysis of the loop filter's parameters. These parameters are useful variables that readily allow us to compare one circuit configuration with another in generalised terms. They are predominated by the loop filter and are only loosely dependant upon the other loop variables. The two most important of these parameters are the “natural frequency of oscillation” of the filter, (referred to as ω_n) or the loop natural frequency for brevity. The loop natural frequency is that at which the loop filter would oscillate if there was no parasitic resistance, or damping, to absorb the energy from that filter. If an impulse was applied to the filter, it would force an oscillation in the loop which would last forever at this frequency. That other important parameter, damping, ζ , (zeta) determines the rate of increase or decrease of the oscillatory part of the response by the filter to the forcing input. The attributes of a system's response that are commonly of interest to us are shown in Figure A3.

Figure A3. Attributes of a system response commonly of interest



Notice that the two decay envelopes pass through the peaks and troughs of the oscillatory response to the step function input. This will allow us to find an equation for the settle time since the peaks' (and troughs') value for time and amplitude can be fixed by taking the derivative of the Inverse Laplace Transform of the impulse or step response:

$$\frac{d}{dt} [r(t)] = 0.$$

The basic formulae for overshoot and settle time as determined by the exponential envelope of the oscillatory response, have been derived in terms of ω_n and ζ in Appendix A for a second order response. By combining the natural loop frequency with the damping ratio we see a pseudo-variable called the damped frequency of oscillation, ω_d , which is the frequency at which the "ring" occurs on most realistic circuit responses.

Before we launch into a full blown analysis of PLLs we should consider how the best results can be obtained from the simple models available to us for the components of the PLL to be assessed. Many of the practical problems that device users encounter when prototyping could be avoided by carrying out some mathematical modelling first. This, along with the feel for how the loop operation alters by varying both components and parameters, will give an invaluable insight into the short-comings on any practical loop. Although the following discussion can be applied to circuit analysis in general, we will limit ourselves to PLLs. Similarly we will restrict our consideration of noise to that caused by interference; internal noise sources and their resulting phase noise, deserve a separate treatise of their own to deal adequately with the physics of those devices.

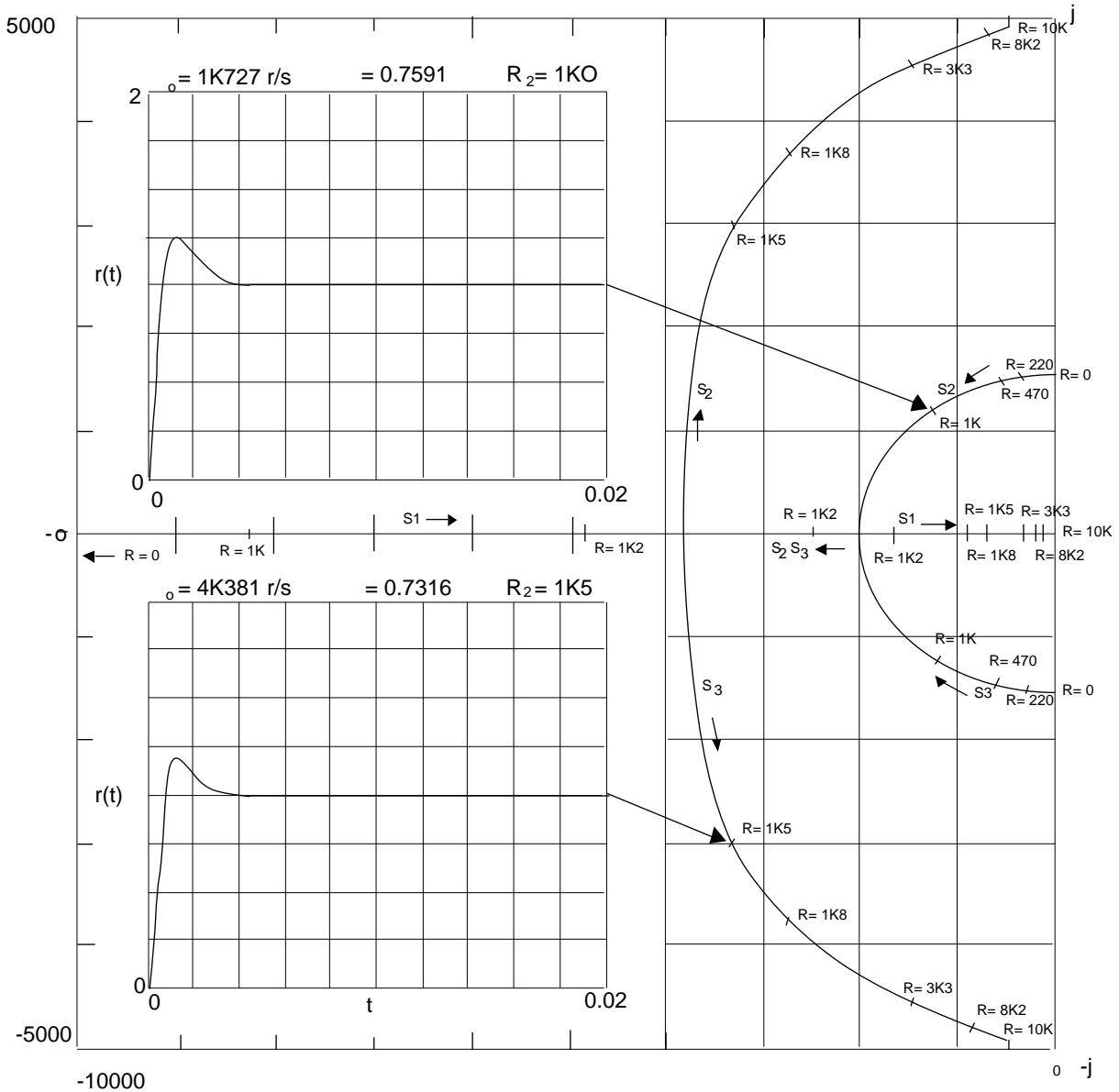
The basic function of a PLL is to multiply a reference frequency by a fixed ratio N, (or PN + A) to another (usually higher) frequency. In a perfect system this would entail one perfect "tone" giving another (higher) frequency at the VCO's output without any "colouration"; the reference would be identical to the output divided by the feedback ratio N(or PN + A). However real systems do alter the output spectrum by adding loop component related frequencies as well as increasing the thermal noise "floor" at the output. The band of frequencies near the output fundamental tend to take on the characteristics of the reference oscillator, whereas those at some distance from the fundamental (some large fraction of the fundamental) tend to take on the characteristics of the VCO, between these two is an area which is determined by the phase comparator and to a lesser extent, the dividers. Harmonics are completely a product of the VCO and are independent of the loop, so will be ignored here. For convenience of analysis, we will only consider the colouration of the output spectrum to be due to signal injection to the VCO's control voltage which is then modulated onto the fundamental "carrier".

Noise injection into a servo-loop will have a varying effect upon the controlled output depending upon where in the loop the injection is being done. With reference to Figure B2 again, it can be seen that any input to the VCO will be modulated directly, then presented to the output. Conversely, any input to the N-divider, reference or phase detector will be altered by the loop filter, before being presented to the VCO for modulation onto the fundamental. Therefore these last parts of the circuit will behave as a low pass filter since they feed into the loop filter, whereas the former will behave as a high pass filter because the feedback from the phase detectors error term will have to “filter” through before it can cancel any disturbance at the VCO. Which effect predominates for a given input is determined by the “break-point frequencies” of the filter and the frequency versus amplitude “slope” of the filter’s roll off, or “skirt”. It should be noted that the filter’s roll off is not abrupt and must be considered across many decades of frequency if a successful implementation of the loop is to be completed. Reference to Appendix C will give an idea of the range of frequencies that must be considered. For this reason, wideband techniques using Laplace Transforms to convert to the complex frequency domain and Inverse Laplace Transforms to convert back to the time domain must be applied to PLL analysis rather than the more usual narrow band “phasor” techniques usually applied to RF circuitry.

Wide band analysis will involve time domain analysis using step functions rather than sine waves. Analysis using Laplace Transforms allow us to obtain the frequency response (when $s = j\omega$) for noise analysis and the time domain response ($s = -\sigma + j\omega$) for step and settle analysis as well as dynamic error assessment. An added bonus is the ability to generate s-plane plots from the Laplace Transforms, which show σ and ω immediately. The s-plane is referred to as the complex frequency plane which can tell us the type of response available (in terms of the steady state frequency response and the time domain transient response) according to how the loop’s transfer function migrates across the s-plane as each variable or parameter is altered. These are expressed graphically in the form of Root Loci or Root Contours when more than one variable is involved. Appendix A develops the background to the s-plane. The root locus method will allow us to predict the stability of the system and to choose rational values for the loop components before any commitment to a design architecture has to be done.

Figure A4 shows the root locii for a Cubic Response, with some typical time domain responses for the evaluation card overlaid on the marked s-plane locations. Note that the resistor value at each pole location has two attendant poles which function in conjunction with the one indicated by the response to contribute to that total response as shown. The migration of the three poles describe their root locii. The generation of the necessary equations for drawing these is explained in Part B.

Figure A4. The root locii of the cubic response for the N588C33 Evaluation card



Analysis using the complex frequency domain is a linear technique rather than a discrete sample technique. This linear approximation is acceptable when analysing a non-linear discrete time sampled system, provided we make an appraisal of the loop variables at each individual frequency output of the loop as it settles to that new value. This should ensure a valid small signal analysis. Next we need to establish the transfer functions for the loop filter and the closed loop transfer function, in order to appreciate the meaning of the above root locii plot.

Part B: Analysis of the Basic Phase-Locked Loop.

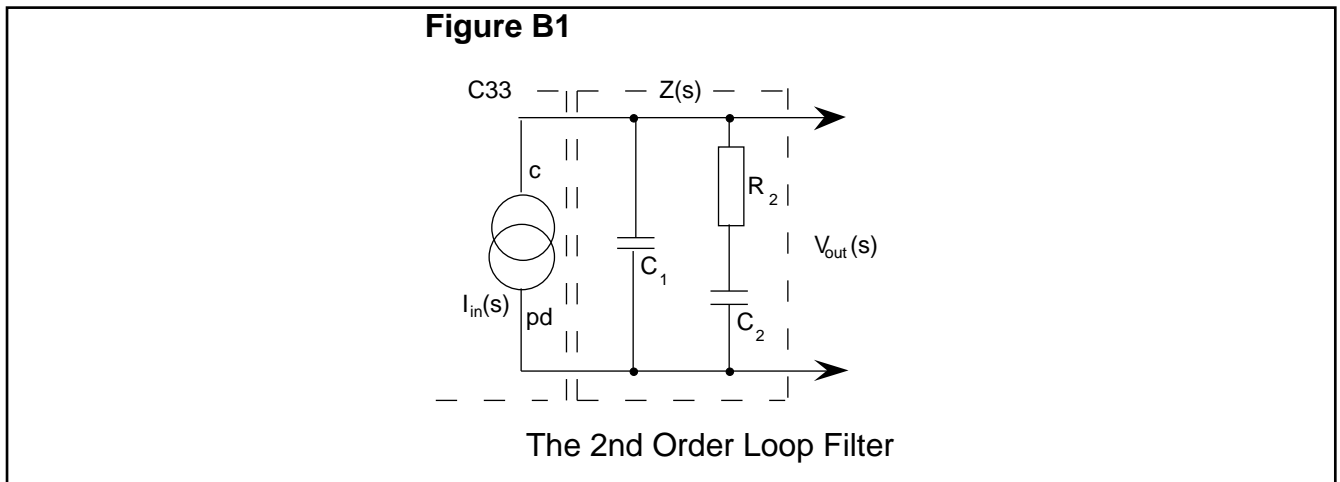
a) The Derivation of the Loop Filter.

To allow an accurate analysis of the PLL function, the loop filter has to be chosen to operate well below the phase detector's comparison frequency. A practical maximum is around one fifth of the comparison frequency, however the attenuation of the fundamental and harmonics of the phase-detector's charge pump pulses must be considered as these will contribute to the VCO's output sidebands, as dealt with in Appendix C and D. To a first approximation we can consider the analysis of the Loop Filter and its forcing current source(s) as a time invariant linear system. This will allow us to use Laplace Transforms to carry out the analysis of the steady state and transient cases provided we assume small-signal conditions. For those unfamiliar with System Analysis, Appendix A gives some useful background to the subject.

The choice of filter structure affects the completed closed loop function. The simplest filter we can use for this loop is a driving point immittance (admittance and susceptance, i.e.; the reciprocals of resistance and reactance), in parallel with the VCO's control voltage. If we choose a simple series RC filter in parallel with the current source we see a network with a transfer function that displays an impedance characteristic; since the output divided by the input has the dimensions of volts per ampere. The transfer function is:

$$Z(s) = R_2 + 1/sC_2$$

where (s) is used to indicate that the impedance is given in terms of the Laplace variable in the complex frequency domain, (for capacitance: $Z_{C_x} = 1/sC_x$ and for inductance: $Z_{L_x} = sL_x$). R_2 and C_2 are the filter components. For the moment just consider the $1/sC_2$ as the impedance of C_2 with $s = j\omega$ and $\omega = 2\pi f$. This filter will give discrete steps in control voltage in response to the charge pump's current pulses. These can be, and usually are, objectionable such that further filtering is required. This can be achieved by adding an integration capacitor across the above RC filter, forming the network shown in Figure B1; the component numbering agrees with that for the evaluation card shown in Figure C2.



The transfer function of this filter is:

$$V_{out} = I_{in} Z(s)$$

That is: the transfer function which controls the "signal" (current and voltage) relationship of a "black box" representation of the filter, is as follows:

$$\begin{aligned} Z(s) &= V_{out}(s) / I_{in}(s) \\ &= Z_{C_1} // R_2 + Z_{C_2} \\ &= 1/sC_1 // (R_2 + 1/sC_2) \\ &= 1/sC_1 // [(R_2 \cdot sC_2)/sC_2 + 1/sC_2] \\ &= 1/sC_1 // [(R_2 \cdot sC_2 + 1) / sC_2] \end{aligned}$$

Consider, that if $Z_1 = 1/sC_1$ and $Z_2 = (R_2 \cdot sC_2 + 1) / sC_2$, then:

AN-94

$$\begin{aligned}
 Z(s) &= Z_1 \cdot Z_2 / (Z_1 + Z_2) \\
 &= \frac{[1/sC_1 (R_2 \cdot sC_2 + 1)]/sC_2}{[1/sC_1 + (R_2 \cdot sC_2 + 1)]/sC_2} \\
 &= (R_2 \cdot sC_2 + 1) / [sC_2 + sC_1 (R_2 \cdot sC_2 + 1)] \\
 &= (R_2 \cdot sC_2 + 1) / (sC_2 + sC_1 R_2 \cdot sC_2 + sC_1) \dots\dots\dots (B1)
 \end{aligned}$$

Equation B1 shows the form of the filter as well as its transfer function. Normally the numerator and denominator of the transfer function will have their polynomials expressed in root form to show the poles and zeros of the complete function, i.e:

$$\begin{aligned}
 Z(s) &= \frac{(R_2 sC_2 + 1)}{s(C_2 + C_1 + s C_1 R_2 C_2)} \\
 &= \frac{(s + 1/R_2 C_2) R_2 C_2}{s[(C_1 + C_2) (1 + \frac{s C_1 R_2 C_2}{C_1 + C_2})]} \\
 &= \frac{(s + 1/R_2 C_2)}{s[(\frac{C_1 + C_2}{R_2 C_2}) (\frac{C_1 + C_2}{C_1 R_2 C_2} + s) (\frac{C_1 R_2 C_2}{C_1 + C_2})]} \\
 &= \frac{(s + 1/R_2 C_2)}{s[C_1 (s + \frac{C_1 + C_2}{C_1 R_2 C_2})]} \\
 &= (s + 1/T_2) / [sC_1 (s + 1/T_1)]
 \end{aligned}$$

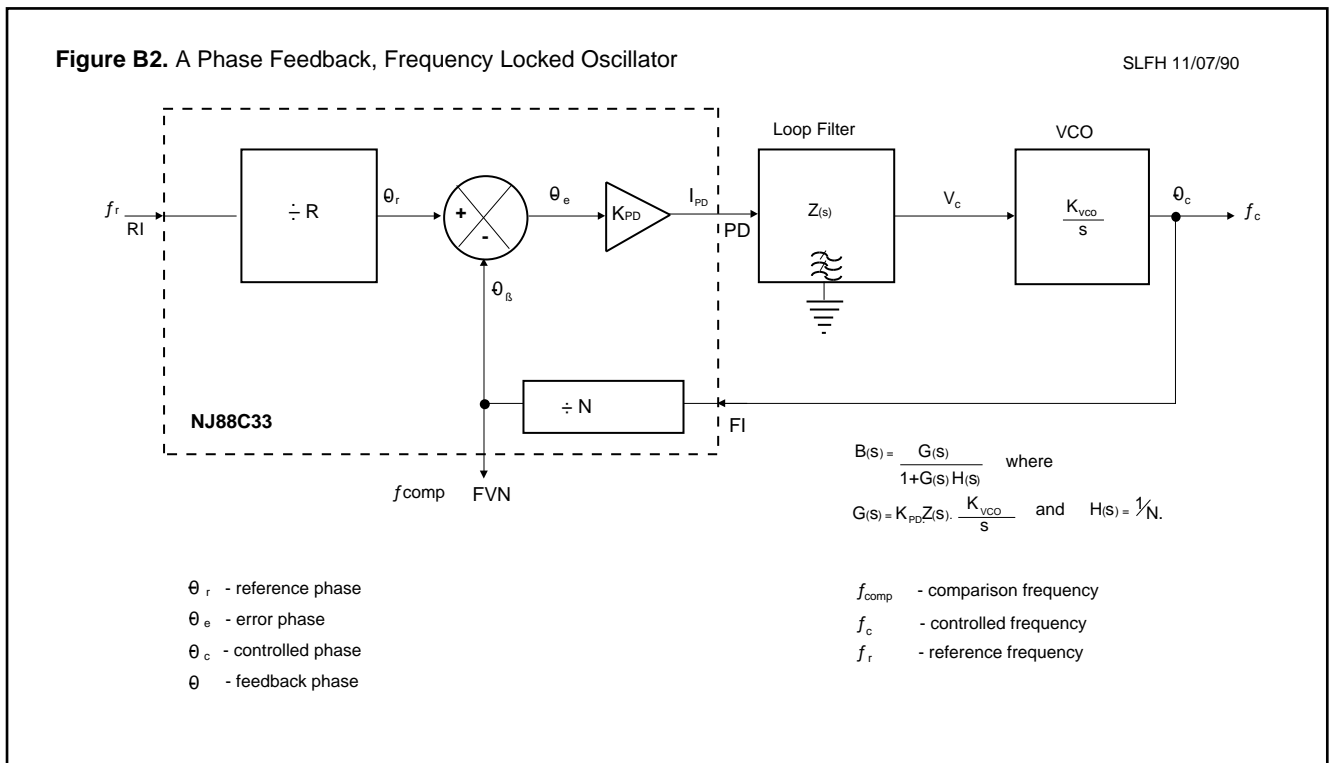
where $T_2 = R_2 C_2$ and $T_1 = (C_1 C_2 R_2) / (C_1 + C_2)$. From this we can see that there is one zero at $s = -1/T_2$ and three poles; one at infinity (due to the zero when $s =$ infinity, which is generally ignored), one at zero and one at $s = -1/T_1$. To ease later calculations we shall express this as:

$$Z(s) = L (s + 1/T_2) / s (s + 1/T_1) \dots\dots\dots (B2)$$

where $L = 1/C_1$. Later on, the term L will be absorbed into K, the general scalar for the loop equation; L is simply used here as a variable to carry over the ratio of C_1 (for the loop filter's impedance) to the loop equation. This is of importance because this ratio affects the damping of the closed loop, precluding us from directly writing an equation for the damping, (zeta). C_2 also effects the apparent "gain" of the filter.

b) The Derivation of the Loop Equation.

This analysis requires a familiarity with control theory and goes as follows. Examine Figure B2, which shows a simple Phase-Locked Loop using the NJ88C33.



We need to know the forward and reverse gains of the loop (the direction of the signal flows are shown by the arrows), as well as the loop's structure, to formulate the closed loop Transfer Function. These functions for each component part of the structure are given in terms of additions, subtractions, multiplications, divisions, integrations and differentiations. The first four are trivial, however the last two are a function of the energy storage in the reactive components in the circuit under consideration. Which function represents a capacitor or inductor will be determined by the components placement in the circuit, for example: a capacitor in parallel with the signal line (or an inductor in series) will behave as an integrator of voltage (current), but will behave as a differentiator of current (voltage); the exact function is determined by node or loop analysis. The use of Laplace Transforms simplify the integro-differential equations that result from the above analysis, as they reduce the equations to multiplication in the complex frequency domain. We will use them here without further proof, reference 1 contains a couple of excellent sections dealing with nodal and loop analysis as well as the use of Transforms. It should be noted that the method of analysis used here is generally applicable to feedback control loops, not just to phase-locked loops.

Once we have formulated the function of each component in the loop, we can derive the closed loop operation for any point in either the forward or reverse direction. Here we are going to assume that the phase detector is completely linear and use phase feedback rather than voltage as for an amplifier analysis. The phase detector (PD) has been split into two parts: one being the phase subtractor the other being the phase multiplier (K_{pd}). From Figure B2 we can see that:

$$e = r -$$

where e is the error produced when the feedback phase (θ_b) is subtracted from the reference phase (θ_r); these operate at the comparison frequency (F_{comp}) as determined by the R-counter and the reference input, RI. We have already said that the loop filter is a driving point immittance and as such it is a complex impedance across the control input of the VCO. The output of the phase detector's current-sources pump charge into that impedance, which then converts the charge into the VCO's control voltage. The form of this voltage will be:

$$V_c(s) = K_{pd} \cdot Z(s) \cdot e$$

where K_{pd} is the current sources' mean output (I_{PD}) and is given in amperes per radian of the comparison frequency's period. The loop filter integrates the PD pulses and holds V_c constant during steady state conditions. The phase detector gain expression is:

$$K_{pd} = (I_{PD})/2$$

AN-94

Now, the VCO is a previously fixed variable giving a controlled output phase ϕ_c of:

$$\phi_c = V_c K_{VCO}/s$$

Where the 1/s term shows that the VCO is an additional integrator in the transfer function for the forward gain. K_{VCO} can be measured or estimated, being given in cycles per second per Volt. From control theory, we can state that the forward transfer function is the product of all of the gain terms from the reference (ϕ_r) to the controlled output (ϕ_c). This is usually written in standard form; from Figure B2 we see that:

$$G(s) = K_{pd} Z(s) K_{VCO}/s \quad \text{and} \quad H(s) = 1/N$$

where $G(s)$ is the forward open loop transfer function, with $H(s)$ being the reverse (or feedback) transfer function. N is the divide ratio of the N-counter. By considering the controlled output phase in terms of these transfer functions we can derive a standardized closed loop forward transfer function:

$$\begin{aligned} \phi_c &= G(s) (\phi_r - \phi_c) \\ &= G(s) [\phi_r - H(s) \phi_c] \\ &= G(s) \phi_r - G(s) H(s) \phi_c \\ &= G(s) \phi_r + [-G(s) H(s) \phi_c] \\ \phi_c + G(s) H(s) \phi_c &= G(s) \phi_r \\ \phi_c [1 + G(s) H(s)] &= G(s) \phi_r \\ \phi_c / \phi_r &= G(s) / [1 + G(s) H(s)] \quad [= B(s)] \end{aligned}$$

which is the standard definition of the closed loop forward transfer function. Put in terms of the loop variables we have:

$$B(s) = \frac{K_{pd} Z(s) K_{VCO}/s}{1 + K_{pd} Z(s) K_{VCO}/s N} \quad \dots\dots\dots (B3)$$

Completing the mathematical model of the operation of the closed loop. We will return to this model later on. The term $B(s)$ is the control ratio of the closed loop from the reference divider's output (at the phase detector's input) to the VCO's output which is the "controlled" output. Notice that this has the dimensions of radians per second. For those who have a problem with this, the operation of the loop is to multiply the input phase by a fixed ratio (the feedback ratio) to produce an output phase at a larger quantity, exactly as the output voltage of an operational amplifier is a multiplied version of the input voltage. The dimensions of K_{VCO} and K_{pd} must be the same, i.e: both in Cycles or Radians, do not mix dimensions. Now, by inserting the values for the variables we can simplify this down to:

$$\begin{aligned} B(s) &= \frac{K(s + 1/T_2)}{s(s + 1/T_1)} \\ &= \frac{K(s + 1/T_2)}{s + \frac{K(s + 1/T_2)}{N s(s + 1/T_1)}} \end{aligned} \quad \begin{aligned} \text{where: } K &= K_{pd} K_{VCO} L, \quad L = 1/C_1, \\ T_1 &= \frac{C_1 C_2 R_2}{C_1 + C_2} \quad \text{and} \quad T_2 = R_2 C_2. \end{aligned}$$

$$= \frac{K(s + 1/T_2)}{s^2(s + 1/T_1) + (s + 1/T_2)K/N} \quad \dots\dots\dots (B4)$$

$$= \frac{K(s + 1/T_2)}{s^3 + s^2/T_1 + sK/N + K/(N T_2)} \quad \dots\dots\dots (B5)$$

Equation B4 is of limited interest to us when we consider the root locii, but is difficult to factorise, so we usually express this in the form of Equation B5. The reason will become clear in later sections, as we will use it to analyse the transient response, the steady state response and the frequency response for the final closed loop form of the PLL. Next we will analyse the range of the elements in Equation B5 and its dynamics.

c) Loop Dynamics

To compare the function of the complete loop with respect to other circuit configurations, we express them in terms of the loop parameters. The relevance of the loop natural frequency (ω_n) and the damping (ζ), will be obvious once we see how they predominate the expressions for overshoot and settle time (refer to Appendix A). These two, in turn, govern the dynamic range and response times for the loop's functional blocks. Dynamic range is a direct function of the VCO's control voltage and the phase detector's output compliance. Both response time and dynamic range affect the stability of the loop. Once these parameters have been decided, the loop variables can be evaluated (these are the functional blocks in Figure B2) and the component values for the loop filter can then be found.

There are two commonly used ways to approach the analysis of the loop. The first uses the s-plane and is approximate. It requires the derivation of a linear expression for the closed loop time domain response to be carried out; then evaluation of ω_n and ζ from the resultant "waveform". The formulae used can be of great utility when it comes to affirming the theory with a practical result. This method is not a direct one since expressions for component values are not easily extracted from the formulae; they have to be estimated and then plugged into the formulae to evaluate the response. Many iterations can be done before a satisfactory ω_n and ζ drop out. Despite the, this method is to be preferred when initially designing a loop since it covers the conditions governing the second approach. A practical maximum for the first route would be where F_{comp} is about five times ω_n . An approach this close in frequency, by ω_n to F_{comp} , will require an analysis of the frequency domain response of the closed loop to assess the loop filter's (lack of) attenuation of the charge pump pulses. These find their way through to the VCO's control input, causing excessive sideband energy at multiples of F_{comp} . Appendix C and D deal with this. The second method available is based upon the first, it examines the loop with ω_n approaching and at F_{comp} ; by considering the loop as a sampled data system and then using z-Transforms. This is considered to be beyond an introductory note such as this.

To assure that sensible values of loop variables and components are to be used, we use root locii methods to obtain an initial idea of the time domain response and the sensitivity of the selected design to changes in the variables and components used. Next, we take a look at this, then obtain the exact result for the time domain responses using the first method.

d) The Characteristic Equation and its Root Locii.

The denominator of the closed loop transfer function $B(s)$ is of interest to us, as it contains all the information needed to show the form of the transfer function's dynamics. The process of partial fraction forming used to solve the Inverse Laplace Transform of the transfer function also helps us understand the dynamics. The method divides the denominator into its component "factorised" fractions, that is, the number of fractional parts are a "product" of the denominator's linear (or first order) factors, these are equated to a sum of these factors scaled appropriately. The form of the response is determined by the number of fractional parts, which in turn are determined by the number of poles in the denominator's polynomial, hence the denominator "characterises" the complex frequency response. The numerator of the transfer function simply alters the scale factor to each fraction; refer to reference 3a and 3b for further details of partial fraction expansions.

The process of finding the time domain response automatically takes care of any pole-zero cancellations, since any polynomial in the numerator will be seen to either cancel factors in the denominators of the partial fractions, since they alter the magnitude of those partial fraction's terms. Sometimes it is convenient to think of the magnitude of the response as being in the form of the z-axis of a three dimensional x,y,z plot. The z-axis is "out of the page" on the (s-plane) plot and is therefore invisible. The z-axis here is distinct from the z-plane. Therefore the study of the denominator will show the form of the response. By ignoring the magnitude of these responses, we can study the roots' effect upon the form of these responses. Appendix A deals with the Quadratic's Responses and introduces the subject of Root Locii.

AN-94

Now, we will consider the roots of the characteristic equation of B(s) when B(s) is expressed in the form of two polynomials: one in the numerator expressing the zeros and the other in the denominator expressing the poles of B(s), as in Equation B5. The denominator of this can be used for the characteristic equation, or the characteristic equation can be calculated by:

$$\begin{aligned}
 \text{C.E.} &= 1 + G(s) H(s) \\
 &= 1 + K_{pd} Z(s) \frac{K_{VCO}}{s N} \\
 &= 1 + \frac{K_{pd} K_{VCO}}{N s} \cdot \frac{(s + 1/T_2)}{s C_1 (s + 1/T_1)} \\
 &= 1 + \frac{K}{N} \cdot \frac{(s + 1/T_2)}{s^2 (s + 1/T_1)} \quad \text{where } K = (K_{pd} K_{VCO})/C_1 \\
 &= \frac{N s^2 (s + 1/T_1)}{N s^2 (s + 1/T_1)} + \frac{K (s + 1/T_2)}{N s^2 (s + 1/T_1)} \dots\dots\dots (B6)
 \end{aligned}$$

Next, the characteristic equation can be made equal to zero allowing us to find the value of its roots; which is the same as saying that the numerator of Equation B6 is equal to zero:

$$N s^2 (s + 1/T_1) + K (s + 1/T_2) = 0 \dots\dots\dots (B7)$$

This shows a factored form of the equation, but not the roots we require for the root locii analysis. To find these we have to expand the expression as we did earlier in Equation B5, then find a set of linear factors whose product is equal to that expression, being:

$$\begin{aligned}
 N s^2 (s + 1/T_1) + K (s + 1/T_2) &= 0 \\
 N s^3 + N/T_1 s^2 + K s + K/T_2 &= 0 \\
 s^3 + 1/T_1 s^2 + K/N s + K/NT_2 &= 0 \dots\dots\dots (B8)
 \end{aligned}$$

Which is the expanded Characteristic Equation. We can express it in the form of a polynomial as in Equation B8, then use a root finding procedure as in Appendix B or the routine in Reference 7 (which is also useful for higher order equations), or else in the form of a set of factors or roots. The Characteristic Equation's information will allow us to study the behaviour of the loop as we alter the values for the loop's components across their range. From this, we can discover the pole locations on the s-plane by equating the characteristic equation to zero, then find the roots' values which make that expression equal to zero. As we alter the values of the components, we produce a "root locus" for each pole as they change their value, i.e: there are as many locii as there are poles in the open loop transfer function, G(s) H(s) which move across the s-plane.

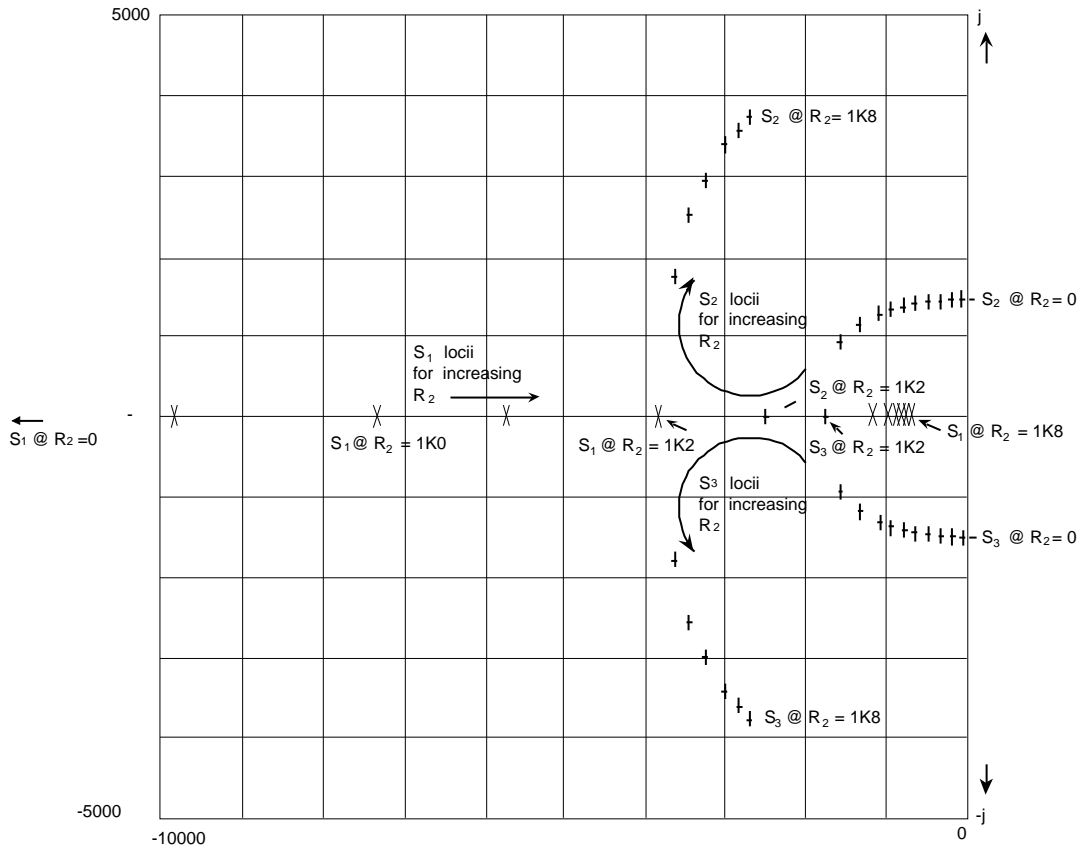
Later analysis of loops using different device types (such as the NJ88C30) will merge with that of the NJ88C33 for the following procedure, since the analysis is now for a generalised third order equation rather than one specifically for the charge pump outputs of the NJ88C33. Appendix B deals with the implementation of the root finding procedure.

To give utility to the roots, we express them on the s-plane as we did in Figure A4. The application of this method can be seen when we change one of the original variables, find the roots, then successively plot them on the s-plane to see the rate of change of the poles with respect to an increment in the original variable. The spacing of the poles will show us the sensitivity of the final design parameters to any variations in those variables, indicating how robust the system will be to component variations.

The plot for Figure A4, was for a variation of R₂ across the range of 1R to 10K with 15R steps. Some locations have been marked for 470R, 1K, 1K2, 1K5 and 1K8. It will be seen that the spacing between 470R and 1K with respect to the spacing between 1K and 1K5, is very much less sensitive. Figure B3 is a plot of the same loop variables, with R₂ being varied across the range of 0 to 1K8 with steps of 100R, to show the relative spacing of the roots' locations at each value.

Figure B3 A plot of $CE = (s + p_1)(s + a + jb)(s + a - jb)$ for $0 < R_2 < 1K8$, in 100R steps

$K_{VCO} = 6 \text{ MHz/volt}$
 $K_{PD} = 2.5 \text{ mA/Hz}$
 $C_1 = 101 \text{ n}$
 $C_2 = 1 \mu\text{O}$
 $N = 6016$



It can be seen that when $R_2 = 0$, s_1 (the real root) is at $s = -\infty$ and the conjugate pair s_2 and s_3 are at the j axis where $= 0$. That is, when R_2 shorts C_1 to C_2 the loop will be unstable; it oscillates at a frequency of $j =$ (which is 1K5 radians per second in this example) with no damping. As R_2 takes a finite value the damping increases, moving the conjugate roots towards the $-$ axis. Initially their locii approximate those of the quadratic function in Appendix A, however the real root decreases in value until it has an effect upon the conjugate roots. The magnitude of this effect is determined by the accuracy to which a result is required since the response settles (in time) from the effect of the higher frequency poles to the effect of the lower frequency poles. Therefore, if the single real pole or the conjugate pair of poles are significantly higher in frequency than the lower frequency pole(s), the lower one(s) will predominate the time domain response. The magnitude of the error in the response can be estimated by: $\text{error (is approximately)} = \exp([F_{\text{lower}} - F_{\text{upper}}] \cdot [n-1])$ where the upper and lower frequencies are for the poles and n is the number of poles involved. If the error is smaller than the accuracy required then the approximation to the quadratic response is valid. This simplification is the reason most designers choose values for the loop components which will allow them to approximate the quadratic response, but is only suited to loops where $\ll F_{\text{comp}} / 100$.

In Figure B3 we see that as the real root (x) approaches the conjugate pair of roots ($+$), the loop's frequency of damped oscillation (ω_d) increases. That is, the loop's natural frequency (ω_n) increases whilst the value of the resistor (R_2) increases rather than remaining constant as it did for the second order response given in Appendix A. This leads to an elongation of the semicircular portions of the locii. The practical effect is for C_1 to be subtracted from the parallel $C_1 C_2$ combination by the increasing value of R_2 . The locii continue towards the $-$ axis with increasing R_2 , until they meet at the s -axis. The angle of approach is at right angles to the axis, where they meet. The positive conjugate root becomes real (it loses its complex part) and moves suddenly to a higher frequency. The negative conjugate root also becomes real, but moves suddenly towards the origin (down in frequency). They now have two distinctly different values. Their movement from the point of meeting is the opposite to the movement of the quadratic response at its "breakout" point. This is the point at which the cubic response deviates dramatically from that for the quadratic response and is unfortunately the point of optimum settle time verses side band attenuation for the cubic response. An approximation of the cubic by a quadratic response will fail miserably and should not be used past where $s_1/4$ is less than the natural frequency of oscillation of the conjugate pair (this results in an error of $\exp(-4) = 1\%$).

AN-94

As R_2 is increased through the area of "critical damping" the singular real root s_1 continues to move towards the origin with the real root pair s_2 and s_3 moving away from the origin. Initially the pair of roots move towards the single root, then they cross over and then recede from it, away from the origin. A point is reached where s_2 and s_3 snap together and breakout again to move as a conjugate pair away from the σ -axis in a straight line, the singular root s_1 continues on towards the origin. As R_2 increases further (about 1K3) the locii of the conjugate pair bends back towards the $j\omega$ axis as the effect of the real root upon them decreases and they approach that of a quadratic again. Across this part of the root locii the real root dominates the cubic response. Finally as R_2 approaches an open circuit the speed of movement across the s -plane by the conjugate roots is decreasing at a lesser rate than the decrease in frequency of the real root, such that they reassert some influence upon the response.

Exactly what does all this movement mean? Fundamentally, the s -plane can tell us graphically the type of response we can expect depending upon the relative location of the roots. We know from Appendix A that a particular set of root locations will produce a set time domain response that is dominated by the pole or poles that are closest to the origin. Be aware that the roots of the characteristic equation are not always the poles of the closed loop (or other function under consideration). However, in this example we can use the term root and pole interchangeably. Remember, the relative positions tell us which poles to discard and which poles will dominate the time domain response. That is, as the value of R_2 is altered from zero to infinity the response of the closed loop cubic transfer function will display an oscillation of about 1K5 radians per second at $R_2 = 0$, this becomes a damped oscillation as R_2 moves away from zero, to become a critically damped exponential as R_2 approaches 1K2. The response up to this point is dominated by the conjugate pair of poles. Between 1K2 and about 1K25, the response is a product of three different exponentials resulting in a time domain response with one reasonably large overshoot. As R_2 increases further the conjugate pair reform and breakout at approximately 3K8 radian per second. The response is then dominated by the single real pole which is at a few hundreds of radians per second. When R_2 exceeds about 2K0, an oscillatory component reappears on the time domain response. With R_2 approaching an open circuit, the loop returns to an unstable state displaying an oscillation at approximately 5K radians per second. It should be noticed that the second order response is unstable for this configuration, i.e: when C_1 and C_2 are shorted by R_2 or when C_1 is removed from circuit by open circuiting R_2 .

The next section will deal with the time domain response from these component values, we will use $R_2 = 1K0$ as a starting point for the analysis. Notice that we can produce s -plane plots for any of the loop variables or filter components in order to optimise a particular part of the response, as we will see later on. The size and shape of the locii will change accordingly, requiring a similar interpretation process.

Figure B4 shows a set of locii for varying R_2 across a range of zero to ten kilohm; these locii intersect the locus generated by holding all the variables except C_1 constant; R_2 is held at 1K0. C_1 is then varied across the range of 1n0 to 1 μ 0. The locus for C_1 forms the small ellipsoid between (- 1K2, +-j1K0) and (- 300, +- j1K3) on the s -plane plot; this locus intersects the other locii where $R_2 = 1K0$.

AN-94

The step response occurs when an instantaneous change from one level of input to another occurs (e.g: when a loop variable such as the N-division ratio is changed). This type of response is used most commonly to demonstrate “the time domain response”. We will use it in conjunction with the settle time and over-shoot formulae from Appendix A. This will allow us to derive the loop natural frequency and damping in terms of the loop components in the next section. It forms the most commonly analysed of the group of responses and conveniently delivers up most of the information we need about the loop’s dynamics.

The ramp response shows the instantaneous error when we slowly vary the value of a component, or input to the circuit (e.g: linear modulation of the loop). This can be demonstrated practically by the use of a triangle waveform, or evaluated analytically for small values of time. If the ramp is equated to the instantaneous rate of change of the waveform of interest, we can find the maximum dynamic error or “velocity deficit” caused by that input, at that point in time. For example, we evaluate the equivalent ramp slope with time to the maximum rate of change in a modulating waveform; for a sine wave input this will be at the zero-crossings where d/dt[f(t)] is at a maximum. It will be found that a practical measurement of the ramp response will be more meaningful than a plot. The sine wave response can be evaluated by using the angle and magnitude criteria of the Phasor Method of analysis. For these two reasons the analytic assessment of the ramp function will not be carried out here as it will unnecessarily complicate the note. The procedure is the same as for the impulse and step responses demonstrated here, so it is left, as they say, as an exercise for the reader.

To find the time domain response we need to find the roots of the Equation B8 as we did for the root locus. We return from the root finding procedure in Appendix B with s_1 , s_2 and s_3 , which are the roots of the characteristic equation’s polynomial. For this particular third order response, the zero is a simple linear polynomial (first order), allowing us to use the roots of the characteristic equation as the poles of the closed loop response. The numerator being the same zero as in Equation B5. The factored form of the closed loop response in the complex frequency domain as follows:

$$B(s) = K \frac{(s + z_1)}{(s + p_1) \cdot [s + (a+jb)] \cdot [s + (a-jb)]} \dots\dots\dots (B9)$$

where $K = K_{vco} \cdot K_{pd} / C_1$ as before, z_1 is the zero at $-1/T_2$, $p_1 = -s_1$, $(a+jb)$ is the complex numerical value of $-s_2$ and $(a - jb)$ is the complex numerical value of $-s_3$, from which we can solve the time domain responses. These transient responses are found from Equation B9 when s_2 and s_3 are complex and an alternate form when the three poles are real. Since the Laplace Transform of an impulse (an infinitely large, infinitely narrow pulse with a time x amplitude “area” of unity) is unity, we find that the Inverse Laplace Transform of the product of B(s) and the excitation is the transform of the loop function alone. The response to the impulse function is therefore:

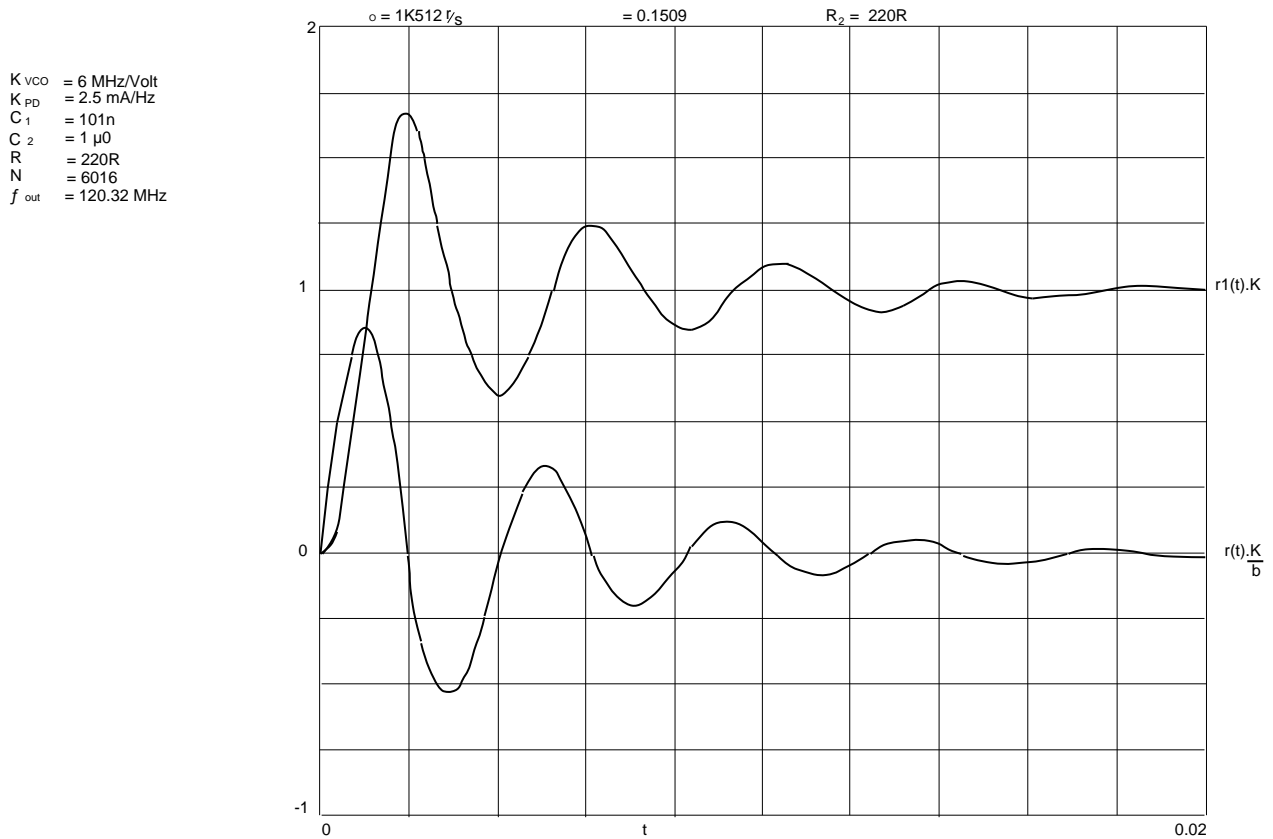
$$\begin{aligned} r(t) &= L^{-1}\{ B(s) \cdot 1 \} \\ &= L^{-1}\left\{ K \frac{(s + z_1)}{(s + p_1) \cdot (s + a + jb) \cdot (s + a - jb)} \right\} \\ &= K \cdot L^{-1}\left\{ \frac{(s + z_1)}{(s + p_1) \cdot [(s + a)^2 + b^2]} \right\} \end{aligned}$$

We can find the Inverse Laplace Transform from a set of tables as in reference 6 and normalise the response by dividing through by the gain factor K:

$$\frac{r(t)}{K} = \frac{(z_1 - p_1)}{[(a - p_1)^2 + b^2]} \cdot \exp(-p_1 t) + \frac{1}{b} \cdot \left[\frac{b^2 + (z_1 - a)^2}{b^2 + (p_1 - a)^2} \right]^{1/2} \cdot \exp(-at) \cdot \sin(bt + \dots\dots\dots) (B10)$$

where $\theta = \tan^{-1}[b/(z_1 - a)] - \tan^{-1}[b/(p_1 - a)]$. This shows an exponential term decaying at a rate determined by the pole at p_1 and an exponentially decaying oscillation which approaches zero as t approaches infinity. The rate of decay is determined by the real part of the conjugate pole at $-(a + jb)$. The period of oscillation is determined by b, the complicated looking fractions are simply scaling for each term, as determined by the poles and the zero. The constant, K, was defined previously by the circuit variables, the result is shown as the lower trace of Figure B5.

Figure B5. Response of an underdamped loop to an impulse and a step excitation



The above response only applies when the discriminant is greater than zero, i.e: the roots represent one real pole and two complex conjugate poles. If the discriminant is less than zero, then the transfer function has three real poles making the response:

$$r(t) = \mathcal{L}^{-1}\{B(s).1\}$$

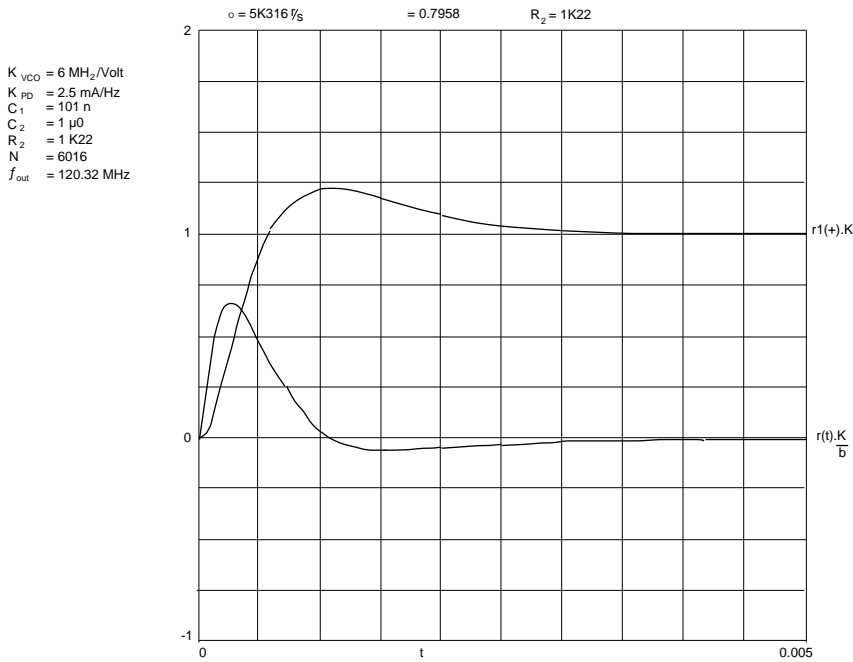
$$= \mathcal{L}^{-1}\left\{K \frac{(s + z_1)}{(s + p_1)(s + a)(s + b)}\right\}$$

which, from transform tables is:

$$\frac{r(t)}{K} = \frac{(z_1 - p_1) \exp(-p_1 t)}{(a - p_1)(b - p_1)} + \frac{(z_1 - a) \exp(-at)}{(p_1 - a)(b - a)} + \frac{(z_1 - b) \exp(-bt)}{(a - b)(p_1 - b)} \dots \dots \dots \quad (B11)$$

showing three exponentials scaled by the respective poles and the zero. The resultant response is the product of two semi-Gaussian pulses with separate time constants which settle back to the baseline that existed before the impulse appeared. The plot of this is shown in the lower trace of Figure B6.

Figure B6. Response of an overdamped loop to an impulse and a step excitation



We can find the time domain response to a unit step-function perturbation of the loop by the same process; the Laplace Transform of the unit step function is 1/s, giving the following response for a discriminant greater than zero (one real and two conjugate poles):

$$r1(t) = \mathcal{L}^{-1}\{ B(s)/s \}$$

$$= K \cdot \mathcal{L}^{-1}\left\{ \frac{(s + z_1)}{s (s + p_1) \cdot [(s + a)^2 + b^2]} \right\}$$

From transform tables the result is:

$$\frac{r1(t)}{K} = \frac{z_1}{p_1(a^2 + b^2)} + \frac{(p_1 - z_1)}{p_1[b^2 + (a - p_1)^2]} \cdot \exp(-p_1 t) - \frac{1}{b(a^2 - b^2)^{1/2}} \cdot \left[\frac{b^2 + (z_1 - a)^2}{b^2 + (a - p_1)^2} \right]^{1/2} \cdot \exp(-at) \cdot \sin(bt + \dots) \quad (B12)$$

where $\theta = \tan^{-1}(b/a) + \tan^{-1}[b/(z_1 - a)] + \tan^{-1}[b/(a - p_1)]$. This response is seen to be an offset, an exponential controlled by the pole at p_1 and a damped oscillation whose amplitude is controlled by the real part of the conjugate poles, a , with its frequency of ring controlled by the imaginary part of the conjugate poles, $\pm j b$. The complicated fractions are again the scaling of each term by the poles and the zero. This is the upper trace in Figure B5.

If the discriminant of the characteristic equation is less than zero, then the response for the three real poles becomes:

$$r1(t) = \mathcal{L}^{-1}\{ B(s)/s \}$$

$$= K \cdot \mathcal{L}^{-1}\left\{ \frac{(s + z_1)}{s (s + p_1) (s + a) (s + b)} \right\}$$

which, from transform tables is:

$$\frac{r1(t)}{K} = \frac{z_1}{p_1 a b} + \frac{(p_1 - z_1) \exp(-p_1 t)}{p_1 (a - p_1) (b - p_1)} + \frac{(a - z_1) \exp(-at)}{a (b - a) (p_1 - a)} + \frac{(b - z_1) \exp(-bt)}{b (a - b) (p_1 - b)} \dots (B13)$$

Here we see an offset with three exponentials, their decay times controlled by the three real poles. This gives an exponential which overshoots once, then settles to the new value exponentially as shown by the upper trace of Figure B6.

The impulse response and step response for the underdamped phase locked-loop are shown in Figure B5. These traces graphically illustrate the output from Equations B10 and Equation B12 for one hundred and twenty-eight discrete time steps between zero and twenty milli-seconds. Figure B6 shows the impulse response and the step response for an overdamped third order loop, being the visualisation of Equation B11 and Equation B13.

The variables used to plot these responses are: $k = K/N = (K_{VCO} K_{PD}) / (C_1 N)$, where $K_{VCO} = 6.0\text{MHz/Volt}$, $K_{PD} = 2.5\text{mA/Hz}$, $N = 6016$ (a prescaler must be used for a divide ratio this high as $N(\text{max}) = 4095$ for the NJ88C33's eleven bit N-counter), $C_1 = 101\text{n}$, $C_2 = 1\mu\text{0}$ and $R_2 = 220\text{R}$. Scattered throughout this note are other time domain responses to the unit step function. These have been drawn using all of the above values with the exception of R_2 . We should examine these with respect to the s-plane plot in Figure A4 as we alter R_2 . With R_2 at 220R, as in Figure B5, we see an oscillatory response near 250 Hz ($1K5\text{rads/s}/(2)$). Increasing R_2 to 1K0 (the upper trace in Figure A4), the step response becomes a single large overshoot which settles to the level of the step, with a train of very small oscillations impressed upon it.

The overshoot decreases, the oscillatory component disappears and the rise time improves in Figure B6, where $R_2 = 1K2$. As we have already seen, this is the point at which the greatest sensitivity of the roots to any change in loop values occurs. It is also the point at which we would wish to operate the loop for optimum settle time and noise performance. Provided care is used to ensure that the loop variables do not cause loop instability (K_{VCO} and K_{PD} are the least controllable), this goal should be able to be achieved.

Continuing the increase in R_2 's value towards 1K5 (the lower response of Figure A4) will display a faster rise time, with the overshoot beginning to increase again. By the time that $R_2 = 8K2$ the response is oscillatory again, displaying a higher frequency component than before; being about 800Hz as in Figure A3. Note that the horizontal scale varies from plot to plot to expand the detail of each; all are in seconds. The plots for each set of values were anticipated from the analysis of the s-plane plots in Figures A4 and B3. Check the positions of the poles on the s-plane for each value of R_2 shown on Figure A4 against each time domain plot.

Notice that an element of the excitation appears at the output in each case. By placing Equations B10 to B13 into a computer program, we can plot the time domain response of the closed loop to each. Figures B5 and B6 are the right hand side of the response formulae scaled by K/N to normalise them to unity. It should be noticed that the terms $\exp(-p_1 t)$, $\exp(-at)$ and $\exp(-bt)$ will result in an underflow error at large values of time. To get around this, a routine should be added to limit $p_1 t$, at and bt to less than the resolution of the machine being used. The predicted responses are for the evaluation card to an "interference" pulse and a step function, the results are drawn in Figure B5 and B6, which have been produced from such a routine. The impulse function's response are all divided by b ; since a factor of each real root must contribute to the scale factor K . Here we have assumed that the divider is perfect, so we could say that these plots are of b in Figure B2. The ramp function's response will be similar to that for the impulse response, but will be lower in magnitude and settle out to a rising straight line which is unbounded.

We see that the impulse response in both the under- and over-damped cases are the differential of each step response; a not entirely unexpected result since division by s in the complex frequency domain is the same as integrating in the time domain. From these it can be seen that the damping term (a) and the oscillatory term (b) are carried from the step response to the impulse response and will be carried through in a similar manner from higher order responses such as the ramp response right down to the impulse response. Therefore we can derive an expression for the loop natural frequency and damping factor from the impulse response in the next section. We shall return to these responses in Part C to examine them in relation to the responses measured from the evaluation card.

f) Loop Natural Frequency, Damping Ratio and Settle Time.

Now that we know what type of response to expect from a third order loop, we should consider how to find an easy method for deriving the loop components values from the loop parameters (ω_o and ζ) and the fixed variables. Usually we will have a set of (fixed) variables over which we have little control; being K_{pd} , which is determined by the phase detector's designer, K_{vco} , which we have selected to cover the range of the application and N , as determined by the above frequency range divided by the comparison frequency. The "flexible" variables which we can readily control are the components C_1 , C_2 and R_2 . We will see that C_1 controls the forward gain; the ratio of C_1 to C_2 controls the range of damping with R_2 fine-tuning the damping and all three affecting the loop's damped frequency, as would be expected from the root-locii plots.

To determine the values of the flexible variables we need to know the loop parameters (ω_o and ζ), which we will deal with here, as well as the ratio of the real pole's frequency to the loop natural frequency. Here we introduce a third parameter t , a time delay, where $t = 1/p_1$ where $p_1 = R$ with R being the ratio of p_1 to ω_o . The ratio R is determined in the next section as a consequence of the roll-off shown in the Bode Plots. First we will formalise ω_o and ζ . We know that from the definition of the roots s_2 and s_3 , that b is equal to the natural frequency of oscillation (ω_o) when the damping term a has been reduced to zero. The characteristic equation then becomes:

$$C.E. = (s + p_1) (s^2 + b^2)$$

Which gives an oscillatory time domain response for the complete equation:

$$\begin{aligned} r(t) &= \mathcal{L}^{-1}\{ B(s) \cdot 1 \} \\ &= \mathcal{L}^{-1}\left\{ \frac{(s + z_1)}{(s + p_1) (s^2 + b^2)} \right\} \\ &= \frac{(z_1 + p_1)}{(p_1^2 + b^2)} \exp(-p_1 t) + \left[\frac{(z_1^2 + b^2)}{(p_1^2 b^2 + b^4)} \right]^{1/2} \cdot \sin(bt + \phi) \dots\dots\dots (B14) \end{aligned}$$

where $\phi = \tan^{-1}(p_1/b) - \tan^{-1}(z_1/b)$. The right hand term is a steady state oscillation, when t approaches infinity. Only the sine term multiplied by a fixed constant is left, since there is no exponential multiplier to represent the rate of damping of the response. The period of oscillation is determined by b and is at the $j\omega$ axis of the s -plane plot. By temporarily assuming that $p_1 > 10b$, we can delete p_1 from the analysis then consider the loop's response to have a quadratic denominator. This would allow us to deal with the analysis the same way that many people have done before. The relevant part being that we can express the complex conjugate pair as:

$$\begin{aligned} s^2 + 2\zeta\omega_o s + \omega_o^2 &= (s + \zeta\omega_o + j\omega_o \sqrt{1 - \zeta^2}) (s + \zeta\omega_o - j\omega_o \sqrt{1 - \zeta^2}) \\ &= (s + a + jb) (s + a - jb) \end{aligned}$$

where $a = \zeta\omega_o$ and $jb = \omega_o \sqrt{1 - \zeta^2}$. We see that a and $(\omega_o^2 - a^2)^{1/2}$ correspond to the real and imaginary projections of the complex conjugate pair for a Quadratic Response as in Appendix A. The definition of damping given there is: $\zeta = \cos \theta$ where $\theta = \tan^{-1}[\text{Im}(s) / \text{Re}(s)]$. When the poles become real, the damping increases but ζ as defined remains at unity since θ remains at zero as the real poles move along the real axis. The conflict is resolved by restricting the use of ζ and ω_o to the values of roots for which the discriminant (for both the Quadratic and Cubic; refer to Appendices A and B) is either equal to or greater than zero.

The proof of the settle time equation is centred around the Quadratic Response, since most higher order responses can be approximated by an adequately scaled Quadratic Response. The full proof is given in Appendix A, the end results we need here are the following Equation A(xi), A(vii) and A(viii) or A(ix), being:

$$= \frac{-\ln}{t_{settle}} \dots\dots\dots (B15)$$

Nominally is chosen to be 0.7071, with = the error expressed as a fraction of the required step and t_{settle} being the time taken to achieve that fractional value, e.g.: the 5% settle time. This allows us to fix the loop parameters. The other two equations are of practical interest for verifying the loop parameters from measured results; we will meet them again in Part C:

$$n = (- [2 n -1] \cot[]) \dots\dots\dots (B16)$$

useful for estimating the first fractional overshoot when n = 1 and:

$$= \left\{ \frac{\text{Pi}(2n - 1)}{\ln(n)} \right\}^2 + 1 \}^{-1/2} = \left\{ \frac{2 (n - m)}{\ln(m/n)} \right\}^2 + 1 \}^{-1/2} \dots\dots\dots (B17)$$

where n = 1 and m = 2 for the first and second peak overshoots of the underdamped response. Apart from a few cases where damping ratio is chosen to be some other value, e.g: greater than unity for an over-damped loop when optimising phase noise, this expression will suffice. The alteration of damping and loop natural frequency for this equation is dealt with in the next section, at which point we may find that we have a conflict of requirements when we choose the (comparison frequency related) sideband rejection level and recalculate Equation B15.

Now that we can numerically evaluate and from the required settle time, we can derive and evaluate expressions for the flexible variables C₁, C₂ and R₂. To do so we have to make a leap of faith and assume an answer, which we will then prove by induction. Conveniently reference 4 has a table of transforms expressed in terms of , and the time delay , one of them has the same form as Equation B8, being:

$$B(s) = \frac{2 (1 + U s)}{(1 + s) \cdot (s^2 + 2 s + 2)} \dots\dots\dots (B18)$$

If we use the denominator of Equation B18, expand it out, then compare its coefficients with those of Equation B8, we can generate a set of equations for C₁, C₂ and R₂ in terms of K_{vco}, K_{pd}, N, and . We need to know that:

$$\frac{(s + z_1)}{(s + p_1) (s + a + jb) (s + a - jb)} = \frac{2 (1 + U s)}{(1 + s) (s^2 + 2 s + 2)} \cdot X$$

where X is some scale factor. We have to prove the right hand side of the equality, taking:

$$\text{LHS} = \frac{(s + z_1) 1/z_1}{(s + p_1) 1/p_1 (s + a + jb) (s + a - jb)} \cdot \frac{z_1}{p_1}$$

Next use s₂, s₃ = [- b ± (b² - 4 a c)^{1/2}]/(2 a), to find the roots of the Quadratic term (s² + 2 s + 2) from the original equality, we can then substitute for (s + a + jb) (s + a - jb):

$$\text{LHS} = \frac{(s + z_1) 1/z_1}{(s + p_1) 1/p_1 (s + + [2 - 1]^{1/2}) (s + - [2 - 1]^{1/2})} \cdot \frac{z_1}{p_1}$$

If we take U = 1/z₁, = 1/p₁ and multiply by 2, we get:

$$\frac{2 \cdot p_1}{z_1} \cdot \frac{(s + z_1)}{(s + p_1) (s + a + jb) (s + a - jb)} = \frac{2 (1 + U s)}{(1 + s) (s^2 + 2 s + 2)} \dots\dots\dots (B19)$$

AN-94

which, if we say that $\alpha < 1$, $a = \alpha$ and $jb = \alpha [2 - 1]^{1/2}$, can be seen to be true with the scale factor $X = \alpha^2 \cdot p_1/z_1$. This now gives us two methods to evaluate the time domain response: with the variables as we did earlier in this part, or in terms of the parameters α , β and γ . Notice that if pole-zero cancellation could be arranged the transfer function, Equation B18 reduces to that of a Quadratic, at other values the response is distorted from that of the quadratic by a factor of p_1/z_1 . Now we use the denominators of Equation B19's left and right hand side after moving the $\alpha^2 \cdot p_1/z_1$ term into the numerator, i.e: into the scale factor K. Notice that the denominator of Equation B5, which is the characteristic equation, can be equated indirectly with the right hand side denominator of Equation B19 since it is equal to the left hand side of Equation B19. For the analysis of other loop types (e.g: the NJ88C30) their characteristic equations should be substituted at this point for that of Equation B5, then follow a similar procedure to that below, to find their coefficients. From the denominator on the RHS of Equation B19 we have:

$$(1 + s) (s^2 + 2\alpha s + \alpha^2) = s^3 + 2\alpha s^2 + (\alpha^2 + 2\alpha) s + \alpha^2$$

Then divide RHS by t to put the result into its standard form:

$$RHS = s^3 + s^2 (2\alpha + 1)/t + s [(\alpha^2 + 2\alpha)]/t + \alpha^2/t$$

If we then take the LHS denominator of Equation B5 and equate it to the RHS equation above, we get:

$$s^3 + s^2/T_1 + sK/N + K/(NT_2) = s^3 + s^2 (2\alpha + 1)/t + s [(\alpha^2 + 2\alpha)]/t + \alpha^2/t$$

So, at long last! We can equate the coefficients of each side of the equality thus:

$$1/T_1 = (2\alpha + 1)/t \qquad K/N = [(\alpha^2 + 2\alpha)]/t \qquad K/(NT_2) = \alpha^2/t$$

From which, we can derive C_1 , C_2 and R_2 ; given the parameters α , β and γ , as well as the fixed variables K_{pd} , K_{vco} and N. Remember that we have made $t = 1/p_1$ and we assumed that R is the ratio of p_1 to z_1 . By rearranging the coefficients in the following order we can find:

C_1 from the coefficients of s:

$$K/N = [(\alpha^2 + 2\alpha)]/t$$

$$\frac{K_{vco} K_{pd}}{C_1 N} = \frac{2\alpha + 2}{t}$$

$$= \frac{(\alpha^2 + 2\alpha) R}{t} \qquad \text{(where } \alpha = 1/p_1, p_1 = R)$$

$$= \alpha^2 (1 + 2/R)$$

$$C_1 = \frac{K_{vco} K_{pd}}{N \alpha^2 (1 + 2/R)} \dots\dots\dots (B20)$$

T_2 from the coefficients for the constants:

$$K/(N T_2) = \alpha^2/t \qquad \text{(remember that } T_2 = R_2 C_2)$$

$$1/T_2 = N \alpha^2 / (K)$$

$$T_2 = K / (N \alpha^2)$$

$$= t / \alpha^2 \cdot \alpha^2 (1 + 2/R) \text{ (K/N from above)}$$

$$= (1 + 2/R) / (\alpha^2 R)$$

$$= 1 / (R + 2/R) \dots\dots\dots (B21)$$

and the ratio of C_2 to C_1 from the coefficients of s^2 :

$$\begin{aligned} 1/T_1 &= (2 + 1) / \\ \frac{C_1 + C_2}{C_1 C_2 R_2} &= 2 + 1 / \quad \left(\text{since } T_1 = \frac{C_1 C_2 R_2}{C_1 + C_2} \right) \\ \left(1 + \frac{C_2}{C_1} \right) \frac{1}{T_2} &= 2 + R \\ C_2 / C_1 &= (2 + R) T_2 - 1 \dots\dots\dots (B22) \end{aligned}$$

Once we find a value for R we can solve the flexible variables by finding C_1 , then the ratio of C_1 to C_2 , this value of C_2 will solve the value of R_2 in the time constant T_2 . These coefficients also allow us to find two more extremely useful Equalities for damping and loop natural frequency in terms of the loop variables. From Equation B21 we have:

$$= \left[\frac{K_{vco} K_{pd}}{R N C_1 C_2 R_2} \right]^{1/3} \dots\dots\dots (B23)$$

and from Equation B21: $= (T_2 - 1/R) / 2 \dots\dots\dots (B24)$

Care must be exercised when using the last two expressions as it is possible to calculate ridiculous values, they should be used in conjunction with the s-plane root locii methods to assure sensible results. Their use should only be to fine tune the loop parameters, or to check changes due to tolerance errors across a small range. For large ranges the ratio R must be evaluated from $-(s_1 /)$ from the routine given in Appendix B; but then we would know and from:

$$= \cos\{ \tan^{-1} [\text{Im}(s_2) / \text{Re}(s_2)] \} \quad = \{ [\text{Re}(s_2)]^2 + [\text{Im}(s_2)]^2 \}^{1/2}$$

anyway, which makes Equations B23 and B24 somewhat superfluous. The expressions will prove useful when comparing different order loops or loop formats, due to the generality of their parameters. They can be useful in finding a quick approximation to a loop's response, by substituting the results from bench measurements into the formula for the Quadratic response (as in Appendix A). The time domain response can be determined in terms of the loop parameters (and) by plugging them into the Laplace Transform of the right hand side of Equation B19, the result is to be found in reference 4.

To finish this section it would be instructive to look at the form of Equations B23 and B24 to help develop an intuitive feel for the loop's function. C_1 is seen to be the only flexible variable which contributes to the loop natural frequency in Equation B23, along with the fixed variables K_{vco} , K_{pd} , N and the positioning of p_1 via the parameter R. These change at a rate of $2^{1/2}$ per doubling of value for K_{vco} and K_{pd} , and at a rate of $2^{-1/2}$ per doubling for C_1 and N. Damping is seen to be a strong function of T_2 from Equation B24; which is heavily dependant upon R_2 , C_2 , K_{vco} and K_{pd} . Damping is inversely proportional to N and C_1 , but has a lesser dependency upon the ratio R which will be determined by the loop filter's transition-to-stopband shape. R will be examined in the next section and is fortunately the only defining parameter still to be decided upon.

AN-94

g) Bode Plots of Phase and Magnitude.

Question: When is a Third Order Loop not a Third Order Loop?

Answer : When it has a zero in it!

The above commentary underlines the function of this particular type of loop. With reference to Figure B4 (which shows the migration of the poles across the s-plane for changing R_2 with various ratios of C_1 to C_2) we see that as the location of p_1 nears the conjugate pair p_2, p_3 , it influences the shape of the root locii of the pair; i.e: the circular shape of the locii distorts towards that of an ellipse. These locii can be shown to represent a Butterworth filter in the first instance and a Chebyshev in the second. The implication of this being that the use of a Butterworth Filter would lead to an unacceptable overshoot in the time domain, whereas the Chebyshev would lead to an unacceptable peaking near in the frequency domain. We hope to minimise both characteristics to approximate something in between the two filter types, which can be done by careful choice of the ratio between the real pole p_1 and the zero z_1 . This results in a response in the time and frequency domain that approaches that of a Bessel filter which has a monotonic response in the time and frequency domains with increasing frequency.

We obtain minimal overshoot and peaking at the expense of rapid slope turnover to the final rolloff in the transition band. This shape can be seen in Figure B7 where the final slope in each case is -40 dB per decade rather than the -60 dB that would be expected from a third order filter. It was to optimise the shape of the transition near that such a lot of energy was devoted to obtaining the complete transfer function, $r(t)$, in terms of the parameters and . These allow a simultaneous solution of the complete loop's transfer function in terms equivalent to those of a second order loop. Note the distinction: "in terms equivalent to ...". This is a third order loop and must be solved as such: the deviation of any of the variables within the loop from their designed values, will make this fact very clear. So be warned: do not try to cut corners by trying to solve this as a second order loop (usually done by ignoring the real pole) by assuming that the real pole is far enough up in frequency to have no effect upon the loop response. The reason the real pole matters is that the components contributing to the real pole also contribute to the zero. Whereas the real pole may be far removed from the conjugate pair, the zero tends to be fairly close and lower in frequency than the conjugate pair; thereby heavily influencing the response of the loop filter and so, the loop's operation.

We saw in Appendix A, that we can state any generalised transfer function for $G(s)$, when $s = j \omega$, (the steady state response) as being:

$$G(j \omega) = M(\omega) e^{j \phi(\omega)}$$

where $M(\omega)$ is the magnitude response and $\phi(\omega)$ is the phase response at the applied frequency ω , notice that the exponent of ω is assumed to contain $j \omega t$ with only ωt expressed. With reference to Appendix A, we can plot out the Magnitude from Equation B9 in the form of Equation A(xii):

$$M(\omega) = \frac{\prod_{i=0}^n (s - z_i)}{\prod_{j=0}^m (s - p_j)} \quad \Big|_{s=j\omega} \text{ Remember that } z_1, p_1 \text{ etc are negative, whereas } M(\omega) \text{ can only be positive.}$$

$$= \frac{(j \omega - z_1)}{(j \omega - p_1) [j \omega - (a + jb)] [j \omega - (a - jb)]}$$

Again we see that we need to know the roots of the characteristic equation; these we take from the routine in Appendix B in the form of $p_1 = -s_1, p_2 = -s_2 = -(a + jb)$ and $p_3 = -s_3 = -(a - jb)$. Since most designs will be seeking to optimise the settle time response where $\zeta = 2^{-1/2}$, we will concentrate on a solution using complex roots, rather than real roots: if an overdamped loop is desired to optimise noise, the following will need reworking with the appropriate values. We can either numerically evaluate the above expression or we can let:

$$a + jb = \zeta \omega_n + j \omega_n (1 - \zeta^2)^{1/2} \quad \text{and} \quad a - jb = \zeta \omega_n - j \omega_n (1 - \zeta^2)^{1/2}$$

at this stage $z_1 = 1/T_2$ from Equations B₂ and B₉, in Equation B₂₁ we see that:

$$T_2 = (1 + 2R) / (R)$$

=>
$$z_1 = \frac{R}{1 + 2R}$$

giving:
$$M(\omega) = \frac{(j\omega + R)(1 + 2R)}{(j\omega + R) \cdot [j\omega + \{ \dots + (2 - 1)^{1/2} \}] \cdot [j\omega + \{ \dots - (2 - 1)^{1/2} \}]}$$

where we have made $p_1 = -s_1 = R$ and $z_1 = R / (1 + 2R)$ from equations B₂ and B₉, since $z_1 = 1/T_2$. We can assume a solution to the complex conjugate part represented by p_2, p_3 , as being similar to the solution obtained in Appendix A, when dealing with the Characteristic Equation of the quadratic, giving:

$$M(\omega) = \frac{(j\omega + z_1)}{(j\omega + R) [\omega^2 + j2 \dots - 2]}$$

Next we normalise the result by taking out a factor of $z_1/(p_1^2)$:

$$M(\omega) = \frac{(j\omega/z_1 + 1)}{(j\omega/R + 1) \cdot [1 + j(2 \dots) - (\dots)^2]} \cdot \frac{z_1}{p_1^2}$$

Since we wish to find the vector form for each factor, we square the real and imaginary parts separately, then find the root of their sums to remove the j operator from each:

$$M(\omega) = \frac{[(\omega/z_1)^2 + 1^2]^{1/2}}{[(\omega/R)^2 + 1^2]^{1/2} \{ [1 - (\dots)^2]^2 + [(2 \dots)^2]^{1/2} \}} \cdot \frac{z_1}{p_1^2}$$

$$= \frac{[1 + (\omega/R \dots (1 + 2R))]^2]^{1/2}}{[1 + (\omega/p_1)^2]^{1/2} \{ [1 - (\dots)^2]^2 + (2 \dots)^2 \}^{1/2}} \cdot \frac{R \dots (1 + 2R)}{p_1^2} \dots (B25)$$

which is plotted in Figure B₇, in normalised form for various values of p_1 and \dots . The magnitude ordinate is in $20 \cdot \log[M(\omega)/k]$ form, where $k = z_1/(p_1^2)$.

Before going any further with this analysis, we would do well to consider the exact meaning of the ordinates of the $M(\omega)$ plot in terms of the operation of the completed phase locked loop. Since the loop is one which uses a phase detector, the fed-back element is phase (by virtue of the N counter's division of the VCO's output frequency; or should we say, multiplication of the VCO's period to the comparison period, or phase?) such that the amplitude indicated by $M(\omega)$ is really the frequency deviation of the VCO's output frequency. The ordinate relates to the rate of deviation of the output frequency of the VCO. Neither of these should be confused with the amplitude and frequency components of the final output spectrum. The relationship of those comparison related side products to the original input at the reference or at the charge pump output to the VCO output is a very complicated function dominated by the Bessel functions given in standard texts on frequency modulation frequency. It is more useful to think of these plots as representing the control voltage to the VCO by assuming that there is a direct correspondence between the control voltage and the output frequency without any real limitation upon the VCO's function, that is, an ideal voltage to frequency conversion. If the first pole in the VCO's control line is well above the assumption is valid, allowing us to consider the effect of the loop upon the control voltage in terms of the comparison frequency attenuation and noise rejection. The shape of the magnitude response allows us to estimate the noise floor contour as well as the ability of the Phase-locked Loop to function as a control system. In a real implementation of a practical Phase-locked Loop, great attention will be paid to the ability of the loop to suppress the VCO's noise sidebands (distinct from the comparison frequency related spurs on a plot of the output's spectrum); giving the controlled output a close-in, phase noise characteristic, typical of the reference input rather than the VCO. We shall return to this subject in Part C, under "Measurement of Noise Bandwidth and Sidebands".

AN-94

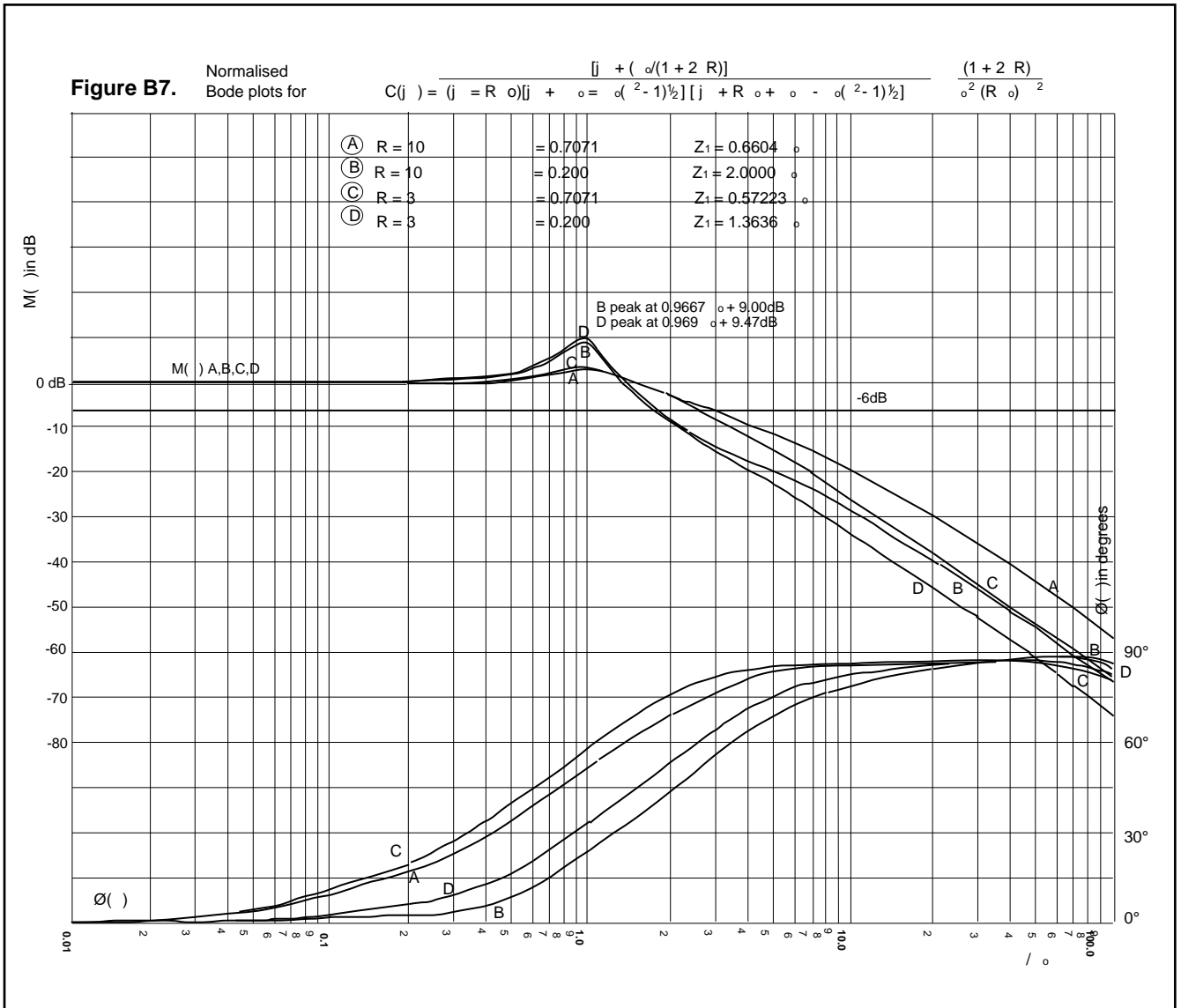
Next we turn our attention to the phase plots for the “Phase-locked Loop”, these make more sense if we consider the alternate name “Phase Feedback Frequency Locked Oscillator”. We consider the phase plot for the phase trajectory during a phase modulation sequence where the divider ratios are used to modulate the loop, or if we are to analyse the loop’s response to a non-sinusoidal waveform. That is, phase analysis tends to be a dynamic consideration rather than a static one. The phase response can become very important since it alters the time relationship between the harmonics of the input waveform, which in turn alters the shape of the resultant waveform at the VCO’s control voltage input. Practical results will show a dramatic change in the character of the loop’s side products for changing loop phase due to the change in timing of the higher harmonics with reference to the lower ones; so reinforcing or cancelling many of the multiple comparison frequency side products. Examination of the relationship of these side products gives a very powerful analysis tool for locating hardware and layout problems associated with the loop filter as well as the interference leakage paths into the VCO around the loop filter, e.g: via the finite ground plane inductance or the power supplies’ output impedance. Reference 3 deals with the Harmonic Analysis of Waveforms. As the full analysis of this technique is well beyond this note, we shall complete this section by merely producing a phase plot of the loop, leaving more complex analysis to others. The phase response plot is drawn by evaluating Equation B9 in terms of the graphical solution outlined in Appendix A, near Equation A(xiii), thus:

$$\phi(\omega) = \sum_{i=0}^n \text{angles of the zeros} - \sum_{j=0}^m \text{angles of the poles}$$

where the angles are the arguments of the fraction formed by the applied frequency ω less the imaginary projection of the pole or zero, divided by the real projection of that same pole or zero. This may take a little bit of thought; with the poles and zeroes placed on a pole / zero plot (same ordinates as an s-plane), we employ basic trigonometry to find the angle subtended by a perpendicular projection from the imaginary axis to the pole or zero, with a projection from the pole or zero to the point of the applied frequency on the positive imaginary axis, the angle of interest is the acute angle so formed. Remember that this equation only applies for $0 < \omega < 1$.

$$\begin{aligned} \phi(\omega) &= \text{atan}\left[\frac{-\text{Im}(z_1')}{\text{Re}(z_1')}\right] - \text{atan}\left[\frac{-\text{Im}(p_1)}{\text{Re}(p_1)}\right] - \text{atan}\left[\frac{-\text{Im}(p_2)}{\text{Re}(p_2)}\right] - \text{atan}\left[\frac{-\text{Im}(p_3)}{\text{Re}(p_3)}\right] \\ &= \text{atan}\left(\frac{\omega}{1 + 2R/R_0}\right) - \text{atan}\left(\frac{\omega}{R_0}\right) - \text{atan}\left(\frac{\omega}{1 + [1 - 2]^{1/2}/R_0}\right) - \text{atan}\left(\frac{\omega}{1 - [1 - 2]^{1/2}/R_0}\right) \end{aligned} \tag{B26}$$

The Bode plot for phase, $\phi(\omega)$, is shown at the bottom of Figure B7. The phase ordinates on the right hand side are in degrees rather than radians, conversion from one to the other being quite straight forward: degrees $\cdot \pi/180 =$ radians.



From Figure B7 we see that the only method available to us to control the comparison frequency related components (typically greater than 10), is by changing the damping and the ratio between α and p_1 , that is the quantity R required in the previous section. Notice that the final rolloff can be moved by a factor of 2:5 in frequency (trace D to A; giving an 8 dB improvement in the rejection), for the displayed values of α , ω and R. The improvement in the comparison frequency's harmonic rejection of trace D must be balanced against the relative lack of overshoot in trace A. Traces D and B have a smaller deviation in d/d (time delay) to those shown in traces C and A.

Conclusion

By examination of the loop analysis equations, we have been able to logically choose rational values for the loop parameters α , ω and R. These are seen to result in improved noise and time domain response characteristics for larger values of α and R for the same value of ω . These gains are made at the expense of the loop filter being able to reject comparison (or other) related energy which may be generated inside the loop.

AN-94

Part C: Using the NJ88C33 and its Demonstration Cards.

After a description of the measurement techniques used to assess the NJ88C33, an example of a stand alone application of the device to a 60 to 100 MHz phase-locked loop is given followed by a less detailed outline of its use with the SP8705 Prescaler IC. Although the set up procedure refers to the use of a purpose built NJ88C33 Programmer card, the instructions should be readily adaptable to any I²C Bus Programmer. Only an outline of the Programmer card is given here as it is anticipated that most users will have access to an I²C Bus programmer or be capable of generating the data streams required.

(a) Measuring Buffer Sensitivity, Phase Detector Gain and Dead-Band.

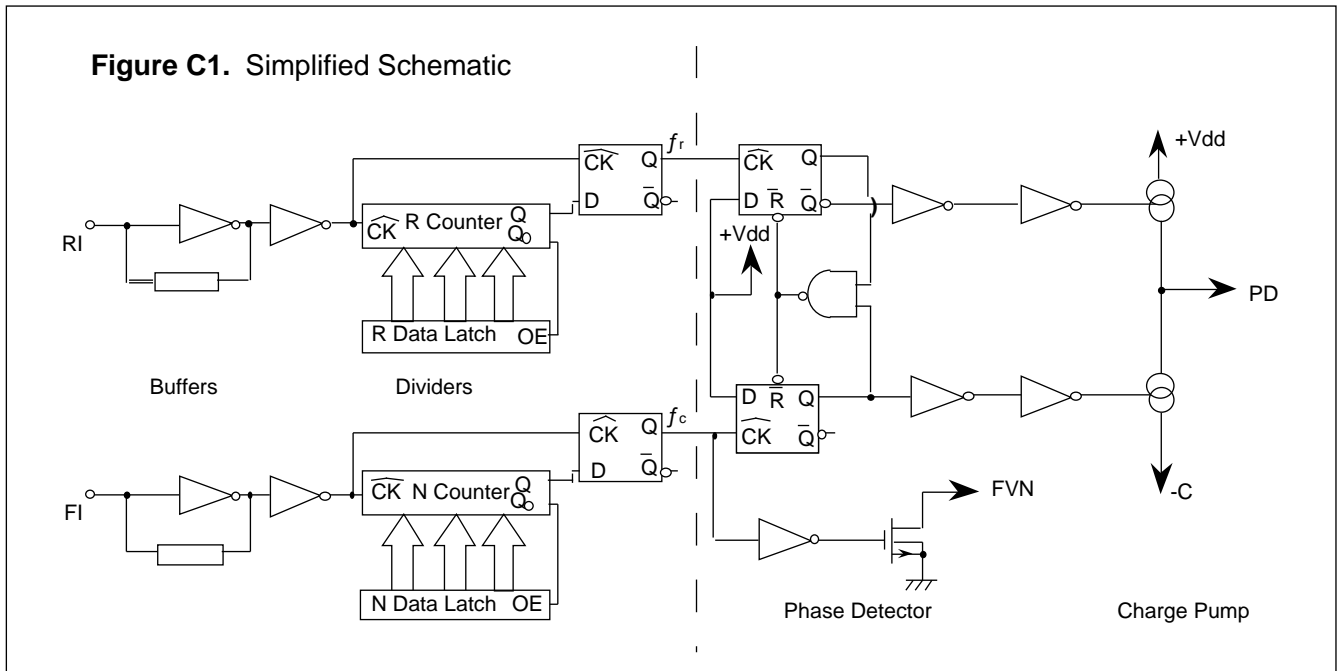
Before any design work for a PLL is to be done, some idea of the input operating conditions for the device must be sought: these will include the level of drive needed to exercise the buffer, divider and phase comparator chain correctly. Similarly, feed-through from the I²C Bus and its related PCB tracks will alter the levels required for correct operation from those given in the data sheet for a quiescent bus. Another consideration is the trade off between input isolation and drive level, both have a direct effect upon the phase noise contribution of the device and need to be decided before the loop parameters are chosen.

It is commonly thought that the buffer/divider sensitivity can be adequately measured by using a technique where the input and output waveforms of the divider are monitored by a frequency/period counter set to the ratio mode. The point at which the dividers cease to produce the programmed ratio is assumed to give their sensitivity. However it will be noticed in practice that any practical loop will fail to deliver this sensitivity for a "clean" phase lock. Under some dynamic conditions the input levels need to be as much as +20dB higher than the level given on the data sheets. So we see that a formal approach must be taken to clarify how the phase detector gain and buffer sensitivity measurement can be reliably assessed in a repeatable manner.

The measurement of the phase detector gain is relatively straight forward; intuitively, we simply have to induce an error of 2 (by stopping one or the other input) then measure the current from the PD pin. However problems can sometimes occur in the form of input noise (with the input shorted) or oscillations (with the input open circuited) produced at the input buffer of the disabled input. These reduce the "phase error" and therefore the apparent phase detector gain. A less error prone technique is proposed here, using "cycle slip". This method is a natural consequence of the buffer sensitivity measurement.

For most practical digital phase detectors, a "dead band" of operation appears due to the propagation time through the signal processing chain. Reference to Figure B2, showing the complete PLL system's loop in block form, should convince us that if the phase detector has a period over which it is inoperative, we will see an open loop system; that is, the feedback path via the phase detector has been isolated. Therefore no cancellation of noise can occur. This tends to allow noise to be injected into the loop, appearing at the output of the VCO with an characteristic due to the loop filter. To produce a high purity loop this deadband may be avoided by providing a small current offset at the charge pump outputs. If we know the dead band period, we can then estimate the maximum acceptable phase error at the phase detector, which in turn sets the maximum comparison frequency that we can use. Normally this will be well above the comparison frequency as determined by the channel frequency spacing. From the chosen comparison frequency and the loop's settle time requirements we decide the value of . Once this is known, we can extrapolate backwards from the output noise bandwidth (\pm) at the VCO output to a voltage on the VCO's control line via a knowledge of K_{VCO} , which we then use to derive the value of offset current from or to the loop filter. Practically this current either pulls or pushes the loop and holds the phase detector just out of its dead band. We produce this current into or from the loop filter by adding a small leakage path from the loop filter to either the C pin or the V_{dd} pin. This method accrues an advantage by enhancing the final settling trajectory of the loop, that is: it prevents the phase detector requiring the VCO's output to continually deviate with a sufficient depth (at an rate) to overcome the dead band, causing the close in phase noise mentioned above.

With these three measurements in mind, we should look at the operation of the phase detector to allow us to logically develop a test method. Given that a simplistic model of the phase detector is of the form of that given in the right hand half of Figure C1 (the phase detector has been drawn for the "+ PD" configuration) we see that the operation of the PD output will be in terms of $f_p = RI / R$, with $f_c = FI / N$, as follows.

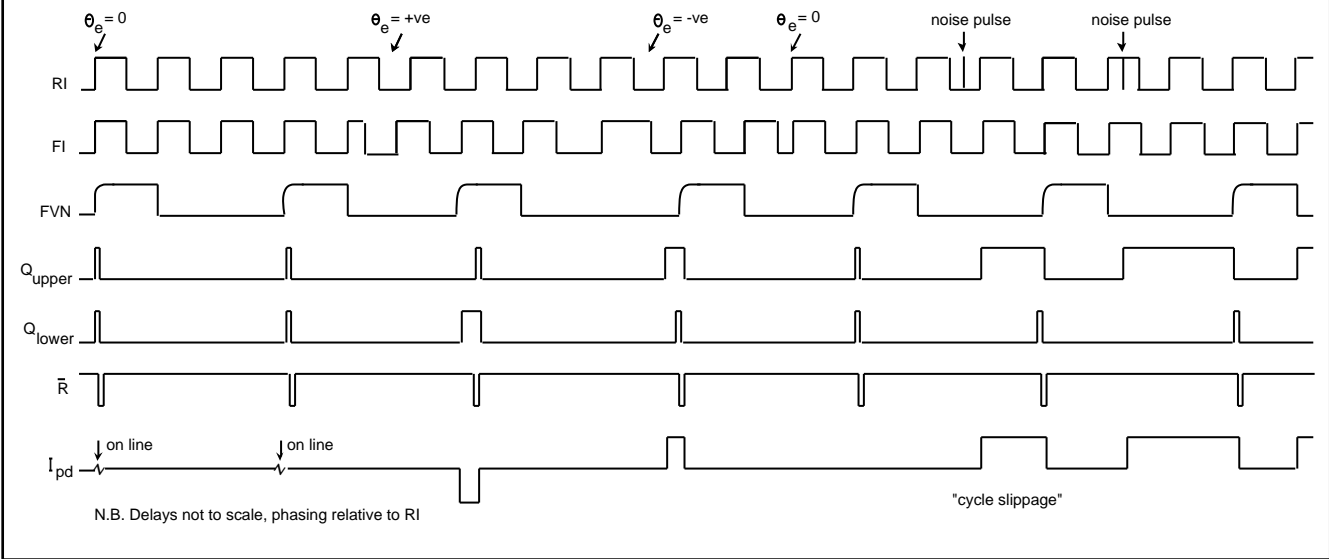


First we assume that $f_r = f_c$, where the rising edges of each train sets the Q outputs of the upper and lower flip-flops (in the phase detector) to the high state, thereby pulling the Not Reset lines low; such that the upper Not Q output then goes high, switching off the upper current source. Meanwhile the lower Q output goes low switching off the lower current source. Here we note that this constitutes the “zero” state for the phase detector and charge pump circuitry. That is, there is no phase error between the RI and FI inputs. This is the situation that we seek to reproduce in our test set-up.

It should be noticed that when $f_r = f_c$ and with FI and RI synchronised, the Not Reset lines to the flip-flops are toggled at the rate of f_r (or f_c) with a very narrow width pulse as determined by the clock-to-reset loop of the flip-flops. This pulse is prevented from arriving at the current sources due to the bandwidth limitation of the Q output buffers between the flip-flop outputs and the charge pumps. This results in a very small “dead band” of 2 to 3ns, where no output from either charge pump occurs. This limits the resolution that the phase detector can achieve near the zero phase error point. The propagation delay through the RI divider determines the delay of the PD output and is seen on the plotted measurements made later, as a shift of 1 ns on the plot towards the “FI leading the RI input”, the shift can appear on either side of the origin depending upon the batch, temperature and comparison frequency. Practically the dead band will appear as “close in” noise modulation. Any impulse energy present will cause the control voltage to “wobble” about inside the limits set by the dead band. The VCO output’s “noise bandwidth” becomes wider for higher comparison frequencies.

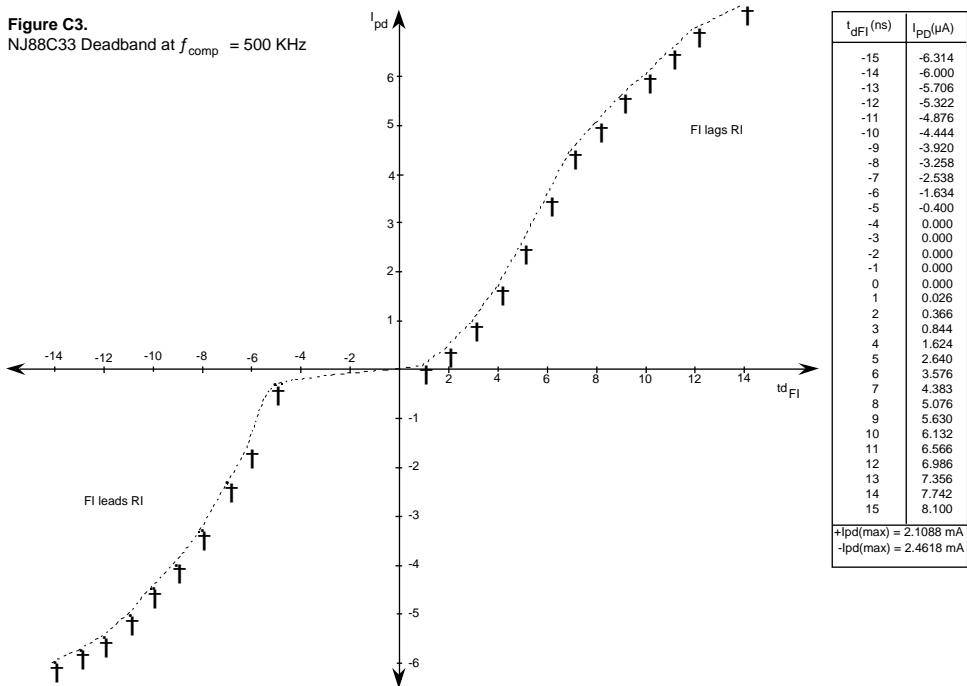
Notice that the flip flop inputs are triggered from the rising edges of the divider inputs by virtue of the fact that each divider chain is resynchronised at its output with that counter’s input clock (FI or RI) by clocking through the divider’s output with the buffered divider input. This can be seen in the left hand part of Figure C1. The function of each counter is completely independent of the other and is loaded from that counter’s latch at its own reset. That is: the change in count is synchronised with its own input which can be seen on the real device when the FVN output appears at the reset of the N counter and is one FI input cycle wide. The resynchronisation of the counters minimises the phase noise of the dividers due to noise on their transitions causing timing jitter. Normally the R counter remains at a static divide ratio and is unlikely to be reprogrammed in operation. However it can be checked at the PD output where it will initiate the positive charge pump output and terminate the negative charge pump output for each comparison frequency period when operated in the positive phase comparator mode. The zero state is shown on the left of Figure C2, where no current ($I_{PD} = 0$) appears at the PD pin. Notice that $R = N = 3$ for this example.

Figure C2.
Relative Phasing of RI, FI and PD



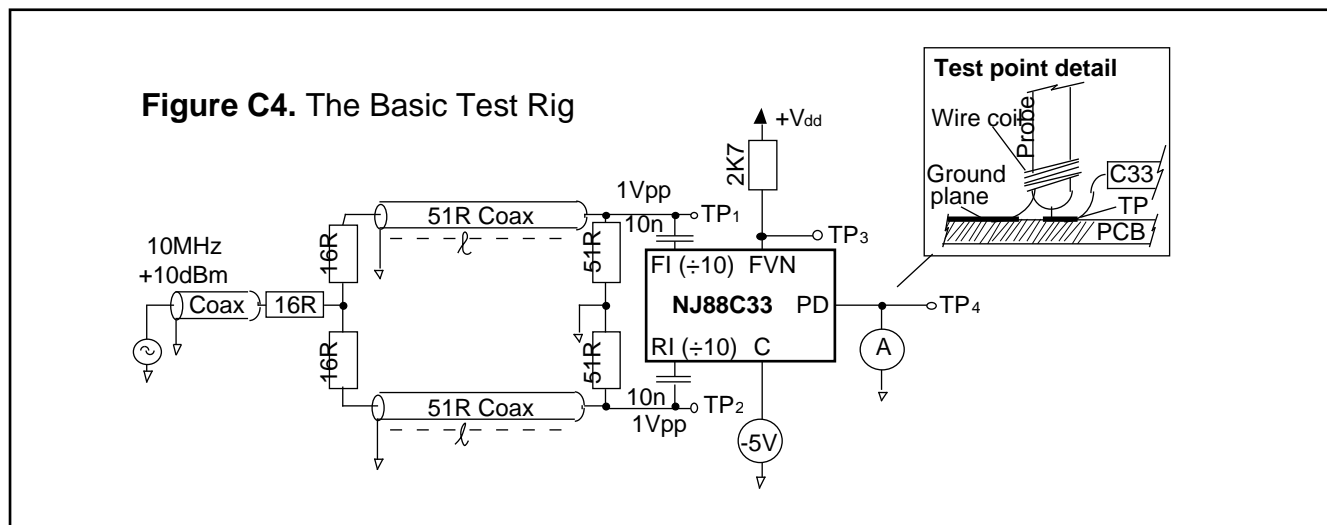
Now, consider when the rising edge of f_c leads the rising edge of f_r in time: the lower Q output is set high, with the negative current generator pumping current at the PD pin after a propagation delay time. At the arrival of the f_r rising edge the upper Q output asserts the Reset line. A propagation delay is seen at the leading and trailing edges of the output pulses, such that the charge pump output is linear in time across $\pm \pi$ to almost zero (f_c leads f_r) with a small delay of about 1 ns. A similar argument applies to the opposite condition where the rising edge of f_c lags f_r , except that f_r initiates the upper positive current source, indicating a lagging phase across zero to $-\pi$. Figure C3 shows part of the range near the origin for a typical device. The extremities of the plot are monotonically linear to ± 2 where the output current is $\pm I_{PD}$.

Figure C3.
NJ88C33 Deadband at $f_{comp} = 500$ KHz



The first quadrant (the upper right hand quarter) of Figure C3 represents the condition where the current out of the PD pin is positive when FI lags RI, the third quadrant represents $I_{PD} = -ve$ and FI leads RI. Notice that the horizontal ordinate is scaled in terms of the time delay from the RI input signal to the FI input signal which then produces the current shown on the vertical ordinate from the PD pin. The horizontal ordinate could be scaled in terms of phase (degrees or radians) provided it is referenced to the comparison period.

This would seem an appropriate point to consider how a test rig could be made to allow us to assess the functionality of the NJ88C33. The base requirement is shown in Figure C4. We use variants of this rig to condition the FI and RI inputs. Measurement of the input and output conditions are carried out easily since the device is operating “open loop”.



We see that the input to FI will be almost identical to the input to RI, provided the two coaxial cables to the FI and RI inputs are the same length (L) and loaded in an identical fashion, this ensures that the timing of the arrival of their input signals are identical, thus they maintain the same phase. Care must be taken over the positioning of the probes and even probe types. The probes to be used, should all be placed onto the same input to verify that they all display the same propagation times, up to 1.5ns difference has been noted even amongst “high quality” probes of the same type!

When powering up the above rig we will see a random output from the PD pin. If we programme the N and R counters for a count of ten we then see a one megahertz output at the PD pin with a random mark space ratio. There is a one in ten chance of the current being zero and a one in ten chance of it being at either a fixed positive or negative offset as determined by the programmed current and the shunt resistance of the ammeter on the PD pin. If we assume for a moment that we are lucky and the output is at zero current (the resets on the R and N counters are occurring coincidentally), we see that if we introduce a slight delay at one or other input by making that inputs coaxial cable longer, we can steer the PD’s output current. A train of output pulses with approximately the width of the delay time and a positive value, will appear at PD if the delay is introduced into the FI chain.

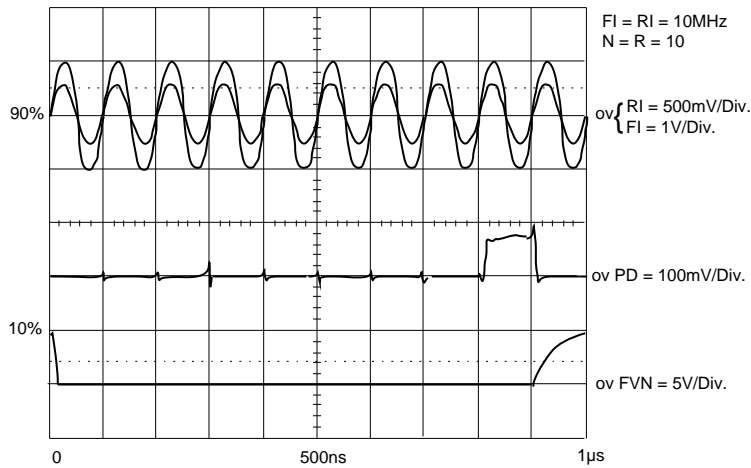
The problem of obtaining synchronism between the counter resets can be overcome by adding an extra pulse as seen in the right hand part of Figure C2. Notice that the addition of these extra pulses causes the PD output to slip back one RI period from the FVN rising edge. This situation is analogous to FI lagging RI by one third of a comparison period or -120° , which is of course one complete RI input period. However we usually restrict ourselves to considering phase errors in terms of the comparison period at the output of the PD pin. We use FVN to synchronise the waveforms as a matter of convenience, since the PD output is likely to disappear. These extra pulses are added by decreasing the input level to either RI or FI. It will be found that for any real device that when the input is reduced, any external interference or 1/f noise will appear to add extra pulses to the inputs. The presence of any impulse energy will add extra transitions to the slew rate limited edges of the input buffers when dealing with low level signals. This is overcome by either increasing the level or “squaring up” the edges of any low frequency inputs. These additional pulses result in a phase noise contribution at the output of the VCO due to the open loop forward gain from the phase detector output to the VCO output; the noise produced is the loop trying to cancel the FI input noise by modulating the VCO. RI input noise directly modulates the loop.

Variants of this test set-up give us some very convenient methods to measure: i) the buffer/ divider amplitude sensitivity, ii) the phase detector’s phase gain and iii) the phase detector’s dead band.

i) Measurement of Buffer Sensitivity.

By adding identical switched attenuators into the coaxial lines to FI and RI we can control the amplitude of each input independently. These two attenuators can then be operated in turn to find the point at which cycle slip occurs. To allow inspection of the pulse timings, a low divide value such as $R = N = 10$ is programmed in. We trigger an oscilloscope on the FVN output; provided the input delays are matched to better than one nanosecond, we will see that the PD output produces a positive output for a reduced level on RI. In Figure C5 we see where noise has produced one cycle slip on the R counter chain. Once such a slippage is produced, returning the input level back to its unattenuated value will lock the oscilloscope display indefinitely, that is: a permanent “phase error” of 36° is maintained due to cycle slip, not an actual input error.

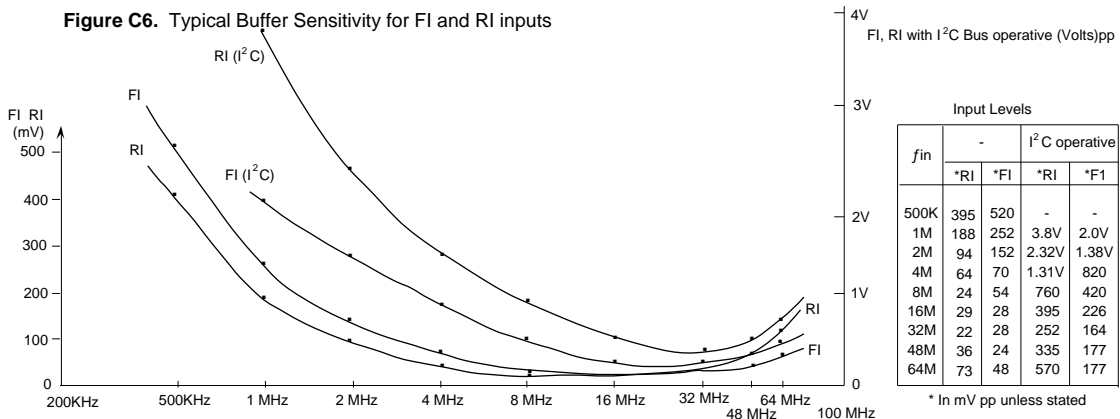
Figure C5. N588C33 FI, RI, FVN and PD relationships



The positive going pulse on PD represents a cycle slip of one RI period, its peak amplitude is about 68mV, being due to the current source's 625µA current being impressed upon the ammeter resistance. An accurate reading of the current is not possible from the scope trace since some error is introduced by the circuit parasitics. Addition of further pulses results in further slippage of the rising edge to the phase detector's output to the left of the above oscillogram. Reduction of the FI input will cause a negative PD cycle slip to start at the point at which FVN goes high at 900ns. A single cycle will terminate at 1000ns, a slippage of two cycles will cause the PD output to reappear at the start of the trace on the left of the oscillogram, terminating at 100ns. The addition of further FI pulses causes the PD output's rising edge to progress towards the right of the oscillogram until "roll-over" occurs, at which point the PD current returns to zero. At this point a comparison pulse "disappears" due to the zero PD current until the next comparison period.

Now, by decreasing the amplitude of the input signals, we reduce the dv/dt of the input waveform such that the input waveform reaches the threshold point of the internal logic at a later time during that input waveforms period; that is, we introduce a progressive delay. This effect exacerbates the phase modulation effect of the cycle slip despite having an exact balance in the frequency and phase of the input signals. It will be seen that when this cycle slip is occurring, the repetition rate of the comparison period remains the same and in direct proportion to the FI/N and RI/R ratios. If an edge detecting type of frequency counter is used to check the divider sensitivity, we see the programmed ratios and assume that the dividers are functioning correctly; the cycle slip is completely missed due to the averaging of the counter. No indication of the problem appears until the cycle slip has reached a point where it has exceeded the division ratio; such that the missing pulses start occurring with a higher frequency than the count repetition rate of the counter. The problem is worse for higher divide ratios, since more cycle slips are required before the division frequency alters due to the missing pulses. The overall effect is to give a false impression of the devices sensitivity.

Figure C6. Typical Buffer Sensitivity for FI and RI inputs



Practically we need to decide upon a minimum number of cycle slips per second, then measure the sensitivity required for that number of slippages. This is the level to be designed for. One slip per second seems sensible for most applications; giving a level of some +7dB above that indicated in the data sheets for a clean lock where no further decrease in the noise floor can be attained for an increase in FI or RI input level. The figure increases to +20dB for applications where the I²C Bus is to be operational continuously. The sensitivity based on this criteria is plotted in Figure C6 for a typical device. The effects of slew rate limiting can be seen to the left of the plots below about 8MHz with the sensitivity falling above about 50MHz. The upper traces are when the I²C Bus is operative.

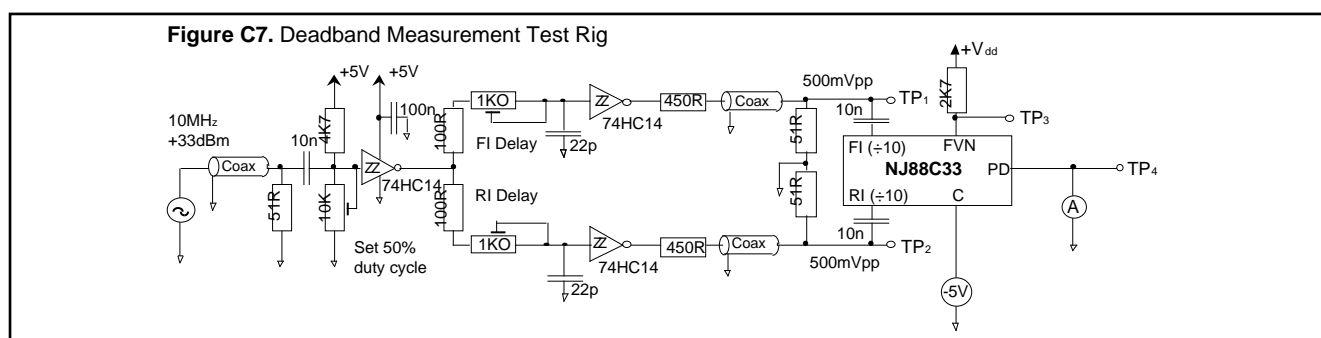
ii) Measurement of Phase Detector Gain.

The condition at which a finite cycle slip exists is an interesting one, since it allows us to make an accurate measurement of the phase detector gain, K_{pd} ; we can then see how K_{pd} varies with comparison frequency. If we reduce the input level of RI, we can choose any integer multiple (of the input frequencies period) of cycles offset between the RI and FI resets. This allows us to choose the mark space ratio of the phase detector's output period. If the integer is made to be exactly half the R and N counter values ($R = N$), we can then scale the integrated current measured by the ammeter at TP4, by two to obtain the value of K_{pd} per cycle of comparison frequency. K_{pd} can be obtained at other values of mark to space ratios but it will be found that a progressive error occurs near the extremes due to a finite settling of the current sources and the integration of the test rig/ meter combination. Strictly speaking the average of the magnitudes for the positive and negative currents should be used as the value of K_{pd} in loop calculations. The measurements carried out here are done with a comparison frequency of 1MHz which represents the practical maximum frequency that can be used since the negative current source runs into speed problems due to its extra level changing circuitry: this can be seen in Figure C10 where the positive and negative current sources are no longer equal to their DC values (as in the data sheet) to which they were trimmed at manufacture.

Notice that with appropriate scaling of the division ratios, this test method can be applied to other PLL synthesiser ICs which use a different type of phase detection scheme; for example the sample and hold, voltage source output of the NJ882X series of Synthesiser ICs.

iii) Measurement of Dead band Time.

An adaption of the principle used to measure buffer sensitivity and phase detector gain can be used to measure the transition from $-I_{PD}$ to $+I_{PD}$ when we change FI leading RI to FI lagging RI. To minimise error in the measurement due to the dv/dt of the input signals and to give an "infinite" resolution to the required time delays, we resort to generating the necessary signals "digitally" with the following set-up as in Figure C7.



Notice that the points TP1 and TP2 are direct coupled to the 51R resistors before the decoupling capacitors to prevent any timing errors in the measurement due to DC shifts moving the trigger point when the mark to space ratios of the driving waveforms becomes asymmetric. This would result in a characteristic "S" shape and a shift in the required transfer function (between I_{PD} and the time delay between RI and FI).

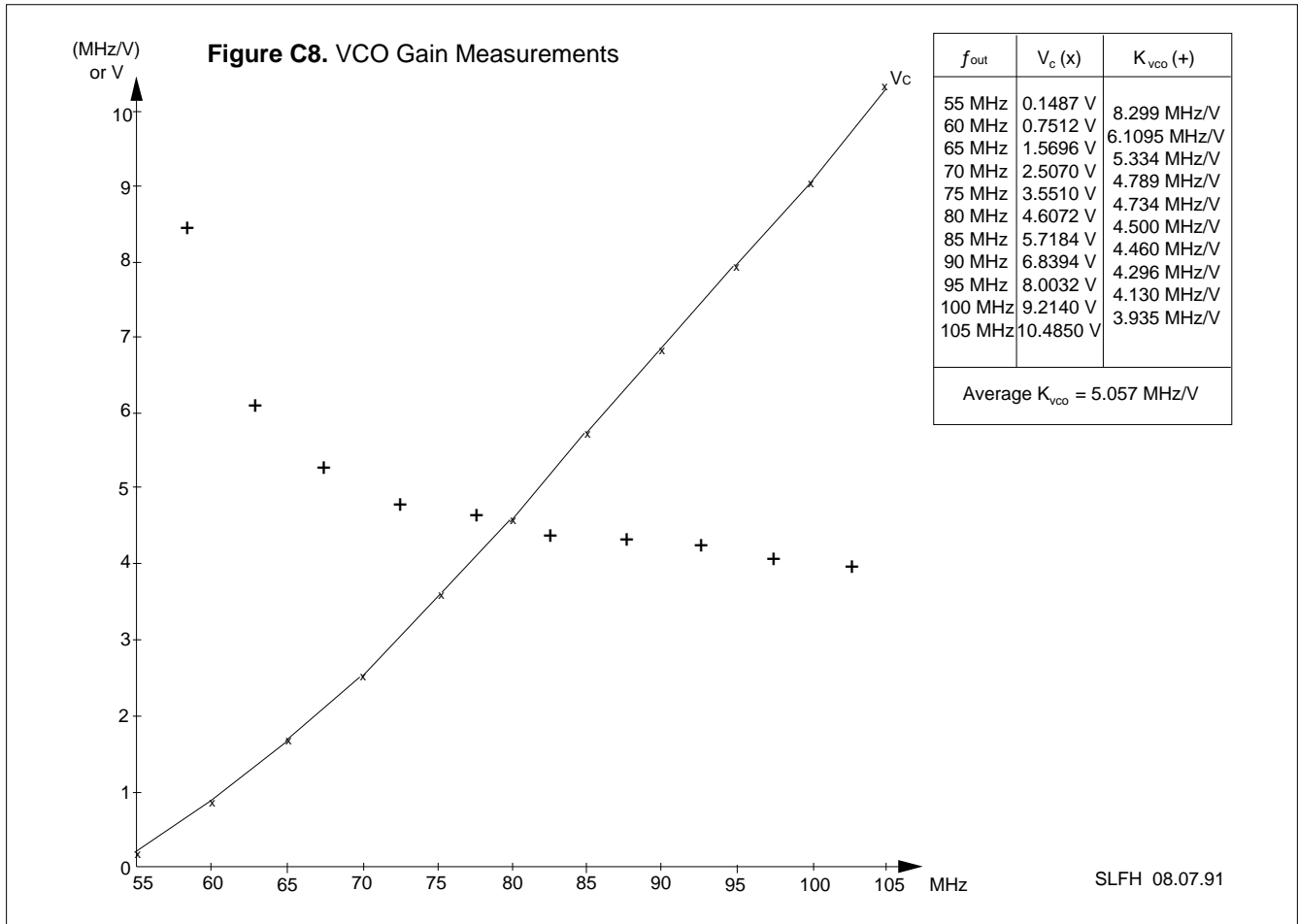
Once the test rig is set up, the two variable resistors are adjusted to give minimum delay at the FI and RI inputs (TP1 and TP2) with respect to the input signal, that is: the 1KΩ pots are set to zero. At power-up, a cycle slippage at the PD output will probably be seen. This can be overcome by disturbing one of the delays momentarily by shorting its 22pF capacitor to ground, repeat until a low value of current is indicated on the ammeter (typically a few nA). Plotting the dead band is simply a matter of introducing a progressive delay into the FI chain, then read off the integrated current at the ammeter and a delay in the RI chain with the FI delay at a minimum value, to plot the negative current. A plot like the one in Figure C3 can then be produced. For the values shown the test rig will give a range of approximately ± 25 ns. The deadband measured here represents less than a one degree error for the one megahertz comparison frequency used.

Foot Note.

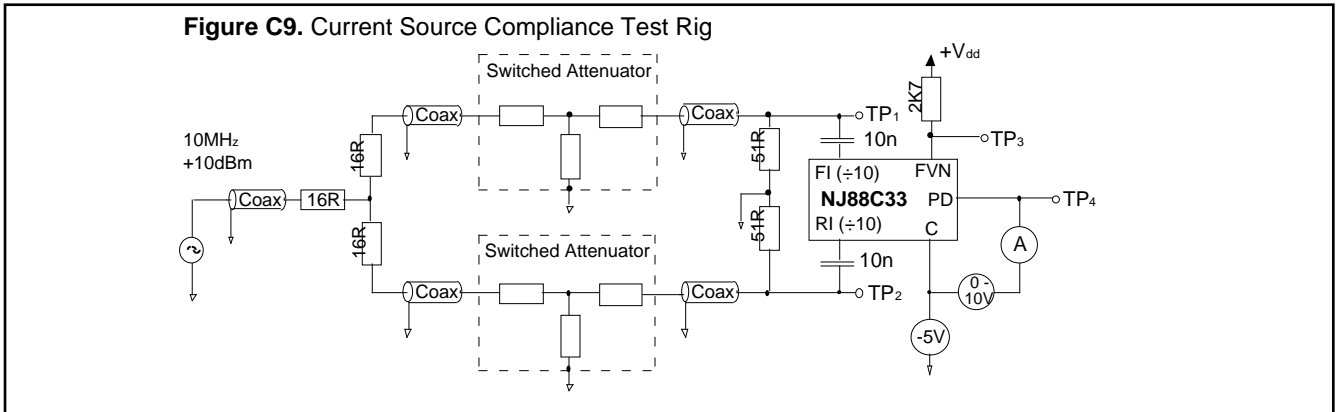
There is a constraint to the low frequency sensitivity measurement: slew rate. This can be derived from the rate of change in voltage for a sine wave input signal and is calculated as the derivative of the sine wave at its zero crossing point. Simply stated, this is the peak voltage times the radian frequency, normally in terms of Volts per microsecond. By direct coupling the inputs, then limiting the rise time, this measurement is found to be slightly less than a $1V/\mu s$ minimum. Thus the minimum edge speed for a logic input to the NJ88C33 dividers should be faster than $3\mu s$ rise time for a 4.5V logic input to RI or FI. This means that at a point of around 8MHz a decreasing sensitivity for a decrease in frequency will be seen. For AC coupling at low frequencies and voltages, the input signals will need "squaring up". If the slew rate criteria is preserved, the basic sensitivities measured above 8MHz will be preserved down to the cut-off of the capacitive coupling at the inputs. When direct coupled the NJ88C33 will operate with a full ground to V_{dd} logic swing right down to DC, making it suitable for applications such as video clock generators locked to a sync pulse derived from an incoming video signal.

(b) Generating the Loop Component Values.

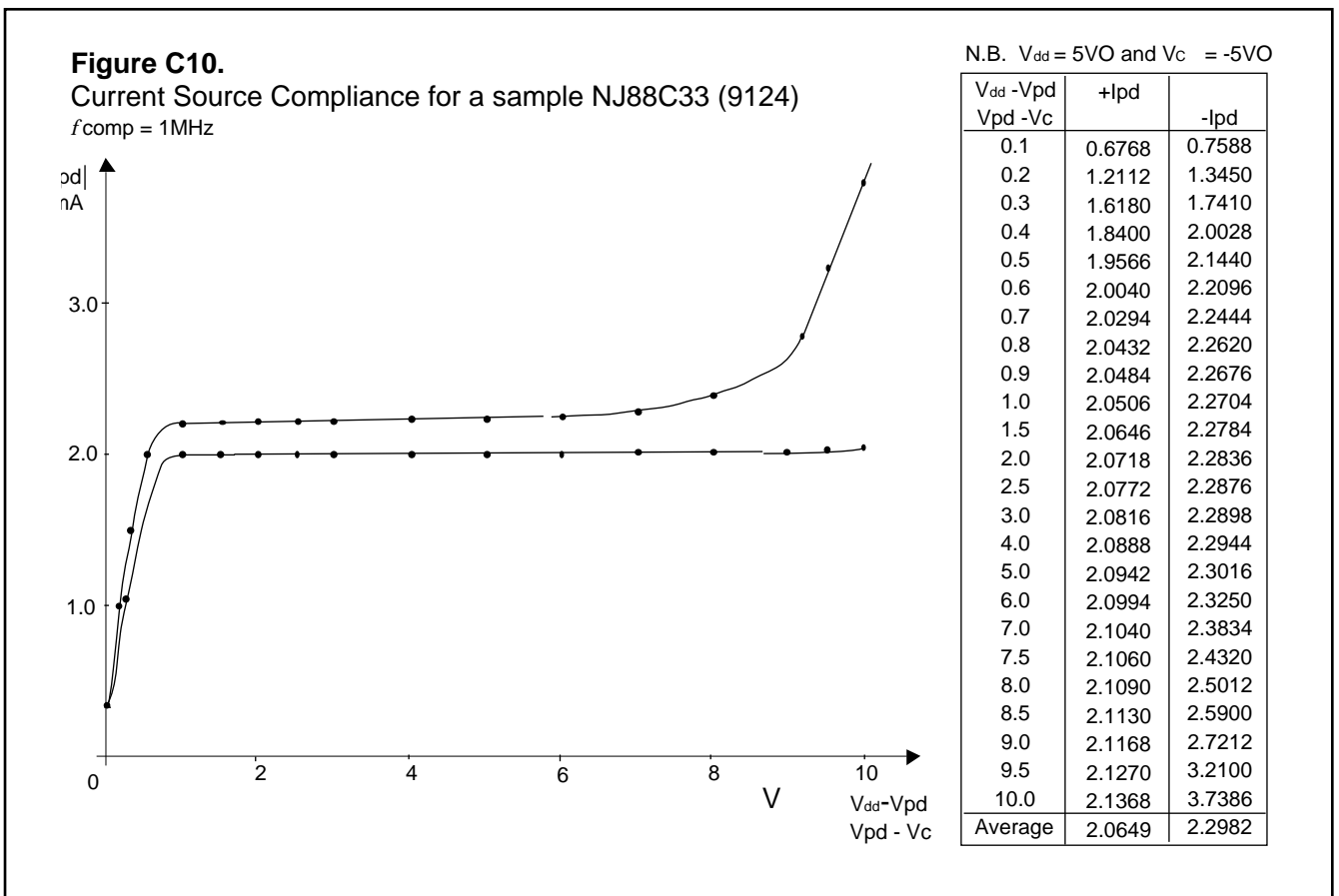
Referring back to Equations B20, B21 and B22, we see that we need to measure, estimate or otherwise find the value of K_{VCO} . For a proprietary device this will be given on the data sheet as a sensitivity in Hz per volt as determined by the change in output frequency for a change in control voltage. Since a VCO will behave as an integrator, this “gain” will be a dynamic value. That is: an offset (or constant of integration) exists in the circuit such that a finite frequency offset will be apparent in the device when a static voltage is applied to the control line. When this is changed to another static voltage, a different frequency output will be seen consisting of the offset from zero frequency, plus the dynamic frequency change per unit of voltage input. To illustrate the point, Figure C8 shows the voltage sensitivity of a typical application board VCO in terms of output frequency against input control voltage. The application board will be dealt with later.



Note that the average dynamic gain for a practical VCO changes according to which part of the curve the control voltage V_c is situated at. An average K_{VCO} for the evaluation card’s VCO would be 5MHz/V, as averaged for a sample of ten units as used here. A reasonably constant gain is maintained across a V_c range of 1.5 to 8.5 volts; the precise value of the static voltage on the control line will be determined by temperature and supply voltage to the VCO circuitry as well as the feedback mechanism of the loop, once closed. The control voltage is measured with respect to the C pin which generates an approximate - 4.7Volt output for a V_{dd} of 5.5Volts. The variability of V_c and K_{VCO} will affect the operation of the closed loop, so must be chosen with care, in order to maintain a good dynamic stability (where V_c and K_{VCO} remain constant) for each discrete value of output frequency. One other factor will have an effect upon the loop in a similar manner: the variability of K_{pD} with V_c , that is: the current sources’ compliance. The measurement of this is relatively straight forward, if we use a modified form of the test rig shown in Figure C4 where we connect a 0 to 10 volt supply between the C pin and the ammeter. This allows us to initiate a positive cycle slip by reducing the input level to the RI input, returning the level to $1V_{pp}$ to hold this value. We then vary the additional power supply across 10 to 0 Volts, to produce the data required to plot a curve for the positive current source’s output current ($+ I_{pD}$) verses its compliance voltage ($V_{dd} - V_{pD}$). The complete test set-up is shown in Figure C9.

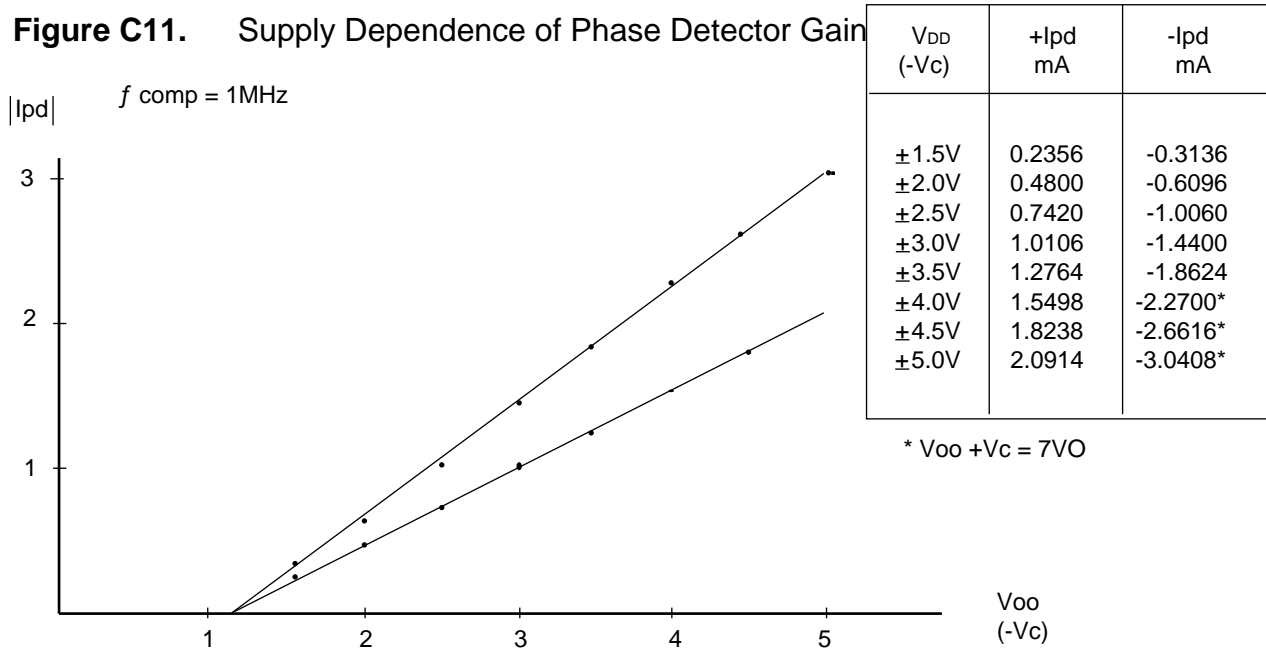


Collating the data from this test gives the following plot in Figure C10. We see that the current for the negative current source deviates appreciably for a compliance voltage above nine volts across that source; this is process related. Considering that the Voltage doubler gives approximately -4.3 volts output at the C pin for a +5V input to V_{dd} , this deviation from a constant will be academic since the usable range for these voltages will be in the region of 0.5V to 8.8V. What is of interest, is the mismatch between the two current sources due to the limited response of their drivers at a comparison frequency of 1MHz. The matching improves as the comparison frequency is decreased. Notice that the acceptance band for $|I_{PD}|$ is nominally from 1.9mA to 3.1mA, a tolerance of $\pm 24\%$. However the specific performance for an individual device across 0.5V to 7.5V will be excellent, with the average K_{pd} across that range for this device being 2.182mA per cycle of the comparison period (347.2 μ A/radian).



There exists one further factor that influences the design parameters: the supply voltage dependency of the phase detector's gain. To test this, we use the test rig in Figure C9, reconnect the ammeter to ground, remove the extra 0 to 10 Volt supply, then adjust the negative five Volt supply to match the V_{dd} supply (use a tracking supply). The result of this test is shown in Figure C11.

Figure C11. Supply Dependence of Phase Detector Gain



As we already know from Figure C10, the change in K_{pd} is virtually independent of any change in V_{PD} , within the limits already set. Note that the last three measurements made for the negative current source are made with seven volts between V_{dd} and the C output pin to minimise the break down effect seen in Figure C10. Therefore any change in $|I_{PD}|$ in Figure C11 will be a consequence of the incremental change in V_{dd} . This is due to the internal current setting resistors being connected from the ground to a current mirror on the V_{dd} line, hence we see the lines plotted for the current source magnitudes terminating at 1.1 Volts, i.e: at this point V_t is 0.8 to 0.9Volts (where no current flows across the current setting resistor), so the offset voltage is made up from a V_t plus the resistor bias for the current sources, V_t is the MOSFET threshold voltage. The actual value of K_{pd} is the average of the two current sources' magnitudes, here it is seen to be 2.567mA per cycle of the comparison period.

The overall conclusion being that a stable supply must be provided. We see that the dependence of K_{pd} is almost directly a function of $V_{dd} - V_t$, having important ramifications upon the final phase noise performance of the completed loop implementation; any noise upon the supply line will modulate the phase detector gain; use a clean well regulated and decoupled supply for the PLL IC. Ensure that the decoupling capacitors used at the supply line are "low K" ceramic types, or better still the polystyrene or polyester types to minimise microphonics from causing modulation of the supply line and hence the loop.

So, we now have all the information we need to implement a practical loop. First we pick an output frequency at which we shall evaluate the loop's performance, say around the middle of the control range for the VCO. We need to be aware that an assessment should be carried out at the extremes of the anticipated output frequency range with the appropriate values of VCO and phase detector gains as previously measured. The deviation of these values may have two effects: instability in the form of increased ringing due to decreased damping or increased the settle time.

Keeping these effects in mind, we choose a value for K_{pd} of 2.5 mA per cycle of the comparison period and a value for K_{VCO} of 5.0 MHz per Volt variation of the control line. Recalling Equation B15 (or A(xi) from Appendix A) we calculate the value of from the settle time (t_s) requirement; the value of and , when using this equation, are scaled for a second order loop, but give us a good starting point for deciding the loop parameters. For example, if we need to step 1MHz and settle to within 100 Hz of the final frequency in 4.15 ms we have an error ratio () of 100ppm. The loop natural frequency is calculated as follows:

$$= \frac{-\ln}{t_s}$$

$$\begin{aligned}
 &= \frac{-\ln(100\mu)}{4m15 \cdot 0.7071} \\
 &= 3K1386 \text{ radians/s (500Hz)}
 \end{aligned}$$

Using Equation B20 and deciding upon an output frequency from the VCO of 70MHz with a comparison frequency of 50KHz, choose the ratio of the real pole ω_0 to be six times higher in frequency, that is $R = 6$, we then determine the value of C_1 as being:

$$\begin{aligned}
 C_1 &= \frac{K_{vco} K_{pd}}{N^2 (1 + 2R)} \\
 &= \frac{5M0 \cdot 2m5}{1K4 \cdot 3K1386^2 \cdot (1 + 2 \cdot 0.7071 \cdot 6)} \\
 &= 95n556
 \end{aligned}$$

We use Equation B21 to find the value of the time constant formed by C_2 and R_2 :

$$\begin{aligned}
 T_2 &= 1 / (R + 2 / \omega_0) \\
 &= 1 / (3K1386 \cdot 6) + (2 \cdot 0.7071) / 3K1386 \\
 &= 503\mu69
 \end{aligned}$$

Then we use Equation B22 to find the ratio of C_1 to C_2 :

$$\begin{aligned}
 C_2 / C_1 &= (2 + R) T_2 - 1 \\
 &= 3K1386 (2 \cdot 0.7071 + 6) 503m69 - 1 \\
 &= 10.721
 \end{aligned}$$

Such that $C_2 = 1\mu0245$ and $R_2 = 491R67$. Since these are not standard values we choose the nearest being: $C_1 = 100n$, $C_2 = 1m0$ and $R_2 = 470R$. These are the values to be found on the 60 to 100 MHz Evaluation cards. Using Equations B23 and B24 we find that these component values nominally result in:

$$\omega_0 = \left[\frac{K_{vco} K_{pd}}{N C_1 (1 + 2R)} \right]^{1/2} = 3K0681 \text{ radians/s (488Hz)}$$

$$\text{and: } \omega_0 = (T_2 - 1/R) / 2 = 0.63766$$

We now have all the information we need to implement a practical loop: the input drive requirement, the output filter requirement and the values of the components. Next, we shall look at drawing these together to produce the Evaluation Cards, then we shall return to making measurements on them to see how close the theory comes to practice.

(c) The Practical Implementation of the Loop.

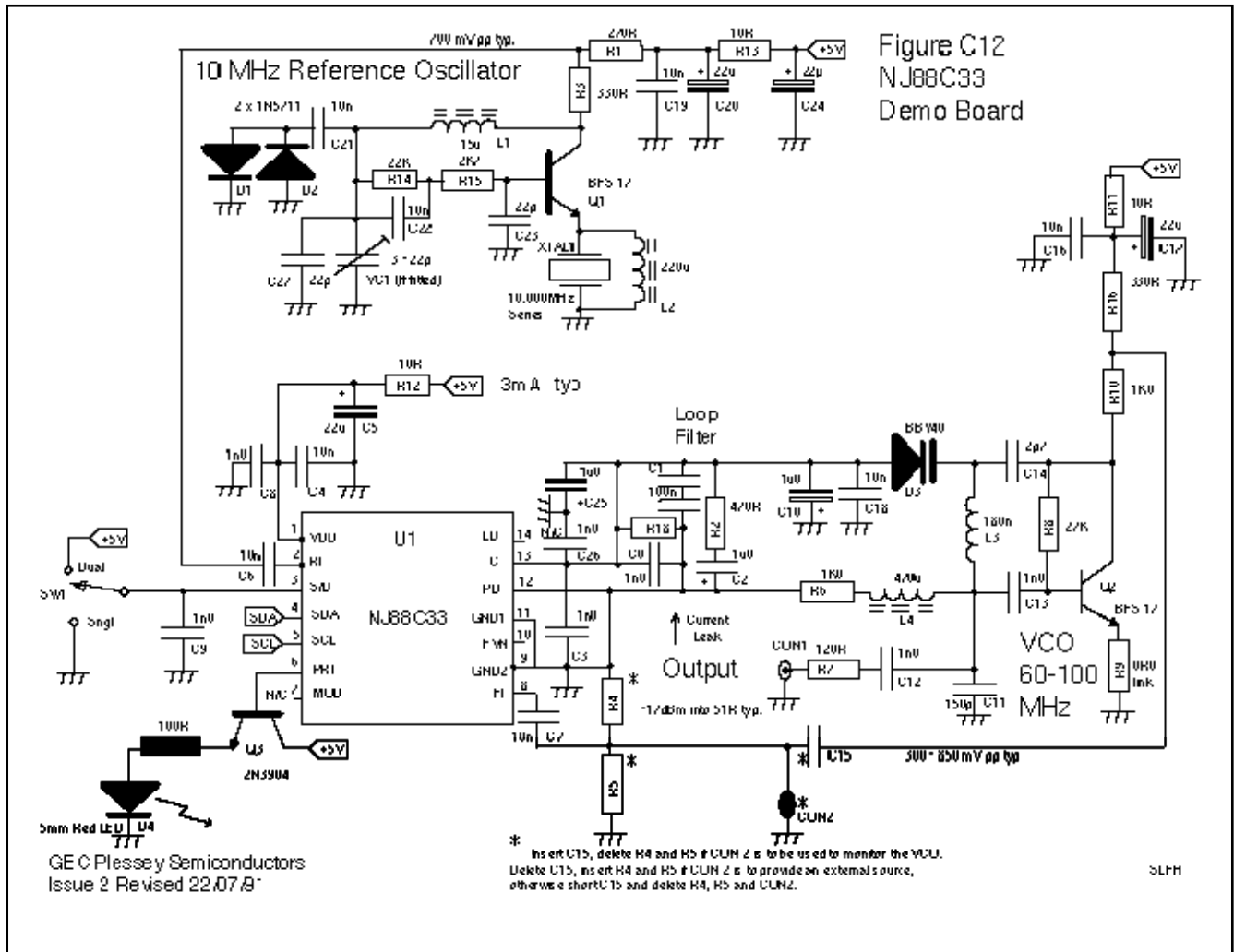
The NJ88C33 contains two divider chains, a phase comparator and a voltage doubler, along with the necessary I²C Bus interfacing circuitry. To complete a synthesiser loop an external frequency reference, voltage controlled oscillator and loop filter must be provided. These have been implemented in the Issue 2 Evaluation Card, with its schematic shown in Figure C12. For synthesizers operating at higher frequencies, operation with the SP8705 is recommended. Details of the Issue 7 Evaluation card using these two devices is given later in this section, with its schematic shown in Figure C14. A brief description of the cards follows, before we return to the measurement of the loop's transients.

i) The Issue 2 Evaluation Card.

To be able to demonstrate the major features of the NJ88C33, the VCO operates near the device's maximum rated input frequency for the N divider. The voltage doubler output has been utilised to generate a nominal minus three volt supply, when $V_{dd} = 3.5V$ or less, to bias the VCO varicap diode. Heavy decoupling of this rail must be provided to minimise reference related frequencies from breaking through the loop filter, as this is aggravated by poor common-mode rejection in the VCO. The oscillator configurations have been chosen to minimise the effects of power supply variations.

The VCO is a loosely coupled inversion oscillator with a resonant circuit Q approaching that of the varicap diode, indicating that this device, rather than any other part of the circuit, limits the phase noise performance of the PLL. The VCO will tune across one octave for approximately a ten volt change in the control voltage. This range gives a large VCO gain (4-6MHz/V) requiring particular care in layout of the printed circuit board if excessive sideband energy is to be avoided. The centre frequency of the VCO can be decreased by changing the resonant circuits inductor to a larger value.

An emitter coupled oscillator is used to generate the reference frequency. Its crystal is operated in a series resonant mode (with a crystal series resistance of less than 30R) to avoid the need for holder capacitance compensation and problems related to changes in the active device's temperature. Two schottky diodes have been used to limit the crystal drive to approximately 3-5mW, ensuring a tolerant circuit suited to a wide range of crystal types. Some frequency adjustment can be effected by adding a small capacitance to the junction of C_{22} , R_{14} and R_{15} (to ground). Overtone crystals can be used providing L_2 is adjusted to null out the resonance resulting from the holder's capacitance with the crystal's fundamental motional inductance, as the NJ88C33 will accept up to a 50MHz reference frequency. "Parallel" resonant crystals can be used, but will operate at the series resonant point, which is lower than the marked value.



The loop filter is a second order combination of C_1 across $R_2 + 1/sC_2$ with the VCO integration adding a third order term. The loop filter is then pumped by either the positive or negative current source in the phase detector. The pumping action is produced by the discrete pulses from the PD output being integrated by the loop filter as the phase comparator samples the output from the N-counter at a rate determined by the R-counter output (at f_{comp}). There are pulses on the loop filter due to the PD output replenishing the charge on the loop filter's capacitors. This effect is utilised to minimise the effects of the deadband by use of a deliberate leakage path as explained in the next section, after we have dealt with the loop transient measurements. The phase detector output and the loop filter capacitors should be treated as a very sensitive sample and hold system.

Loop characteristics are dominated by the choice of filter component value; being a compromise between a fast settle time for a high gain VCO, (with a high loop natural frequency and a high comparison frequency), or a low gain "quiet" VCO to give reduced output sideband energy. The first approach being suited to "digital" modulation by altering the divider ratios, the second for "analogue" modulation summed into the VCO's control input. To reduce the spurious radiation from the NJ88C33's dividers, both inputs are driven from a low source impedance. Any length of line to these inputs should display this same impedance (use pcb microstrips) to prevent input buffer instabilities resulting from uncontrolled high input impedance; the buffers must be driven from a source of less than 1K Ω to assure unconditional stability. The edge rise times of the dividers will provide energy well up into the gigahertz range, as do the edge currents from the charge pump. The line impedances and ground return paths must be well controlled to prevent excessive side product generation in the completed system. The recommended layout for the 'C33 is given in Figure C13. A parts list for the Issue 2 Evaluation card follows that figure.

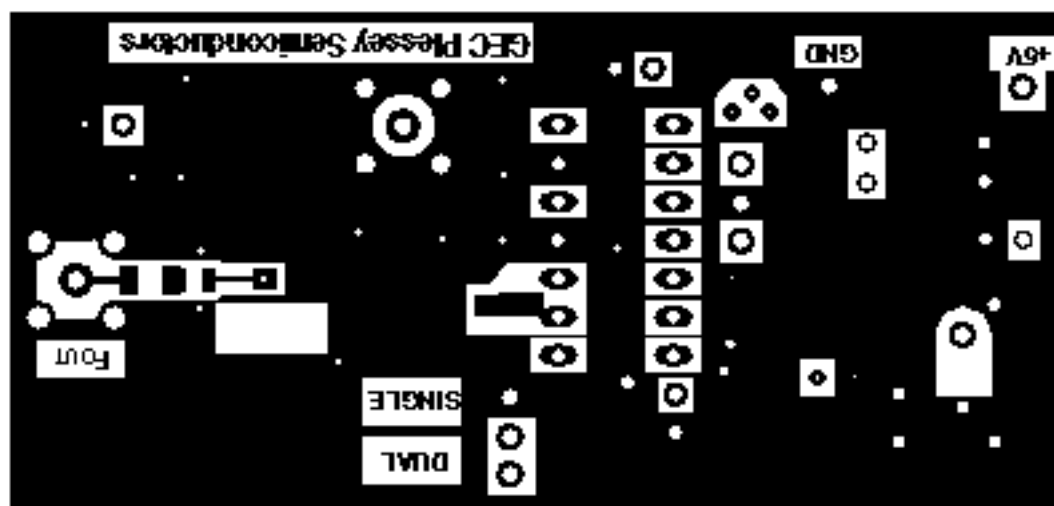
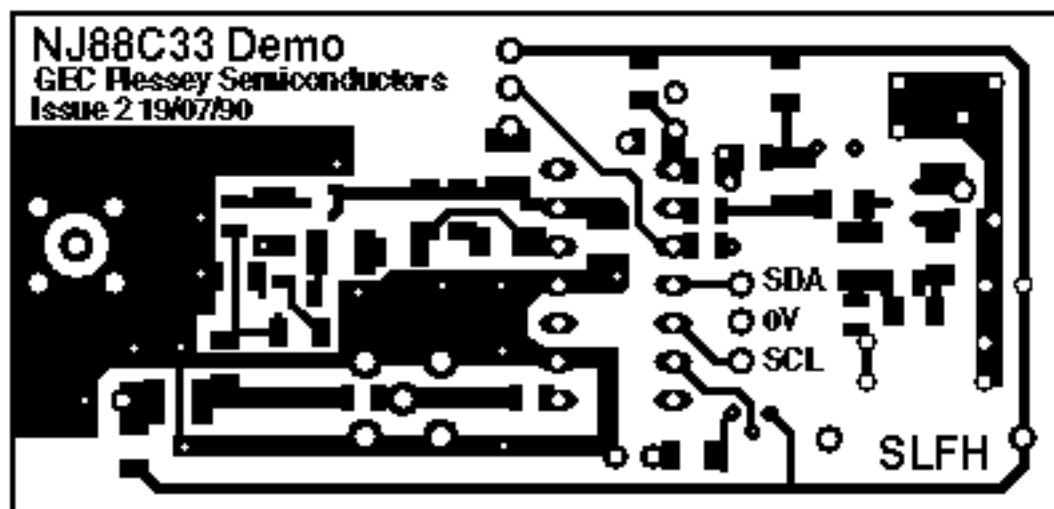


Fig. C13-1 Track and groundplane layout for the NJ88C33 demonstration board, scale 2x actual

AN-94**C33ISS2 EVALUATION CARD: PARTS LIST.**

Revised 20-08-91 SLFH

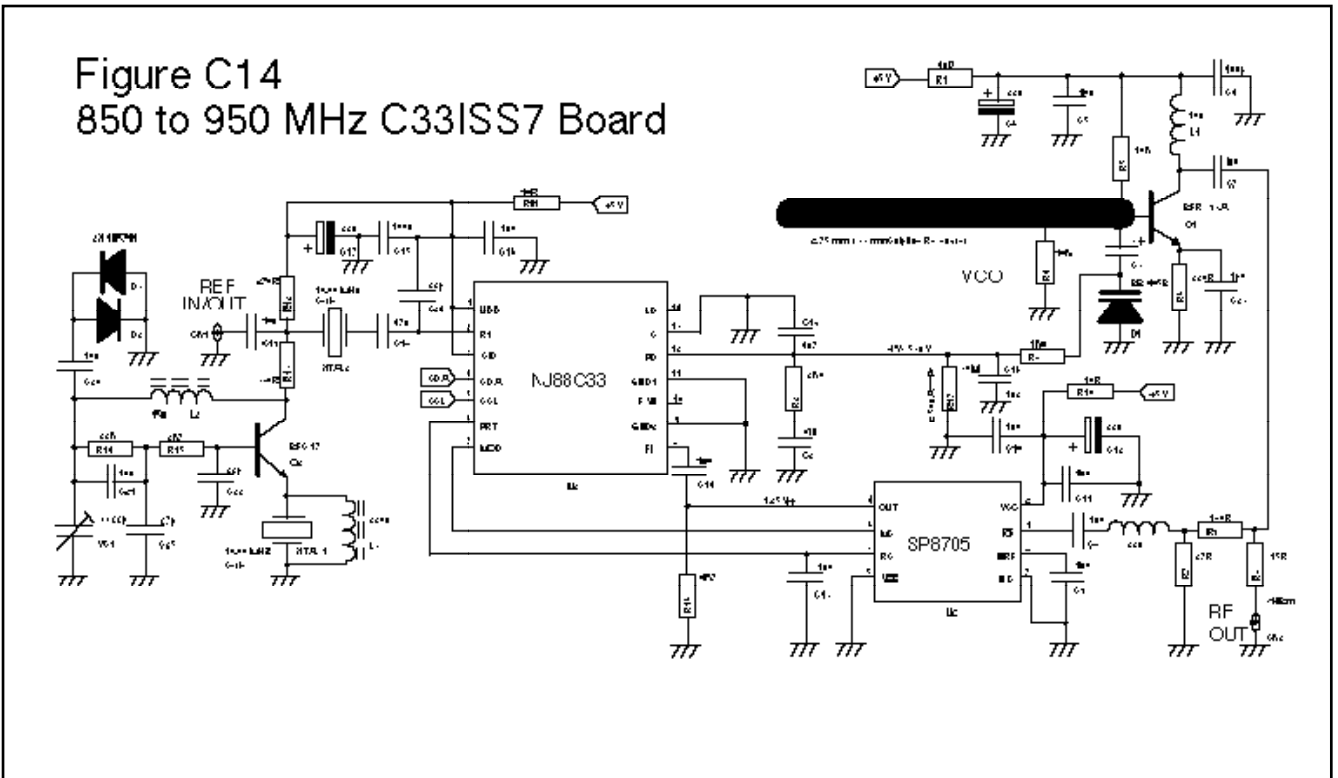
Board Reference	Component Type	Library Symbol
C0	1n0/X7R 10%	SMD0805
C1	100n/X7R 10%	SMD1206
C2	1u0/tant.	SMD1206
C3	1n0/NPO 10%	SMD1210
C4	10n/X7R 10%	SMD0805
C5	22u/35V electro.	RADIAL2.5x6.3
C6	10n/X7R 10%	SMD0805
C7	1n0/X7R 10%	SMD0805
C8	1n0/X7R 10%	SMD0805
C9	1n0/X7R 10%	SMD0805
C10	1u0/35V Tant	SMD1210
C11	150p/NPO 5%	SMD0805
C12	1n0/X7R 10%	SMD0805
C13	1n0/X7R 10%	SMD0805
C14	2p7/NPO 0p5	SMD0805
C15	10n/X7R 10%	SMD0805
C16	10n/X7R 10%	SMD0805
C17	22u/35V electro.	RADIAL2.5x6.3
C18	10n/X7R 10%	SMD0805
C19	10n/X7R 10%	SMD0805
C20	22u/35V electro.	RADIAL2.5x6.3
C21	10n/X7R 10%	SMD0805
C22	10n/X7R 10%	SMD0805
C23	22p/NPO 5%	SMD0805
C24	22u/35V electro.	RADIAL2.5x6.3
C25	1u0/35V Tant.	SMD1210
C26	10n/X7R 10%	SMD1206
C27	22p/NPO 5%	SMD0805
VC1	3p5-22p	Trimcap
R1	270R/0.25W 2%	SMD1206
R2	470R/0.25W 2%	SMD1206
R3	330R/0.25W 2%	SMD1206
R4	100R/0.25W 2%	SMD1206
R5	100R/0.25W 2%	SMD1206
R6	1K0 /0.25W 2%	SMD1206
R7	120R/0.25W 2%	SMD1206
R8	27K /0.25W 2%	SMD1206
R9	0R0 /link	SMD1206
R10	1K0 /0.25W 2%	SMD1206
R11	10R /0.25W 2%	SMD1206
R12	10R /0.25W 2%	SMD1206
R13	10R /0.25W 2%	SMD1206
R14	22K /0.25W 2%	SMD1206
R15	2K7 /0.25W 2%	SMD1206
R16	330R/0.25W 2%	SMD1206
R17	100R/0.25W 2%	SMD1206
R18	33M /0.5W 10%	
L1	15u 10%	SMD1210
L2	220u 10%	SMD1210
L3	180n 20%	SMD1210
L4	470u 10%	SMD1210
D1	1N6263 schottky	DO-35
D2	1N6263 schottky	DO-35
D3	BBY40 varicap	SOT-23
D4	5mm Red LED	LED0.25

Q1	BFS17 RF NPN	SOT-23
Q2	BFS17 RF NPN	SOT-23
Q3	2N3904 Switching	TO-92
U1	NJ88C33	
P1-P2	1mm pins	
P3-P5	0.1" 3 way header	SPCO
XTAL1	10.00MHz Series	HC-43/U
SW1	0.1" 3 way header	SPCO
LINK	0.1" Jumper	
CON1	SMC socket	SMPCPB
CON2	SMC socket	SMPCPB
PCB	C33ISS2	

ii) The Issue 7 Evaluation Card.

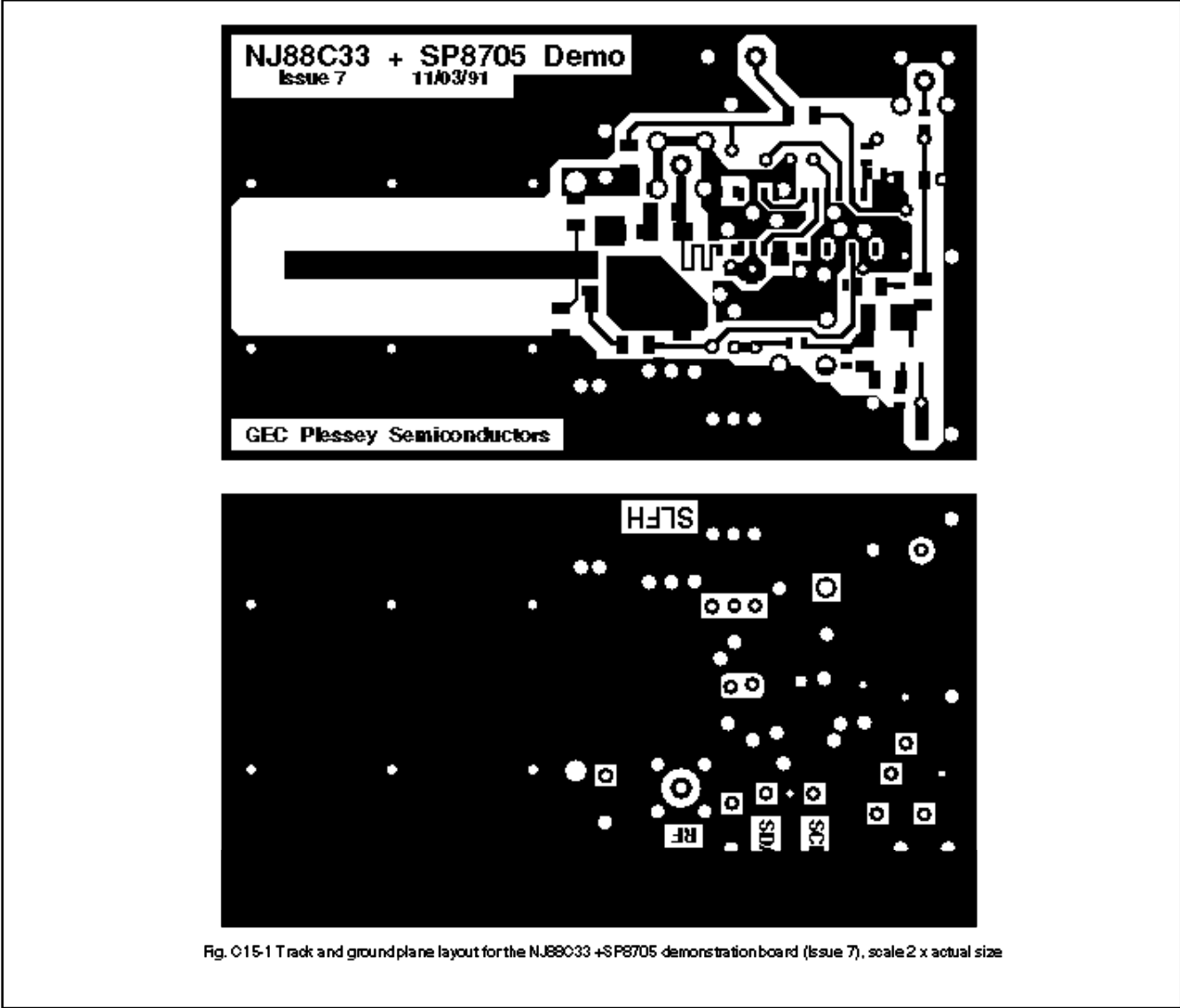
To demonstrate the recommended layout and interfacing between the SP8705 and the NJ88C33 devices, a cheap and cheerful microstrip VCO has been designed for the upper UHF band. The line length has been adjusted to give the best power match between the active device Q₁ and the micro strip in keeping with good low noise design practice. Conjugate matching has been used at the transistor's collector and the Prescaler's input to provide the best power transfer and isolation between the VCO and the Prescaler IC. The addition of a pull down resistor on the output of the SP8705 device assures an adequate level of drive to the FI input of the NJ88C33. The output drive from SK₂ is in the region of 0dBm. The VCO sensitivity varies from board to board, being around 25 to 33 MHz per Volt, typically 28 MHz per Volt.

Figure C14 shows the schematic for the Issue 7 Evaluation card, it can be seen that it has many common elements with the Issue 2 Evaluation card.



AN-94

The reference oscillator is novel due to the use of matching crystals to generate (XTAL₁) and filter (XTAL₂) the reference signal before it is presented to the RI input of the NJ88C33. Tuning of the oscillator is achieved by altering the phase change at the L₂ junction with R₁₅ and C₂₂. The reference can be monitored from SK₁, or else an input can be feed into SK₁ if R₁₃ is removed from the circuit. The loop filter values have been calculated for an ω_o of 2K7Hz, for use with a comparison frequency of 200KHz. This by no means represents the limit of operation, probably an ω_o of 20KHz would be possible with a comparison frequency of 200KHz, at the expense of increased comparison related side products. Figure C15 shows the recommended layout for the NJ88C33 when used with a prescaler IC such as the SP8704/5. A parts list follows.



C33ISS7 EVALUATION CARD: PARTS LIST.

Revised 15-07-91 SLFH

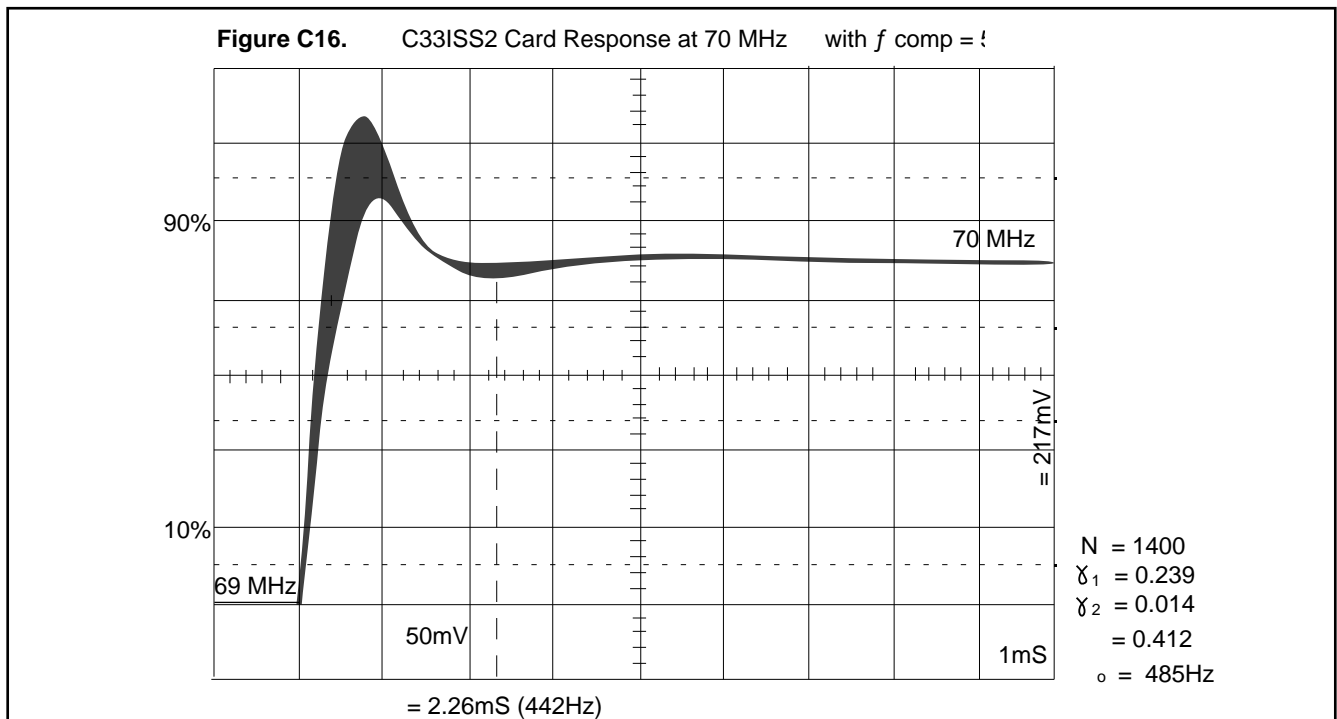
Board Reference	Component Type	Library Symbol
C1a	4n7/X7R 10%	SMD1206
C1b	1n0/NPO 5%	SMD1206
C2	33n/X7R 10%	SMD1206
C3	33p/NPO 5%	SMD0805
C4	100p/NPO 5%	SMD0805
C5	10n/X7R 10%	SMD0805
C6	22u/35V electro.	RADIAL2.5x6.3
C7	1n0/X7R 10%	SMD0805

C8	1n0/X7R 10%	SMD0805
C9	1n0/X7R 10%	SMD0805
C10	1n0/X7R 10%	SMD0805
C11	1n0/X7R 10%	SMD0805
C12	22u/35V electro.	RADIAL2.5x6.3
C13	1n0/X7R 10%	SMD0805
C14	1n0/X7R 10%	SMD0805
C15	47n/X7R 10%	MKT7.2x3.5
C16	1n0/X7R 10%	SMD0805
C17	22u/35V electro.	RADIAL2.5x6.3
C18	47n/X7R 10%	SMD0805
C19	10n/X7R 10%	SMD0805
C20	10n/X7R 10%	SMD0805
C21	10n/X7R 10%	SMD0805
C22	22p/NPO 5%	SMD0805
C23	1p0/COG 0p5	SMD0805
C24	22p/COG 5%	SMD0805
C25	27p/COG 5%	SMD0805
VC1	3p5-22p	Trimcap
R1	10R /0.25W 2%	SMD1206
R2	2K0 /0.25W 2%	SMD1206
R3	1K0 /0.25W 2%	SMD1206
R4	10K /0.25W 2%	SMD1206
R5	10K /0.25W 2%	SMD1206
R6	220R/0.25W 2%	SMD1206
R7	27R /0.25W 2%	SMD1206
R8	15R /0.25W 2%	SMD1206
R9	180R/0.25W 2%	SMD1206
R10	10R /0.25W 5%	0.6 Axial
R11	10R /0.25W 2%	SMD1206
R12	270R/0.25W 2%	SMD1206
R13	330R /0.25W 2%	SMD1206
R14	22K /0.25W 2%	SMD1206
R15	2K7 /0.25W 2%	SMD1206
R16	4K7 /0.25W 2%	SMD1206
R17	33M /0.50W 5%	0.6 Axial
L1	10n 20%	SMD1210
L2	15u 10%	SMD1210
L3	220u 10%	SMD1210
D1	BB105B varactor	SOD-23
D2	1N6263 schottky	DO-35
D3	1N6263 schottky	DO-35
Q1	BFR93A RF NPN	SOT-23
Q2	BFS17 RF NPN	SOT-23
U1	NJ88C33	
U2	SP8705	
XTAL1	10.00MHz Series	HC-43/U
XTAL2	10.00MHz Series	HC-43/U
SK1	SMC socket	SMCPCB
SK2	SMC socket	SMCPCB
P1-P2	1mm pins	
P3-P5	0.1" 3 way header	SPCO
PCB	C33ISS7	

d) Measurement of Transients/ Damped Frequency of Oscillation.

Once the Evaluation cards have been built we will then have a test bed to carry out some more complicated measurements that require the loop to be closed. With the provision of a +- 5Volt power supply and a programmer card (or a logic pattern generator), we can make some dynamic measurements on the boards. In normal use only a single 5Volt supply is needed; however for testing purposes we over-ride the negative supply from the C pin output, otherwise the transient output at the PD pin will contain an element of negative supply recovery transients. The voltage doubler has a limited ability to source current; about 40mA in the divide four mode and about 80µA in the divide two mode (bit 6 of the status byte set to true or false respectively). The - 625µA or - 2.5mA currents from the PD pin must be taken from the decoupling capacitors on the negative supply line, causing it to collapse. Poor common mode rejection in VCO control input will then confuse the output spectrum and transient measurements. The Voltage doubler supply from the C pin is only suitable for static PLL designs. For modulated loops the C pin must either be connected directly to ground (bit 7 of the status byte is set to false) or the negative supply over-ridden by an external supply. Note, the voltage doubler can be left on in this mode but it should be switched off to minimise reference divide two or four related harmonic energy from leaking out of the device and into the VCO's resonant circuit.

First we shall look at the step response of the Issue 2 Evaluation card to see how well the measured loop natural frequency and damping compare to those we predicted earlier on. Figure C16 shows the control voltage V_C for a step in the VCO output frequency of 1MHz (a change in N of 20) to a new settled frequency of 70MHz. The 70MHz point is used to try to keep K_{VCO} at the value used in the calculations (5MHz/V).



The part of the trace that we are interested in is a line nearest a horizontal line projected through the 70MHz value, The ragged edges are due to the comparison period related charge pump pulses being integrated onto the loop filter. Compare the inner line of Figure C16 with the upper plot of Figure B6, where $\zeta = 0.8$; we see that that value is much closer to the real result than the approximation that follows.

The display is triggered from a synchronisation output from the programmer board which gives an edge when the stop bit is transferred on the I²C Bus. Some variation will occur in the trigger point since the N counter begins its new count when the current count is complete, that is: it loads synchronously to its own reset. There is no reason why the device used to programme the I²C Bus should not be locked to the Reference for a fully predictable set-up time for the counters, provided the restrictions on the input levels to RI and FI are met. The above oscillogram is produced by monitoring the VCO control line with an oscilloscope probe in the same manner as for the phase error test-rig. We can approximately evaluate the loop natural frequency by using the relationship between the observed ring (ζ) in Figure C16 and the equation $\zeta = \frac{d}{\omega_0} (1 - \zeta^2)^{-1/2}$ once the damping has been found. We can do this in terms of a second order loop from Equations A(viii) or A(ix) to be found in Appendix A:

$$\zeta = \left\{ \left[\frac{2(n - m)}{\ln m / n} \right]^2 + 1 \right\}^{-1/2}$$

The result will give us the damping for the “best fit” second order response that approximates our third order response. An error can creep in if we use the first peak in the response when the real pole approaches the conjugate pair of poles; the effect of the real pole is still a decreasing factor and influences the overshoot of the response. If we use the second and third peaks (or later ones) this can be minimised. Here we can use the first and second peaks since the real pole is at about six times the loop natural frequency. We see that the first peak overshoots by a factor of 0.239, with the second peak overshooting by 0.014. Therefore:

$$= \left\{ \left[\frac{2(1 - 2) p}{\ln(0.239/0.014)} \right]^2 + 1 \right\}^{-1/2}$$

$$= 0.412$$

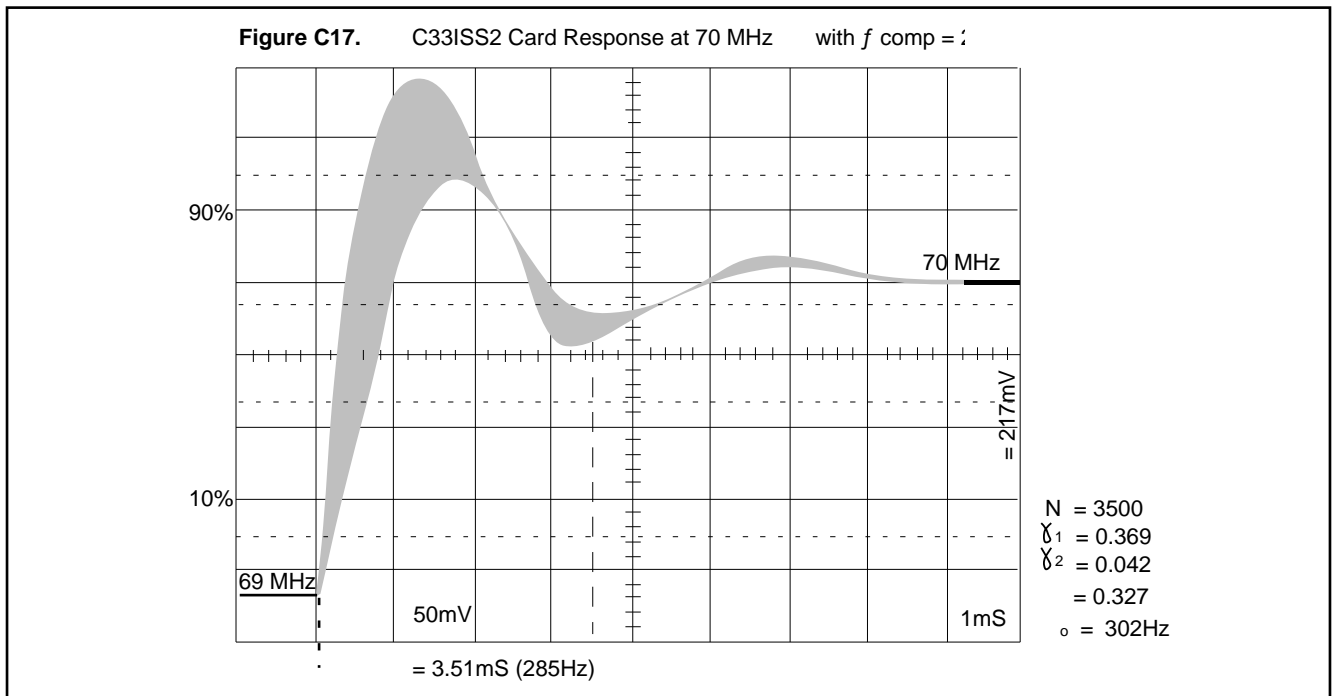
Using this result and the 2.26ms period of the ring (442Hz) in Figure C16, we write the expression for the loop natural frequency as follows:

$$= \frac{1}{d} (1 - 2\zeta^2)^{-1/2}$$

$$= 442 (1 - 0.1697)^{-1/2}$$

$$= 485\text{Hz}$$

Compare this with the expected result of 488Hz and 0.63766 for the Issue 2 Evaluation Card, a small error has crept into the result due to the VCO gain being 4.6MHz per Volt rather than the calculated 5MHz per Volt. Just for interest’s sake we change the comparison frequency to 20KHz and N to 3500 and take the measurement again to see how it alters the loop parameters. The result is shown in Figure C17.

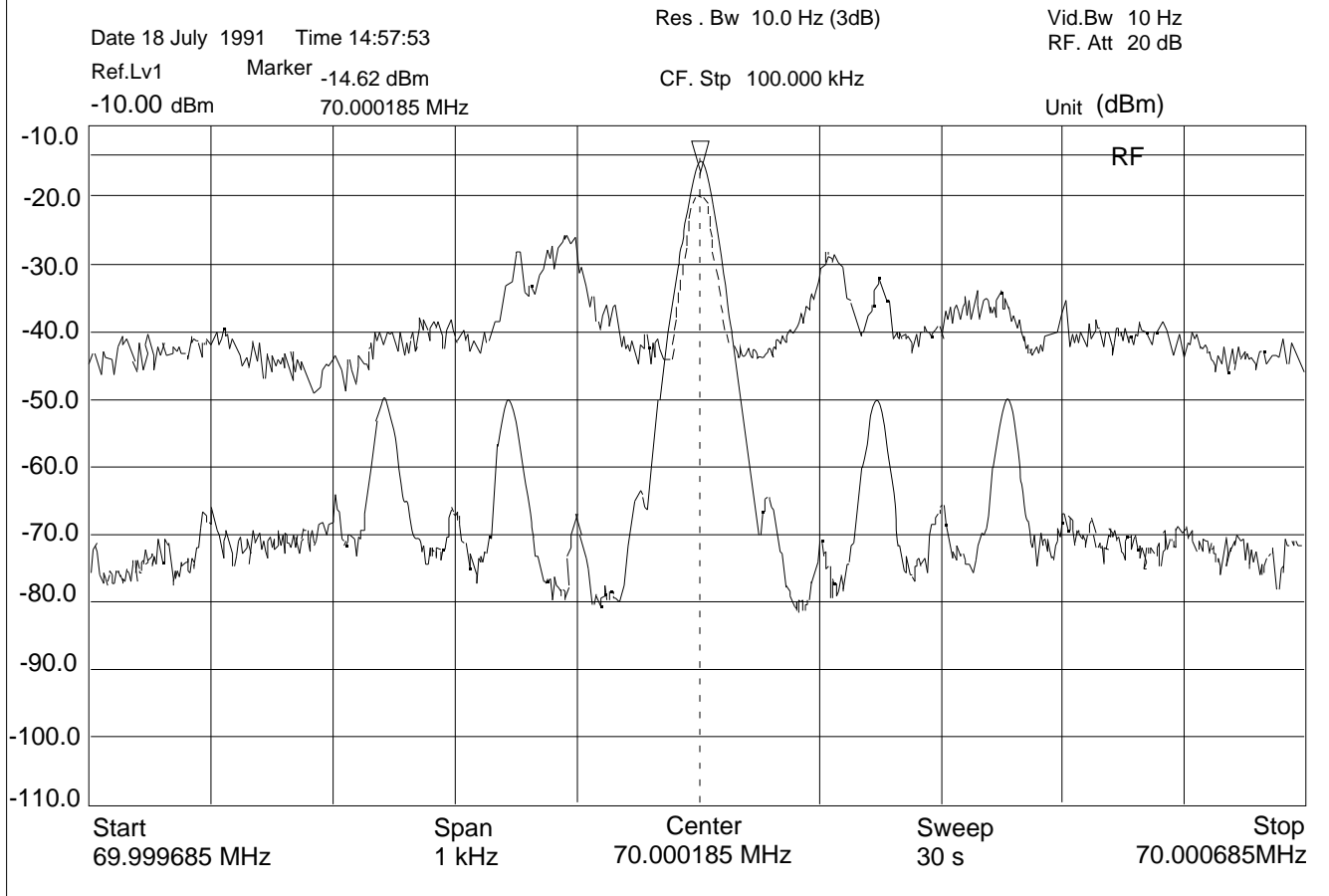


Using the same equations as before we see that the damping has decreased to 0.327 with the damped frequency of oscillation dropping to 285Hz giving a loop natural frequency of 302Hz. It was found that the ring was 384Hz at 91MHz with K_{VCO} of 4.08MHz per Volt. Remember that these are best fit second order values but can be seen to be of reasonable practical use for design verification, at the prototype stage.

e) Measurement of Noise Bandwidth and Sidebands.

Once we are satisfied that our design is practical, we should examine the frequency domain output of the VCO to find out how successful we have been in implementing the design. The test set-up needs nothing more than the Evaluation card, some form of programmer and a Spectrum Analyser. Initially a couple of problems will be apparent: a high level of close in noise, as in the upper trace of Figure C18 and the mains voltage (at harmonics of 50Hz) related spurs seen in the lower trace of Figure C18.

Figure C18. C33ISS2 Evaluation card spectra showing the noise related side bands.
The top trace is the basic unmodified loop, the lower trace is with 30M resistor on the filter.



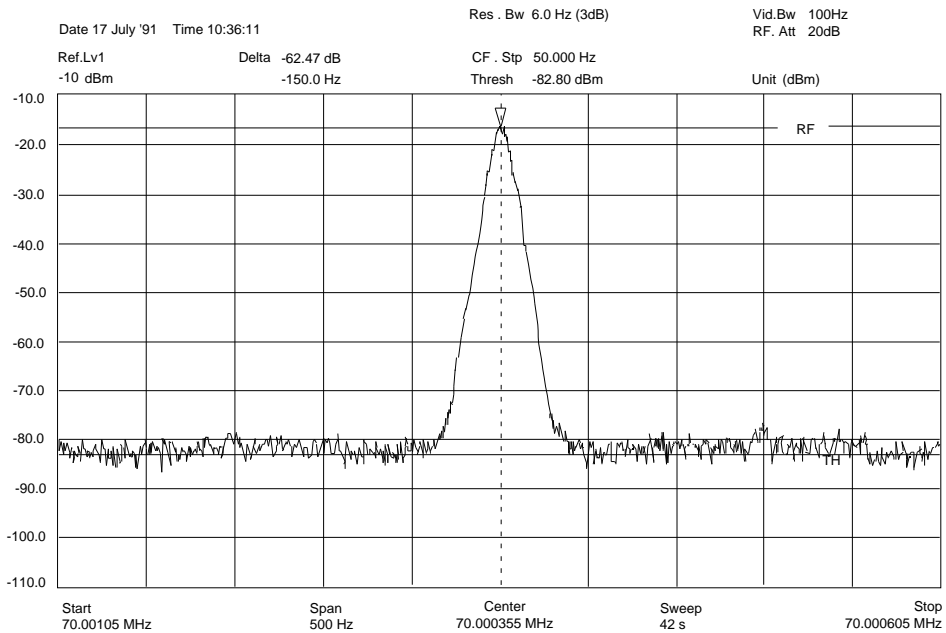
The close in noise (of the upper trace in Figure C18) can be decreased by adding a small current sink to the loop filter; in this case a 30 megohm resistor from the loop filter (PD pin) to the negative supply giving a current sink of about 83nA (resulting in the lower trace of Figure C18). This offset current produces a ramp voltage by bleeding charge off the loop filter. It can be shown with some working that this current can be considered to be integrated onto C_1 only (rather than the whole loop filter C_1 , C_2 and R_2) with little error in the result. A balance must be reached between an acceptable close in phase noise and the comparison related side products. Using a current sink consisting of just a very high value resistor from the control line to ground will give increased phase noise at low tuning voltages and increased comparison related spurs at higher tuning voltages with respect to those at the centre of the VCO's tuning voltage range. Under certain circumstances it may be found that the reverse leakage current in the Varactor diode will be sufficient to fulfil the function of the current sink.

The resulting voltage is:

$$\begin{aligned}
 dV_{C_1} &= (I_{leak} \cdot dt) / C_1 \\
 &= 83n \cdot 50\mu / 100n \\
 &= 42mV
 \end{aligned}$$

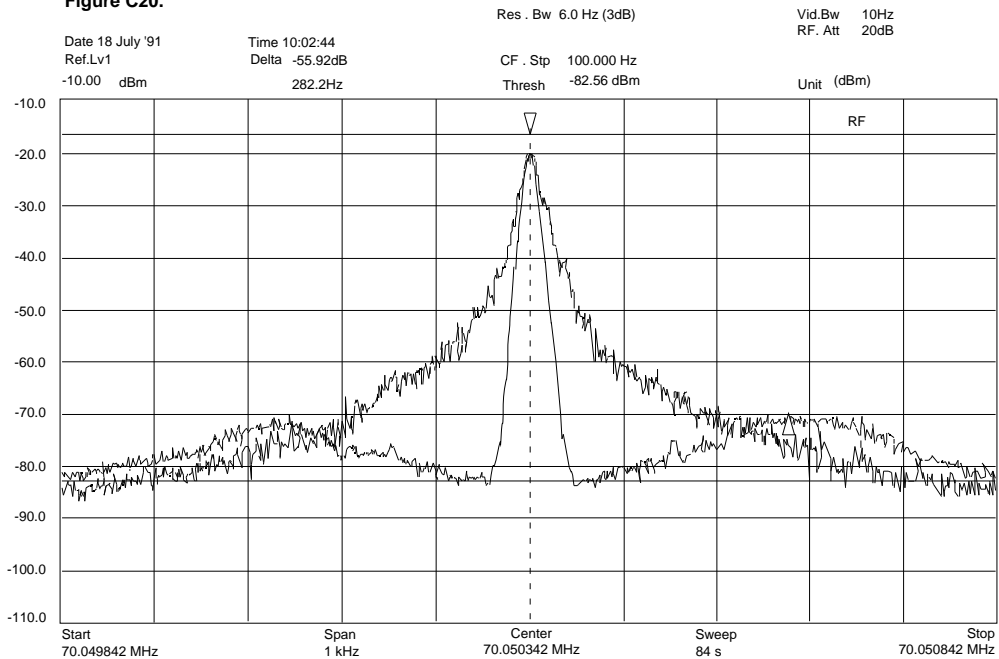
If this voltage is multiplied by the VCO gain of 5MHz per Volt we would see an output "excursion" of 207Hz, a comparable value to that of the loop's natural frequency. The exact relationship between the optimum value of leakage and the loop's natural frequency is still to be established. This value of current would seem to be a maximum. The reduction of close in noise can be seen in the lower trace of Figure C18. We now have a poor side band performance caused by the lower (50Hz) harmonics from the power supply modulating the loop. The effect can be minimised through use of highly regulated supplies or batteries as for the circuit used to produce Figure C19. Close-in noise has all but gone; only a residual 150Hz harmonic remains at - 62.5dBc. The noise level at an offset of 50Hz from the carrier of 70MHz is - 75dBc/Hz. This equates to approximately a 20dB noise figure at the phase detector.

Figure C19. Issue 2 Evaluation Card close in noise spectrum. Peak is at -15.6dBm



By moving the carrier one comparison frequency away from 70MHz to 70.05 MHz and using a lower battery voltage (4.0V), we see a different type of noise produced by the basic loop in Figure C20. The reduction of the noise bandwidth in the upper trace of Figure C20 with respect to the upper trace of Figure C18 is due to the fact that we have moved the carrier away from a harmonic of the voltage doubler frequency. This gives a lower noise injection from the voltage doubler via the V_{dd} line. Now, the lower trace of Figure C20 shows a distinct shoulder due to the loop reducing the noise of the VCO. The centre of this shoulder is at f_d (282Hz) showing how much the parameters have changed from the calculated values due to reduced supply affecting the phase detector and VCO gains.

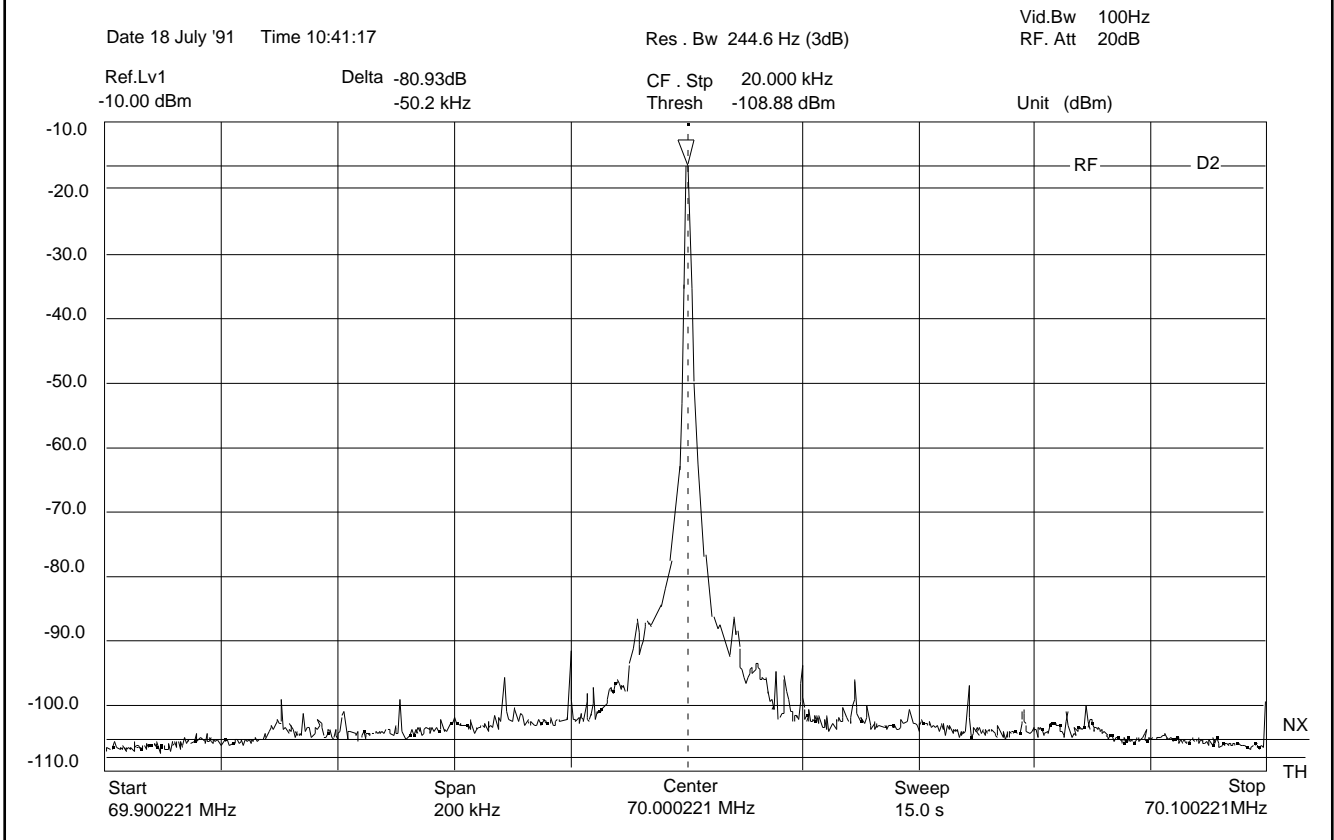
Figure C20.



C33ISS2 Evaluation Card close in noise when supplied from batteries. $V_c = -4V$, $V_{dd} = 4V5$
The top trace is the basic board, lower trace is with a 30M resistor on the filter.

In Figure C21 we see a wider bandwidth plot of the C33ISS2 Evaluation card's spectrum displaying a comparison frequency related side band level at - 81dBc along with various spurs due to feed through from the power supply line.

Figure C21 C33ISS2 Evaluation Card spectra showing the comparison frequency related side bands. The NX line is 3dB up on the threshold of the spectrum analyser.

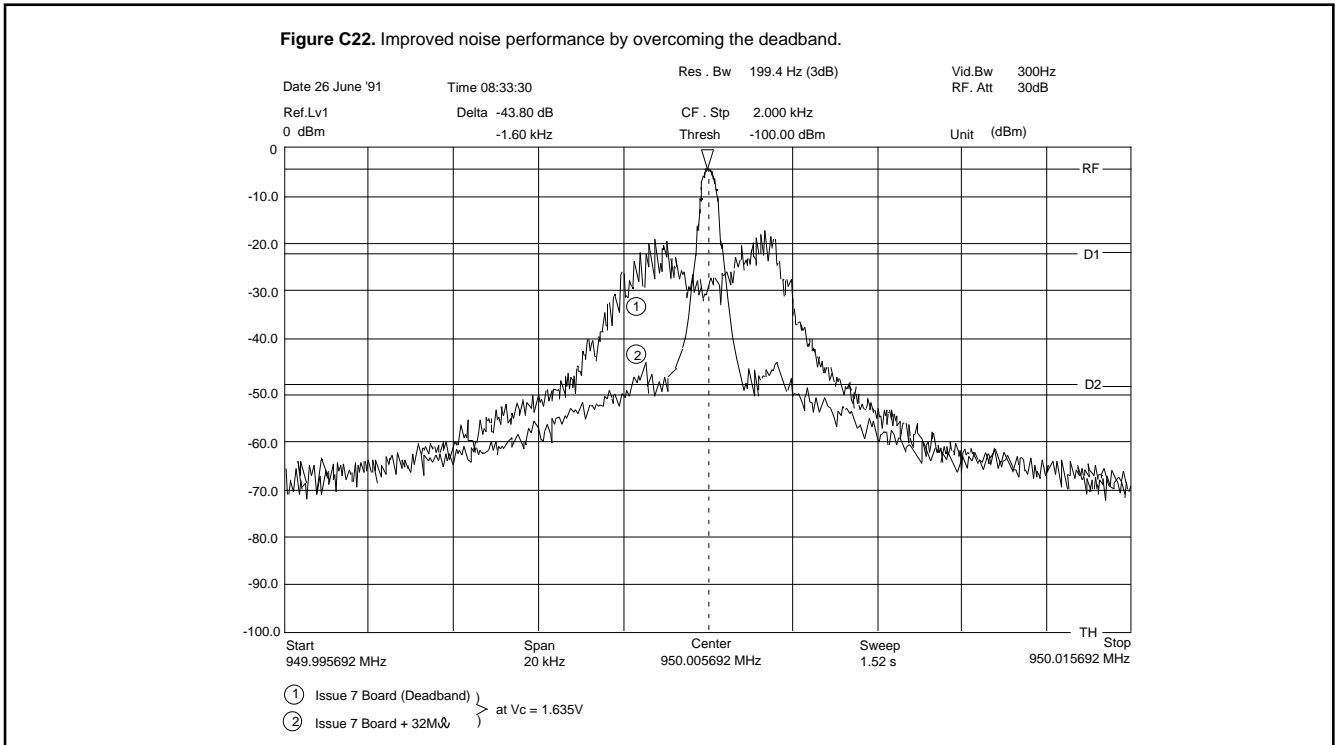


The VCO tank circuit is seen to be approximately 100KHz wide at the point at which the noise floor has increased by + 3dB (indicated by the NX line in Figure C21). If the VCO noise figure was equal to the spectrum analyser's noise figure of 19dB, this would indicate a "Q" about 700. However if we assume a VCO noise figure of typically 10dB, the point at which the VCO noise floor rises above the thermal noise floor by 3dB will be approximately three octaves wider than that measured, if we assume a typical far-out noise contour of - 3dB/ octave. This is narrow enough for tuned amplification of any interference within one comparison frequency spacing of the carrier to cause problems. It is strongly recommended that exacting layout techniques are used around the power lines, the loop filter and the VCO to minimise such noise feedthrough. For low noise applications the Voltage Doubler should not be used, short this pin to ground. It is always worth while checking that bit 7 of the status byte is false, otherwise the voltage doubler current pulses will cause havoc when the carrier is set to a low integer number of comparison frequency spacings away from the doubler harmonics.

A method to measure the actual bandwidth (not shown here) is to use an unrelated fixed frequency marker injected into the tank circuit at about - 40dBc. By tuning the VCO's carrier progressively away from the injected carrier's frequency, the injected carrier's amplitude will remain constant until the carrier is removed by some 150KHz (at which point it has reduced by some - 3dB over its close in value) giving a bandwidth of 300KHz and a Q of 233.

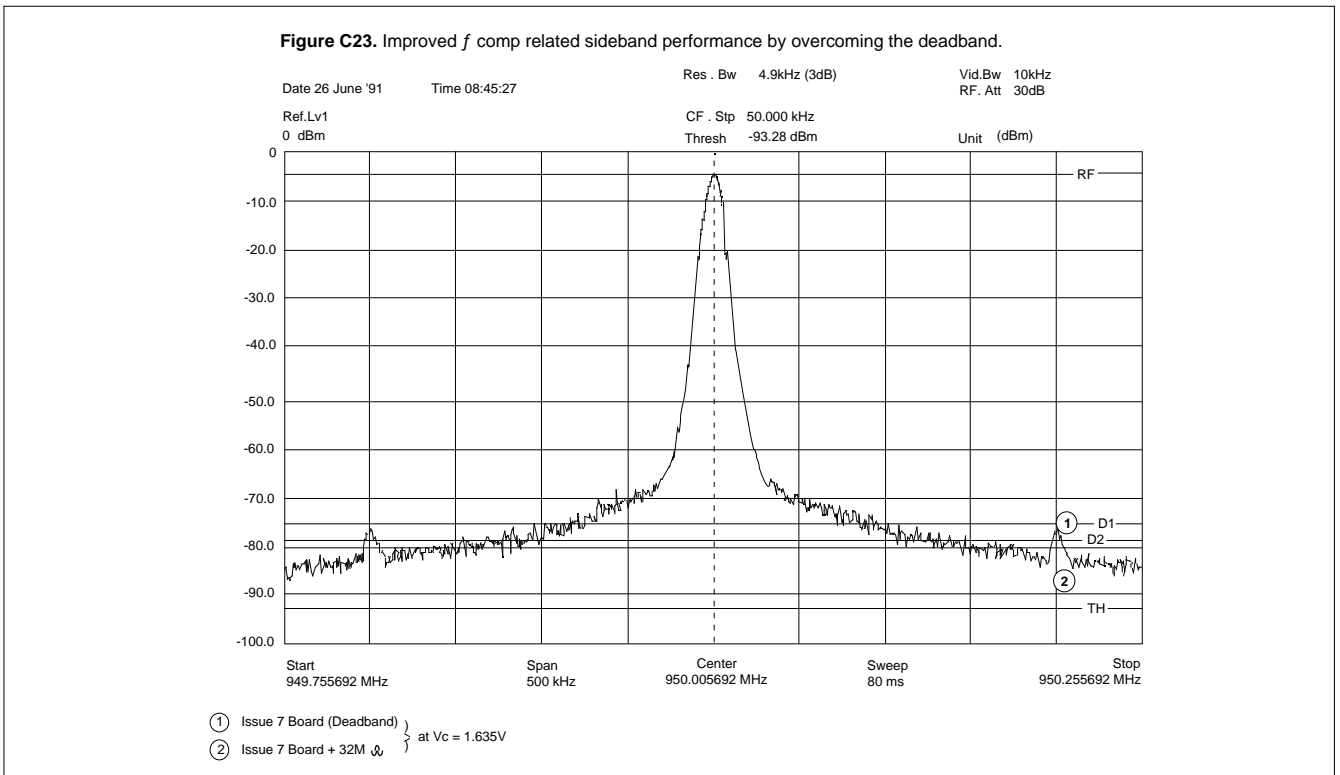
So we see that the practical implementation of the circuit gives an increased effective Q over that for the basic tuned circuit. This is due to the negative output resistance of the oscillator's active device partially cancelling the series resistance in the tuned circuit. Consider the position of the conjugate poles on the s-plane required to produce a constant level of output (by the oscillator) with respect to the position of the conjugate poles for the slightly lossy tuned circuit alone. The energy lost in the damping of the tuned circuit(the angle from the real axis to a projected line to the conjugate pole) must be replaced by the amplifier, in order to effectively move the poles onto the complex axis where damping is zero, hence the Q is infinite by definition since the output oscillations do not decay away (whilst powered-up).

Figure C22 shows the measurement of the close in phase noise of the Issue 7 Evaluation Card.



The upper trace is for the basic evaluation card, which displays the effect of the deadband upon the close in noise. The lower trace shows the effect of adding a current sink of 50 nA to the loop filter, producing the offset current referred to earlier on.

Figure C23 shows an approximate 3dB reduction of the comparison frequency related side products that occur when the current sink is added to the loop filter.



Figures C22 and C23 show the Issue 7 Evaluation Card with a current sink of 50 nA added to it as for the Issue 2 card. The similarity of the current magnitudes is incidental, since the ratios of the comparison frequencies, loop natural frequencies and the VCO sensitivities are similar. The exact value of current must be calculated for each implementation of the loop, here we see that the effect of the offset current and the phase comparator's correction pulses is a ramp voltage of 53mV which calculates out to a VCO output frequency of 1K4Hz, again comparable to the loop's natural frequency of 2K7Hz.

Footnote

The function of the ramp voltage is not seen at the output of the VCO due to the very high value of “Q” for the VCO tank circuit. That is; the VCO’s tank circuit displays a finite response time which is related to its Q, (as would be expected from our previous work on under damped responses by relating their conjugate pole positions to the damping and its reciprocal, Q) since the envelope of its response time is exponentially related to the value of the real projection of the conjugate poles’ position on the s-plane, as in Appendix A under the section covering transient responses. The tank circuit resists any change to its frequency of resonance such that it settles to a new short term frequency in a similar manner that the loop settles to a new frequency at the VCO output. The settle time is related to the damping of the tank circuit since energy must be subtracted or added to the tank; therefore a very high Q VCO resonator cannot be used in a fast settling loop since it will take too long to alter the point of resonance. This time to respond can add an extra pole to the controlled loop.

The non linearity of the phase detector gain near the point of zero phase error, results in a lengthening of the calculated settle time for a carrier settled to less than the dead band offset frequency as calculated by:

$$f_{\text{offset}} = \frac{t_{\text{deadband}} \cdot f_{\text{output}}}{t_{\text{comparison}}}$$

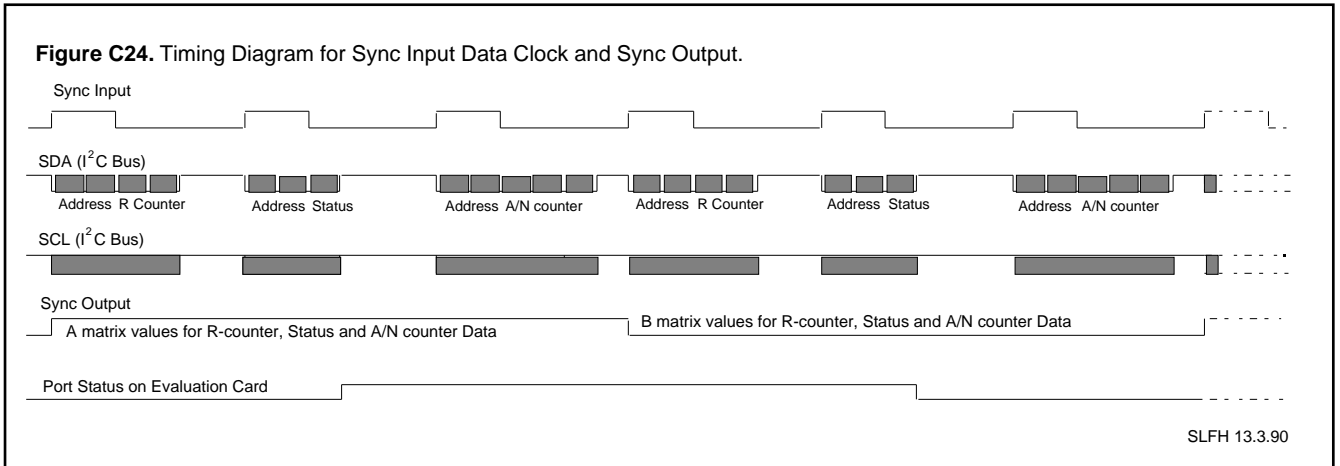
Giving values of 7K56 for the Issue 2 Evaluation Card and 1M03 for the Issue 7 Evaluation Card. These offsets represent the points at which the phase detector is dominated by non linearities caused by the finite rise and fall times of the charge pump drivers and output devices having a longer duration than the actual phase error indicated at the phase detector. Practically, the loop will need to be examined using a spectrum analyser in the receiver mode; where a plot of time verses frequency is produced. It will be seen that the loop will go from being optimally damped for large steps as in Figures C15 and C16, to being under damped as the phase detector gain increases (due to the almost vertical portion of Figure C3) as we approach a frequency offset indicated by the above equation due to the dead band. Then the gain drops away to a very low value dominated by the current sink (source) causing the loop to be overdamped at close in frequencies inside the area governed by the deadband. Such plots will display flat areas in the frequency settling due the dead band whilst the output frequency remains constant but the phase is changing: this can take a number of comparison periods before the error builds up to a level where the opposite charge pump becomes operative. The effect will be one sided (as the current sink pulls the VCO’s control voltage across the dead band) and will be seen on the final trajectory to a stable output frequency dominated by wideband noise of a few tens of hertz for the Issue 7 Evaluation Card. The settle time trajectories for a step up or down in frequency will be different depending upon which side of the settled (loop filter) voltage the bleed resistor is placed, that is: to the supply or ground (doubler output). With care these effects can be minimised, but the systems designer needs to be aware that they exist and needs to resort to an empirical assessment to assure that the design specifications are reached.

(f) Programming the NJ88C33.

At the time of product development, no I²C Bus Programmers were available with the capability of being able to operate at the 5MHz clock speed proposed for the NJ88C33. The requirement was met by a dedicated card based around standard high speed CMOS logic ICs. The implementation was based around the address and data sequence shown in the data sheet. This shows the exact construction of the data trains required to programme up the NJ88C33. Details of the card are available if required, however it is recommended that on of the proprietary I²C Bus compatible microprocessors are considered as these will reduce the hardware costs involved at the prototype stage.

The board is effectively a dual programmer featuring a clock rate of either the I²C Bus standard of 100KHz or at an arbitrary rate of 2MHz, which is well below the NJ88C33’s maximum rate of 5MHz. The programmer has two banks of switches which alternately determine the NJ88C33’s register contents, allowing the device to be cycled between two sets of values for step and settle time measurements. For convenience, the programming sequences are the same as the data sequences shown in the NJ88C33 Data Sheets. The primary and sub-address word is fixed by the PCB implementation to that of the NJ88C33. The succeeding data bytes are variable.

With reference to Figure C24, it can be seen that the programming sequence repeats on every seventh input sync pulse. A sync pulse is either a TTL type input signal or a depression of the on-board “step” switch; this initiates one of the six possible address/data strings in a preset sequence. Following a “start” condition (the data line is taken low whilst the clock line is high) the primary address byte is sent serially across the I²C Bus (the data is clocked on the clock’s rising edges, whilst the data only changes state during the clock’s low period), with the programmer board releasing control of the data line whilst continuing to exercise control of the clock line. If a device “acknowledges” (the ninth bit of each transmitted byte is high impedance allowing the NJ88C33 to take control of the data line in order to respond by keeping the data line low), the programmer then sends the sub-address byte; this sequence repeats for subsequent data bytes to make up a complete string. These strings are of either three, four or five bytes in length. Each string of data is terminated by a “stop” sequence (the data line is taken high whilst the clock line is high). The sequence of strings being: a-matrix R counter, a-matrix status, a-matrix N counter, b-matrix R counter, b-matrix status and then the b- matrix N counter; the sequence then repeats.



The two switch matrices allow for programming of individual differences between the a-matrix switch settings and the b-matrix switch settings. Consequently, every third sync input or press of the step button, will toggle the desired function. At the start of each sequence (before the address word of the R counter string) a sync output transition is given; the transition is from low to high for the a-matrix of switches and from high to low for the b-matrix switches. The sync. output transition controls the A/B matrix indicator LEDs. Figure C24 has been drawn to illustrate the string sequence and composition for dual modulus programming; the third and sixth strings have five bytes rather than four as in single modulus sequences, since the extra byte is used to describe the A value for the A/N counter. Notice that the contents of the NJ88C33's registers are latched through when the "stop" condition is generated, however a new start condition will also have the same effect on a previous sequence if that sequence was not terminated by a stop condition. Note that the maximum programming repetition rate with this board for the 100KHz clock is 500 programming cycles per second or 1500 input sync pulses per second. The maximum rates for the 2MHz clock are twenty times faster.

Reference should be made to the I²C Bus Specification if a reconfiguration of the programming sequence is contemplated. Minor modifications to the board are possible, for example: isolating the track to the wiper of SW21 then connecting it to pin 9 of IC37b. This allows the programmer to control two evaluation cards at once: a dual modulus NJ88C33 via the a-matrix and a single modulus NJ88C33 via the b-matrix, one for each half of the above sequence, as each NJ88C33 requires just three strings to programme it.

Notice that when the A counter of the NJ88C33 is set to zero, it counts to 128 FI input cycles, not zero as may be expected. Therefore to set N to a particular integer value, we subtract one from the desired value and then set A to 64 for a 64/ 65 Prescalar, or set A to 0 for a 128/ 129 Prescalar. In each instance, N must be larger than A to give the correct count sequence.

Using on the C33ISS7 board with a comparison frequency of 200KHz we have:

F_{vco}	N	A	Division Ratio	$(N \cdot P + A)$
850MHz	66	26	4250	4250
900MHz	70	20	4500	4500
960MHz	74	64	4800	4800

AN-94

We see that the last entry gives the same result as $N = 75$ and $A = 0$. If we had a comparison frequency of 100KHz, we would programme the following values:

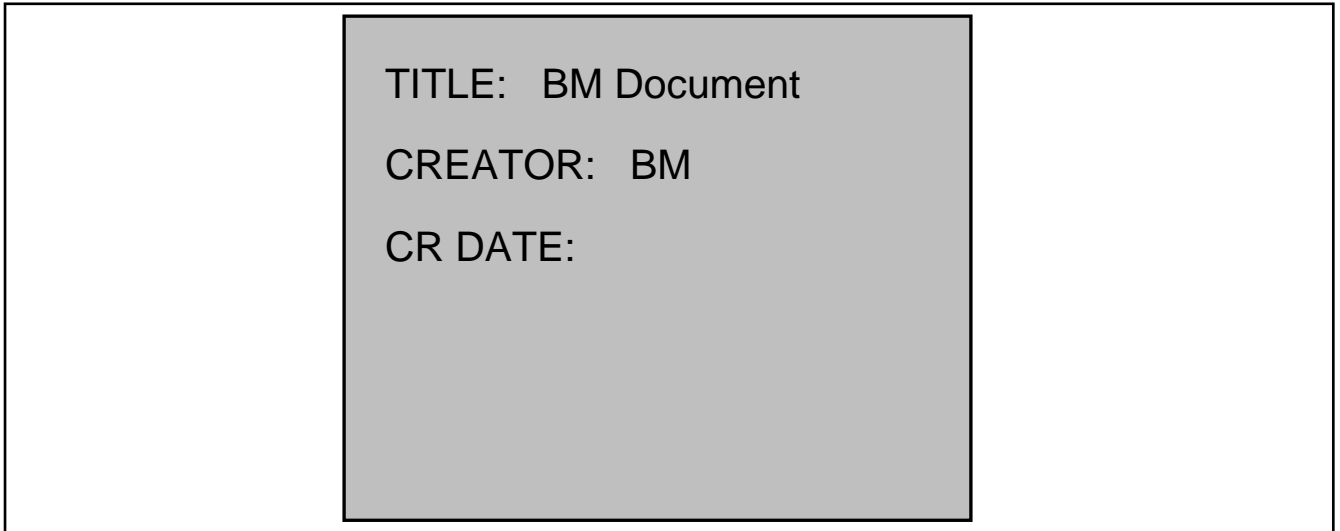
F_{vco}	N	A	Division Ratio	$(N \cdot P + A)$
850MHz	66	52	8500	8500
900MHz	70	40	9000	9000
960MHz	74	0	9600	9472

In the last entry we see that although we program zero into the A counter, it actually counts 128 making up the missing count for N; effectively we get an N count of 75 and an A count of zero as we would expect if the counters followed a contiguous set of values.

Appendix A: The Derivation of the Second Order Response and Some Useful Equations

A Real Network

Whenever a network of components contains more than one energy storage element (inductance or capacitance) any energy injected into that network will be passed between those reactive elements in a characteristic way. Here we are concerned with a generalised approach to analysing this response; particularly when the energy storage of the components is equal. We wish to examine the network's frequency response as well as its transient output with time. To do so, we will use Laplace transforms to study the simple RCL network as follows:



A special case arises when we have a conjugate network, that is the reactance of L and C cancel. Consider the Quadratic Equation describing the transfer function of a series RLC network, given that at time $t = 0+$ and assuming a zero initial condition; $v_C = 0$ and $dv_C/dt = 0$ regardless of the input excitation since the inductor "stands off" the input signal. Now, we have:

$$v_i(t) = v_R(t) + v_L(t) + v_C(t)$$

which is determined by the current loop around the network. If we wish to make v_C the output and given that:

$$v_C(t) = \frac{1}{C} \int_0^t [i_C(T)] dT \quad \Rightarrow \quad i_C(t) \frac{d}{dt} = C \frac{d}{dt} [v_C(t)]$$

we see that:

$$\begin{aligned} v_R(t) &= R i_C(t) & \text{and:} & \quad v_L(t) = L di/dt \\ &= R C \frac{d}{dt} [v_C(t)] & & = L d/dt[C dv_C(t)/dt] \\ & & & = L C \frac{d^2}{dt^2} [v_C(t)] \end{aligned}$$

We arrive at:

$$v_i(t) = v_C(t) + R C \frac{d}{dt} [v_C(t)] + L C \frac{d^2}{dt^2} [v_C(t)]$$

In order to find the time domain response of this network, we can rewrite it in Laplace Transforms to find the complex frequency domain form of the transfer function. To simplify the equations' structure we use a short hand "Dot Notation" form

(from reference 3). For example, we write $d/dt (v_C)$ as \dot{v}_C . The transfer function is calculated as follows, by accounting for the initial conditions:

AN-94

$$L \{v_C\} = \bar{v}_C$$

$$L \{\dot{v}_C\} = s \bar{v}_C - v_0$$

N.B: $v_0 = v_C$ at $t = 0$

$$L \{\ddot{v}_C\} = s^2 \bar{v}_C - s v_0 - v_1$$

and: $v_1 = \dot{v}_C$ at $t = 0$

Where the $L \{v_C\}$ and \bar{v}_C terms mean the Laplace Transform of the capacitor voltage. The $L \{\dot{v}_C\}$ term is Laplace Transform of the first derivative of the capacitor voltage; $L \{\ddot{v}_C\}$ meaning the Laplace Transform of the second derivative and so on. Similarly v_0 indicates the initial condition at $t = 0$ of $v_C(t)$ and v_1 is the initial condition of the first derivative of the capacitor

voltage, $dv_C(t)/dt$ or $\{\dot{v}_C\}$. Both of which were set to zero earlier on. Now if we take these and insert them into the transfer function for the RLC circuit:

$$v_i(s) = L \{v_i(t)\}$$

we get:

$$\begin{aligned} v_i(s) &= L \{v_C\} + R C L \{\dot{v}_C\} + L C L \{\ddot{v}_C\} \\ &= \bar{v}_C + R C [s \bar{v}_C - v_0] + L C [s^2 \bar{v}_C - s v_0 - v_1] \end{aligned}$$

Substitute in initial conditions at $t = 0$, that is $v_C(t) = v_0 = 0$ and $d/dt [v_C(t)] = v_1 = 0$:

$$v_i(s) = \bar{v}_C + R C [s \bar{v}_C] + L C [s^2 \bar{v}_C]$$

Rearrange for \bar{v}_C :

$$v_i(s) = \bar{v}_C (L C s^2 + R C s + 1)$$

Which tells us what the complex frequency domain transfer function is, given that the output at the capacitor divided by any non zero input will tell us the transfer function between them:

$$\begin{aligned} G(s) &= \frac{v_o(s)}{v_i(s)} && \text{where } v_C = L \{v_C(t)\} = v_C(s) = v_o(s) \\ &= \frac{1}{(L C s^2 + R C s + 1)} \\ &= \frac{1}{L C} \cdot \frac{1}{s^2 + (RC)/(LC) s + 1/(LC)} \dots\dots\dots A(i) \end{aligned}$$

which is about as far as we can go without resorting to an explanation in terms of the complex frequency domain form of $G(s)$. Consider the meaning of the Laplace variable s , when it is used to define the Laplace Transform: (N.B: $a = \text{infinity}$)

$$F(s) = \int_0^{\infty} e^{-st} f(t) dt$$

we see that if $s = \sigma + j \omega$, we are defining a transient part ($e^{-\sigma t}$) and a steady state part ($e^{-j \omega t}$) of the transformation. To see the parts more clearly we consider the time domain response or the Inverse Laplace Transform of e^{-st} over the range of $s = -\text{infinity}$ to infinity , which will produce orthogonal functions:

$$f(t) = \frac{1}{2j} \int_{-j}^{+j} e^{-st} F(s) ds$$

$$= \frac{1}{2} \int_{-j}^{+j} [e^{-\sigma t} e^{-j\omega t} F(s)] ds$$

it can be proved with working that the roots of the function F(s) will produce a chain of simple and complex exponentials of the form:

$$e^{-\sigma t} [1/2(j\omega e^{j\omega t} + -j\omega e^{-j\omega t}) - 1/2(j\omega e^{j\omega t} - -j\omega e^{-j\omega t})] = e^{-\sigma t} (\cos \omega t - j \sin \omega t)$$

$$\Rightarrow e^{-\sigma t} \sin(\omega t + \phi) \dots\dots\dots A(ii)$$

where $\phi = \text{atan}(\text{imag./real}) = \tan^{-1}(1/-1)$ and each factor is scaled by a product determined by partial fraction forming when decomposing the roots. Equation A(ii) has two relevant parts: a transient real exponential on the left and a complex conjugate pair of exponentials on the right which are factored into a sinusoidal wave. Together they form an exponentially damped sinusoidal wave; i.e: a "ring", thus:

TITLE: BM Document
 CREATOR: BM
 CR DATE:

Equation A(ii) shows us the form of the time domain response and allows us to calculate the Amplitude and Phase responses of any transfer function represented by F(s). Notice that s in the e^{-st} (amplitude) term determines the rate of decay of the oscillatory waveform. Similarly the ω in the $e^{-j\omega t}$ (frequency) term controls the steady state or frequency part of the response. It is this form of response that will allow us to analyse high order systems in terms of second order ones: the coefficients of any response will be scaled by the Residues of the transfer function and the excitation at the partial fraction forming stage, these coefficients can then be truncated to approximate the response of a low order system. Further detail can be found in reference 5, page 155 onwards.

Returning to our transfer function, we wish to generate a similar mathematical statement in terms of a generalised transient and steady state solution. This will allow us to compare the above equation's coefficients with those of the solution to find the transfer function in terms of the natural frequency of oscillation ω_0 and damping ζ . From these we may compare completely different circuit topologies in generalised terms, i.e. they can be considered as "figures of merit".

If the resistor in the above network is small in comparison with the reactive values of the capacitor and inductor we see that any transient applied to it will excite an oscillatory response from it, that is resonance. At resonance $|X_L| = |X_C|$, we can say:

$$2 \omega L = 1/\omega C$$

and if we make $s = j\omega_0 = 2 \omega f$ we see that:

$$|j\omega_0 L| = |1/-j\omega_0 C| \Rightarrow 1/(LC) = \omega_0^2$$

Allowing us to write the previous transfer function in Equation A(i) as:

$$G(s) = \frac{\omega_0^2}{s^2 + R/L s + \omega_0^2}$$

AN-94

leaving just the coefficient R/L to solve. If $R = 0$ we see that the transfer function reduces to:

$$G(s) = \frac{\omega_0^2}{s^2 + \frac{R}{L}s + \omega_0^2} \Rightarrow G(t) = L^{-1}\{G(s)\} (= \sin \omega_0 t)$$

Which is the steady state undamped oscillation. It is reasonable to suppose that R is linked directly to damping. To further understand these responses, we need to examine the effect of the coefficients of the polynomials. We see that the bottom line of each of these transfer functions can be written in the form of:

$$a_2 s^2 + a_1 s^1 + a_0 s^0$$

which describes a second order polynomial known as the Quadratic Equation. From basic algebra we can find the two roots which characterise this particular transfer function. An intuitive guess would be that the form of these roots will be determined by the resistor R and hence the damping. We introduce the Damping term zeta, ζ , which is related to R in G(s) and controls the magnitude of the coefficient of s, a_1 , in the following way. Consider when:

$$|X_L| = |X_C| = R$$

By considering the roots of the Quadratic Equation in terms of s, with values of s which set the denominator of the transfer function to zero, we can determine the relationship between R,L,C in terms of ω_0 and ζ . By comparison of the coefficients of each form of the denominator polynomial we can "characterise" the transfer function. First assume that $\zeta = R/2$, we now write:

$$s_1, s_2 = \frac{-a_1 \pm [(a_1^2 - 4 a_2 a_0)]^{1/2}}{2 a_2}$$

Where a_2 , a_1 and a_0 are the coefficients of the denominator to the above transfer function.

$$s_1, s_2 = \frac{-(R/L) \pm \{(R/L)^2 - 4 \omega_0^2\}^{1/2}}{2}$$

The term inside the { } brackets is known as the discriminant and has a special meaning for the Quadratic Equation: the type of roots available from the expression are determined by the value of the discriminant, if positive they are real and different, if zero they are real and equal, and if negative the roots are complex and conjugate ($s_1 = s_2^*$). So, if we take the discriminant as being equal to zero we see that the roots will have one particular value only; that is: $-a_1/2$, allowing us to solve the problem:

$$(R/L)^2 - 4 \omega_0^2 = 0$$

$$\Rightarrow (R/L)^2 = 4 \omega_0^2$$

$$\Rightarrow R/L = 2 \omega_0$$

now by inserting a new variable zeta (ζ), which we set to unity, we can write:

$$R/L = 2 \omega_0$$

Zeta is defined as the ratio of R to $R_{critical}$, where $R_{critical}$ is the variable which determines the magnitude and sign of the determinant, here it has attained the value required to make the above expression true, it will obviously take on other values as R is altered so altering the damping:

$$\zeta = \frac{R}{R_{critical}} \quad \text{which is seen to be a dimensionless ratio.}$$

Accepting this initial definition at present will allow us to continue the argument, returning to the subject of zeta's precise definition later on. We now write the complete transfer function:

$$G(s) = \frac{\omega_o^2}{s^2 + 2 \zeta \omega_o s + \omega_o^2} \dots\dots\dots A(iii)$$

a not entirely unexpected result! Notice that when the discriminant is greater than zero, the damping term changes it meaning: the roots become real with no imaginary component. That is, the natural frequency of oscillation is split into two separate frequencies ω_1 and ω_2 since these are now related to either the inductor or the capacitor separately. The point at which $\zeta = 1$, R has reached its critical resistance and the numerical values of $|X_L| = |X_C| = R$ and when $\zeta = 0$ it can be seen that G(s) reduces to that of a steady state undamped oscillation as before.

An important observation should be made at this point: the equivalence of the denominators of Equations A(i) and A(iii):

$$s^2 + (RC) / (LC) s + 1/(LC) = s^2 + 2 \zeta \omega_o s + \omega_o^2$$

Which allows us to directly relate the coefficients of each equality:

$$\omega_o = (RC)/(LC) \quad \text{and} \quad \omega_o^2 = 1/(LC)$$

which implies that: $\zeta = (LC)^{-1/2}$ and $\omega_o = R (C/L)^{1/2}$

By writing out the transfer function for any second order network then factorising in a similar way, we can evaluate it in a similar manner so deriving a generalised expression for many different circuit topologies.

To gain a further insight into the relationship expressed in Equation A(iii), we can plot its complex frequency domain function, G(s), onto an s-plane plot to illustrate the positions of the roots of the polynomials of the numerator (zeros) and the denominator (poles) that make up that transfer function. The real part of the roots of G(s) are overlaid on the s-axis, whereas the imaginary parts are overlaid on the j -axis. The form of this plot can be seen with a forward reference to Figure A(iii). The s-plane plot is a generalised tool for examining the excitation, transfer and response of complex frequency domain functions, as well as the root-locus described by an alteration of one or more variables contributing to those functions, as is seen in Figure A(iii).

Plotting the Root Locus on an S-plane.

Returning to the original Transfer function G(s), we can consider a specific solution to the function's roots (in both the numerator and denominator polynomials) to find the network response to a chosen excitation. Usually the excitation will be a step function: $e(t^-) = 0, e(0) = 0$ then $e(t^+) = 1$; leading to: $E(s) = 1/s$, the response to this excitation will be considered later on. First, we will consider an impulse excitation since this makes the maths easier. We are interested in the paths that these roots will follow across the s-plane when we vary ζ . These paths are the locii through which the numerical values of the roots of the denominator pass, when the original variables are altered. The reason for choosing the denominator is that one method for finding the time domain response of a network is to form a sum of partial fractions based around the roots of the denominator of the response function (which is a product of the excitation and the transfer function: $r(t) = L^{-1}\{E(s).G(s)\}$, where E(s) is the excitation) then take their Inverse Laplace Transforms, the process will be demonstrated shortly. The sum of these transforms describes the required real response from the network. The numerator (zeros) merely contributes to the scaling of each of the component parts of the response; which on the s-plane is at right angles, "out of the paper" and is irrelevant to the factored form of the response and therefore the assessment of the root localities, but is important to the amplitude of the time domain response. That is; the response is "characterised" by the form of the denominator's roots and is referred to as the Characteristic Equation.

AN-94

To expand upon this idea, take the Characteristic Equation as:

$$\text{C.E.} = s^2 + 2\zeta\omega_n s + \omega_n^2$$

then consider the form of the roots of this equation for different values of ζ . We see three apparently different forms for the factored Characteristic Equation which are really the same thing; however, the form of the time domain response using these roots will be very different. Generally:

$$\begin{aligned} \text{C.E.} &= [s + \zeta\omega_n + \omega_n(\zeta^2 - 1)^{1/2}] \cdot [s + \zeta\omega_n - \omega_n(\zeta^2 - 1)^{1/2}] \\ &= (s + \zeta\omega_n)^2 - \omega_n^2(\zeta^2 - 1) \\ &= s^2 + 2\zeta\omega_n s + \zeta^2\omega_n^2 - \omega_n^2\zeta^2 + \omega_n^2 \\ &= s^2 + 2\zeta\omega_n s + \omega_n^2 \end{aligned}$$

When damping is greater than unity, this expression consists of two real roots which are easy to manipulate and enter into a calculator; when the damping is equal to unity the expression in root form reduces to:

$$\begin{aligned} \text{C.E.} &= (s + \omega_n) \cdot (s + \omega_n) \\ &= s^2 + 2\omega_n s + \omega_n^2 \end{aligned}$$

and when the damping is less than unity the square-root of the discriminant results in an imaginary number. As a matter of convenience we can express the complex factors of the Characteristic Equation as:

$$\begin{aligned} \text{C.E.} &= [s + \zeta\omega_n + j\omega_n(1 - \zeta^2)^{1/2}] \cdot [s + \zeta\omega_n - j\omega_n(1 - \zeta^2)^{1/2}] \\ &= (s + \zeta\omega_n)^2 + \omega_n^2(1 - \zeta^2) \\ &= s^2 + 2\zeta\omega_n s + \zeta^2\omega_n^2 + \omega_n^2 - \zeta^2\omega_n^2 \\ &= s^2 + 2\zeta\omega_n s + \omega_n^2 \end{aligned}$$

So we see that the three equations are the same, the Characteristic Equation when $\zeta = 1$ is really a special case of the first expression, leaving a choice of either a real or complex factorisation of the Characteristic Equation depending upon the value of damping which in turn is directly dependant upon the value of the resistor in the original RLC circuit in Figure A(i). By evaluating the above equations for the range of $0 < \zeta < a$ we can plot the locations of the roots on (the left hand half of) a complex plane of coordinates referred to as the s-plane. For example:

When $\zeta = 0$	$p_1 = (0, j\omega_n)$	$p_2 = (0, -j\omega_n)$
When $\zeta = 0.71$	$p_1 = (0.71\omega_n, j0.71\omega_n)$	$p_2 = (0.71\omega_n, -j0.71\omega_n)$
When $\zeta = 1$	$p_1 = (-\omega_n, j0)$	$p_2 = (-\omega_n, -j0)$
When $\zeta = a$	$p_1 = (a, j0)$	$p_2 = (0, -j0)$

Where p_1 and p_2 are the poles of the transfer function $G(s)$ and are the same as the roots of the Characteristic Equation (s_1 and s_2). The particular root locations are drawn on the s-plane in Figure A(iii). The root locii are labelled to show the path that the roots follow for the variation in damping factor ζ . The root locii only show the position of the poles in the complex frequency domain (the s-plane) and do not consider the magnitude of the response which is in a third dimension, "out-of-the-page", and will be explored later on.

By considering the form of the time domain response from this network, we can build up an appreciation for what the pole locations in the complex frequency domain mean in terms of the behaviour of the practical implementation of the network. To do this, we will find the Inverse Laplace Transform of the transfer function $G(s)$ for damping both less than and greater than unity as follows. The simplest time domain response is the network's output response to the impulse function (where the excitation is of the form $e(t-) = 0$, then $e(0) = 1$ and $e(t+) = 0$), which is simply the Inverse Laplace Transform of $G(s)$, since $E(s) = 1$, that is:

$$r(t) = L^{-1} \{E(s) \cdot G(s)\}$$

$$= L^{-1} \left\{ \frac{\omega_0^2}{s^2 + 2\zeta\omega_0 s + \omega_0^2} \right\}$$

When damping is greater than unity, the time domain response takes the form of:

$$r(t) = L^{-1} \left\{ \frac{\omega_0^2}{[s + \omega_0(\zeta + \sqrt{\zeta^2 - 1})] \cdot [s + \omega_0(\zeta - \sqrt{\zeta^2 - 1})]} \right\}$$

which we break down with partial fractions as detailed in Reference 3a as follows:

$$r(t) = \omega_0^{-1} \left\{ \frac{A}{[s + (x + y)]} + \frac{B}{[s + (x - y)]} \right\}$$

where $x = \zeta\omega_0$ and $y = \omega_0(\zeta^2 - 1)^{1/2}$, next we use the "cover-up rule" to solve A and B:

$$A = \frac{\omega_0^2}{-2y} \quad \text{and} \quad B = \frac{\omega_0^2}{2y}$$

resulting in :

$$r(t) = \frac{\omega_0^2}{2y} \cdot L^{-1} \left\{ \frac{1}{[s + (x - y)]} - \frac{1}{[s + (x + y)]} \right\}$$

$$= \frac{\omega_0^2}{2y} \cdot [e^{-(x - y)t} - e^{-(x + y)t}]$$

which is, when x and y are substituted out:

$$r(t) = \frac{\omega_0}{(\zeta^2 - 1)^{1/2}} \cdot e^{-\zeta\omega_0 t} \cdot \left[\frac{\omega_0(\zeta^2 - 1)^{1/2}t - \omega_0(\zeta^2 - 1)^{1/2}t}{2} \right]$$

$$= \frac{\omega_0}{(\zeta^2 - 1)^{1/2}} \cdot e^{-\zeta\omega_0 t} \cdot \sinh[\omega_0(\zeta^2 - 1)^{1/2}t] \quad (\text{by hyperbolic identities})$$

which is the product of two exponentials which build to a peak then decay to zero monotonically, since the $e^{-\zeta\omega_0 t}$ term decays faster than the sinh term expands. To plot this response we normalise it to unity by removing the scale factor $\omega_0 / (\zeta^2 - 1)^{1/2}$, then plot the remaining expression. This would allow us to compare the network's response against any similarly normalised responses for other network configurations. Normally an optimum response time is achieved when the damping is at $\zeta = 1/\sqrt{2}$, which is in the region where the network is said to be under-damped. Since most designers will choose this point, the above response is seldom encountered; however it can be of use when analysing the second order network's response for optimum Phase Noise, which can be shown to occur near $\zeta = 2$, for the Quadratic Characteristic Equation.

AN-94

We will now concentrate on the under-damped response from the LCR network, which is where the roots of the Characteristic Equation are complex and $\zeta < 1$. We have:

$$r(t) = L^{-1} \left\{ \frac{\omega_o^2}{[s + \omega_o + j \omega_o (1 - \zeta^2)^{1/2}] \cdot [s + \omega_o - j \omega_o (1 - \zeta^2)^{1/2}]} \right\}$$

which we break down into partial fractions as before:

$$r(t) = L^{-1} \left\{ \frac{A}{[s + (x + jy)]} + \frac{B}{[s + (x - jy)]} \right\}$$

where $x = \omega_o \zeta$ and $y = \omega_o (1 - \zeta^2)^{1/2}$ and by the "cover-up rule", A and B are:

$$A = \frac{\omega_o^2}{-2jy} \quad \text{and} \quad B = \frac{\omega_o^2}{2jy}$$

resulting in :

$$\begin{aligned} r(t) &= \frac{\omega_o^2}{2jy} \cdot L^{-1} \left\{ \frac{1}{[s + (x - jy)]} - \frac{1}{[s + (x + jy)]} \right\} \\ &= \frac{\omega_o^2}{y} \cdot \left[\frac{e^{-(x - jy)t} - e^{-(x + jy)t}}{2j} \right] \\ &= \frac{\omega_o^2}{y} \cdot e^{-xt} \left[\frac{jyt - -jyt}{2j} \right] \\ &= \frac{\omega_o^2}{y} \cdot e^{-xt} \cdot \sin yt \quad \text{(from Euler's identity)} \end{aligned}$$

which is, when x and y are substituted out:

$$r(t) = \frac{\omega_o}{(1 - \zeta^2)^{1/2}} \cdot e^{-\zeta \omega_o t} \cdot \sin [\omega_o t (1 - \zeta^2)^{1/2}]$$

Which is an exponentially decaying sinusoid of the same form as Equation A(ii). We now have the appropriate equations to express the time domain response of the network under all conditions; the root locii are plotted in Figure A(iii) with their attendant impulse responses.

TITLE: BM Document

CREATOR: BM

CR DATE:

We see that the two poles move along a semicircular path of radius w_0 for $0 < \zeta < 1$, they meet at the real axis when $\zeta = -\zeta_0$ and $\zeta = 1$. Then the $+j\zeta_0$ pole (p_2) migrates towards the origin along the negative real axis. The $-j\zeta_0$ pole (p_1) moves to the left towards $-\zeta_0$ along the negative real axis for $\zeta > 1$. Across this range of roots the impulse response is seen to change from being oscillatory at $\zeta = 0$ to being a critically damped exponential at $\zeta = 2^{-1/2}$, then to zero at $z = 1$. When $\zeta = 2^{-1/2}$ the impulse response is as shown on the plot; with this being the point at which the step response ceases to display an overshoot, more of this later on. Notice that when the roots are complex, they have both a real and an imaginary part; both of which are contributed to by R, L and C as indicated by the work we have already done equating the coefficients of s^1 and s^0 (i.e.: a_1 and a_0). For the simple response shown here, we can rapidly assess ζ_0 - the radius of the locii described by the conjugate roots when altering ζ (i.e.: R alone). We see that:

$$\zeta_0 = [(\text{Re}(s_1))^2 + (\text{Im}(s_2))^2]$$

and

$$= \sin(\text{Im}[s_1]/\zeta_0)$$

$$= \cos(\text{Re}[s_1]/\zeta_0)$$

this last statement we usually interpret as a magnitude only, that is: $\zeta = |\cos \theta|$, where θ is the acute angle formed at the origin, by the radius from the complex root location (s_1) to the sigma axis. We now have a complete definition for damping.

AN-94

A further insight into the response of the network can be gained if we consider its time domain transient response for the range $0 < \zeta < 1$ (that is, whilst the poles are “migrating” around the semicircle) when a step function is used to excite the network. These are derived in the next section. Notice that the responses on the diagram are impulse responses not step responses; similarly, only the “zeros” of the denominator are plotted, the numerator of the transfer function is ignored when forming the root-locii of the characteristic equation. The root locus technique used here is similar in form, but is distinctly different from that for the complete response. It can be applied to any polynomial but requires interpretation to appreciate the form of the time domain response available when the polynomial relates to a particular network. The consideration of the zeros of the numerator and denominator polynomials of the transfer function with its forcing function is fundamental to the study of network responses, it is considered to be beyond a note such as this; reference 5 gives further reading.

The adoption of a graphical technique allows a plethora of trigonometric solutions to be brought to bear, allowing seemingly trivial equations to be written for the time domain response, component values and the (so-called) “frequency domain” response (angle and magnitude criteria).

Transient Response.

Consider: if the R L C network is at its zero state and is then excited by a step-function, $u(t)$, where $e(-t) = 0$ and $e(t) = 1$, we get the following time response:

$$\begin{aligned}
 v_C(t) &= L^{-1} \left\{ \frac{1}{s} \cdot \frac{\omega_o^2}{s^2 + 2\zeta\omega_o s + \omega_o^2} \right\} \\
 &= L^{-1} \left\{ \frac{1}{s} \cdot \frac{\omega_o^2}{(s^2 + 2\zeta\omega_o s + \omega_o^2) + (\omega_o^2 - 2\zeta^2\omega_o^2)} \right\} \quad \text{(by manipulation)} \\
 &= L^{-1} \left\{ \frac{1}{s} \cdot \frac{\omega_o^2}{(s + \zeta\omega_o)^2 + \omega_o^2(1 - \zeta^2)} \right\} \\
 &= L^{-1} \left\{ \frac{1}{s} - \frac{s + 2\zeta\omega_o}{(s + \zeta\omega_o)^2 + \omega_o^2(1 - \zeta^2)} \right\} \quad \text{(by partial fractions)} \\
 &= L^{-1} \left\{ \frac{1}{s} - \frac{(s + \zeta\omega_o) + \zeta\omega_o}{(s + \zeta\omega_o)^2 + \omega_o^2(1 - \zeta^2)} \right\} \\
 &= L^{-1} \left\{ \frac{1}{s} - \frac{(s + \zeta\omega_o)}{(s + \zeta\omega_o)^2 + \omega_o^2(1 - \zeta^2)} - \frac{\zeta\omega_o}{\omega_o(1 - \zeta^2)^{1/2}} \cdot \frac{\omega_o(1 - \zeta^2)^{1/2}}{(s + \zeta\omega_o)^2 + \omega_o^2(1 - \zeta^2)} \right\} \\
 &= 1 - (-\zeta\omega_o t) \cdot \cos[\omega_o t(1 - \zeta^2)^{1/2}] - \frac{\zeta\omega_o}{(1 - \zeta^2)^{1/2}} \cdot (-\zeta\omega_o t) \cdot \sin[\omega_o t(1 - \zeta^2)^{1/2}] \\
 &= 1 - (-\zeta\omega_o t) \cdot \left\{ \cos[\omega_o t(1 - \zeta^2)^{1/2}] + \frac{\zeta\omega_o}{(1 - \zeta^2)^{1/2}} \cdot \sin[\omega_o t(1 - \zeta^2)^{1/2}] \right\}
 \end{aligned}$$

The term $\omega_o(1 - \zeta^2)^{1/2}$ is referred to as the natural frequency of damped oscillation: ω_d . This is the frequency of the “ring” seen when the lightly damped network is excited by an impulse or step function. Notice that the frequency of oscillation is affected by the damping factor. The expression can therefore be rewritten as:

$$\begin{aligned}
 v_C(t) &= 1 - (-\zeta\omega_o t) \cdot \left[\cos(\omega_d t) + \frac{\zeta\omega_o}{(1 - \zeta^2)^{1/2}} \cdot \sin(\omega_d t) \right] \\
 &= 1 - \frac{(-\zeta\omega_o t)}{(1 - \zeta^2)^{1/2}} \left[(1 - \zeta^2)^{1/2} \cdot \cos(\omega_d t) + \zeta\omega_o \cdot \sin(\omega_d t) \right]
 \end{aligned}$$

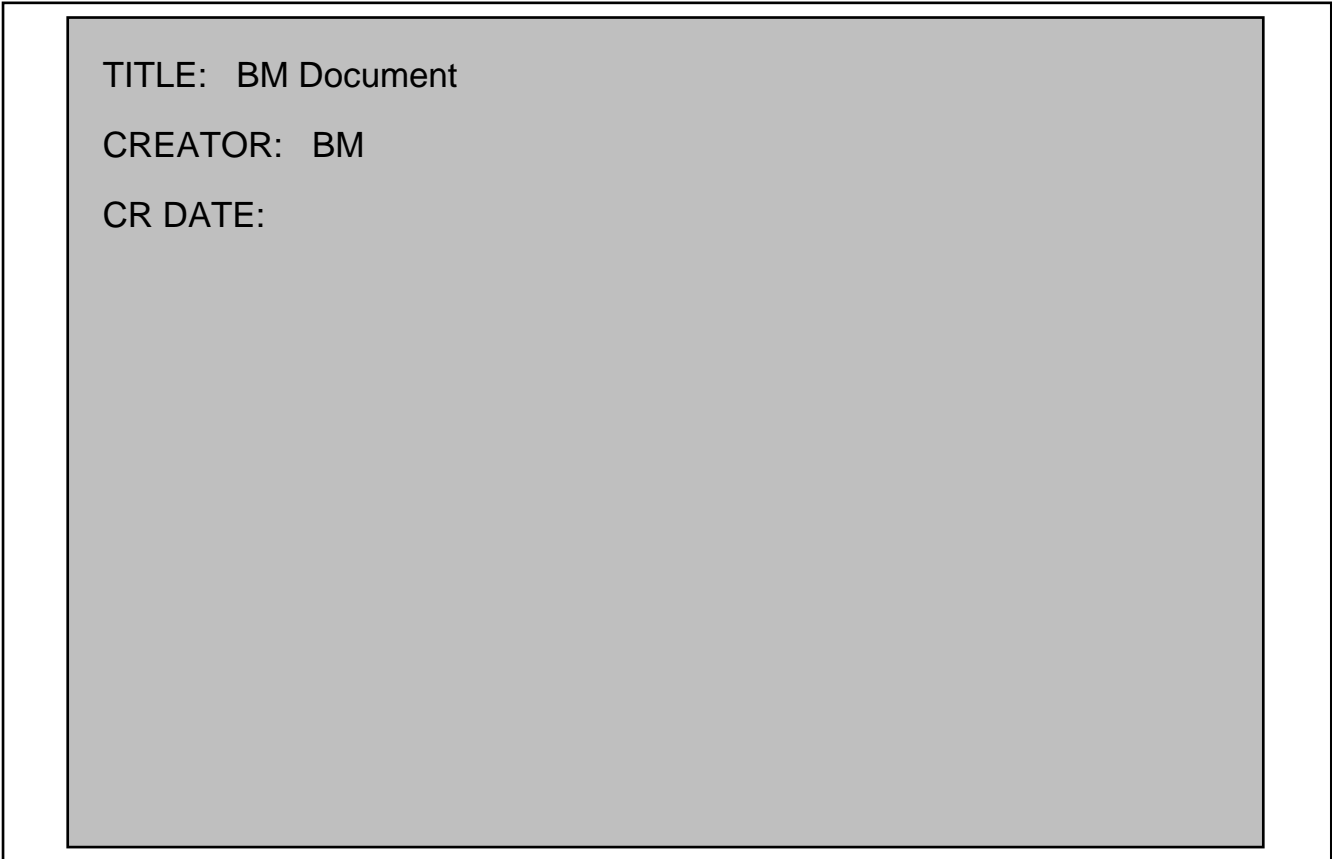
Now, damping is always in the range of $0 < \zeta < 1$, allowing us to simplify the expression further using basic trigonometric ratios; if $\zeta = \cos \phi$ (where ϕ is the angle from the root to the s axis) we can say that $1 - \zeta^2 = 1 - \cos^2 \phi = \sin^2 \phi$. So the expression can be rewritten:

$$v_C(t) = 1 - \frac{e^{-\zeta \omega_n t}}{(1 - \zeta^2)^{1/2}} \cdot [(\sin^2 \phi)^{1/2} \cdot \cos(\omega_d t) + \cos \phi \cdot \sin(\omega_d t)]$$

$$= 1 - \frac{e^{-\zeta \omega_n t}}{(1 - \zeta^2)^{1/2}} \cdot \sin(\omega_d t + \phi) \dots\dots\dots A(iv)$$

(by basic trig. identities)

where $\omega_d = \omega_n (1 - \zeta^2)^{1/2}$, for $0 < \zeta < 1$ and $\phi = \cos^{-1}(\zeta)$. The response that the network gives to the step function is drawn in Figure A(iv), being the visualisation of Equation (B4) with ω_n normalised to one second and ζ equal to 0.2.



Here we see that the amplitude of the oscillatory response is directly related to the damping ratio ζ , which indirectly affects the oscillatory frequency ω_d . The positioning of the oscillatory train moves closer to the step function's rising edge (responds faster) with decreased damping since the phase angle ϕ becomes smaller, therefore $\sin \phi$ is smaller, leading to reduced delay in the response time. Once the time domain response can be drawn (or measured on the bench) it becomes relatively easy to calculate ω_n and ζ from the frequency of oscillation and the rate of decay of the oscillatory ring's envelope.

AN-94

Overshoot

To find σ_o and ω_d we need to follow a somewhat tortuous route to derive formulae for these, first we find the damping, then solve the above response for σ_o . This is done by measuring the time and amplitude between the start of first peak of the first positive (or negative) peak of the overshoot, where $d/dt[v_C(t)] = 0$. By assuming that the response being studied has only two dominant conjugate poles such that the successive peaks are monotonically decreasing with time, we can derive a formula for the overshoot expressed as a fraction of the unit step function initiating that overshoot. Given that:

$$\begin{aligned} \frac{d}{dt} [v_C(t)] &= \frac{d}{dt} \left[1 - \frac{e^{-\sigma_o t}}{(1 - \zeta^2)^{1/2}} \cdot \sin(\omega_d t + \phi) \right] \\ &= 0 - \frac{1}{(1 - \zeta^2)^{1/2}} \cdot \frac{d}{dt} [e^{-\sigma_o t} \cdot \sin(\omega_d t + \phi)] \\ &= - \frac{1}{(1 - \zeta^2)^{1/2}} \cdot \frac{d}{dt} [u \cdot v] \end{aligned} \quad \begin{aligned} \text{where } u &= e^{-\sigma_o t} \\ v &= \sin(\omega_d t + \phi) \end{aligned}$$

Now: $\frac{d}{dt} [u \cdot v] = v \cdot du + u \cdot dv$ where $du/dt = -\sigma_o e^{-\sigma_o t}$
and $dv/dt = \omega_d \cos(\omega_d t + \phi)$

$$= \sin(\omega_d t + \phi) [-\sigma_o e^{-\sigma_o t}] + e^{-\sigma_o t} \cdot \omega_d \cos(\omega_d t + \phi)$$

such that; $\frac{d}{dt} [v_C(t)] = \frac{d}{dt} \left[\frac{e^{-\sigma_o t}}{(1 - \zeta^2)^{1/2}} \cdot \cos(\omega_d t + \phi) \right] - \frac{\sigma_o e^{-\sigma_o t}}{(1 - \zeta^2)^{1/2}} \cdot \sin(\omega_d t + \phi)$

This expression allows us to find the time between the peaks of the time domain response's "ring" when equated to zero. It is simplified as follows, by using $\omega_d = \omega_o(1 - \zeta^2)^{1/2}$ and $\phi = \cos^{-1} \zeta$. Given that:

$$\begin{aligned} \frac{e^{-\sigma_o t}}{(1 - \zeta^2)^{1/2}} \cdot \sin(\omega_d t + \phi) &= \frac{e^{-\sigma_o t}}{(1 - \zeta^2)^{1/2}} \cdot \cos(\omega_d t + \phi) \\ \Rightarrow \frac{e^{-\sigma_o t}}{(1 - \zeta^2)^{1/2}} \cdot \omega_o \sin(\omega_d t + \phi) &= \frac{e^{-\sigma_o t}}{(1 - \zeta^2)^{1/2}} \cdot \omega_o \cos(\omega_d t + \phi) \\ \Rightarrow \omega_o \sin(\omega_d t + \phi) &= \omega_o \cos(\omega_d t + \phi) \end{aligned}$$

Next substitute in: $\phi = \cos^{-1} \zeta$, and $\omega_d = \omega_o(1 - \zeta^2)^{1/2} = \omega_o(1 - \cos^2 \phi)^{1/2} = \omega_o \sin \phi$, to give:

$$\begin{aligned} \omega_o \cos \phi \cdot \sin(\omega_d t + \phi) &= \omega_o \sin \phi \cdot \cos(\omega_d t + \phi) \\ \Rightarrow \frac{\omega_o}{\omega_o} \cdot \frac{\sin(\omega_d t + \phi)}{\cos(\omega_d t + \phi)} &= \frac{\sin \phi}{\cos \phi} \\ \Rightarrow \tan(\omega_d t + \phi) &= \tan \phi \end{aligned}$$

That is, when $\tan(\omega_d t + \phi) = \tan \phi$, then the amplitude of $v_C(t)$ has reached a maximum or a minimum ($d/dt = 0$) such that $\tan(\omega_o t) = \tan(k \phi)$, where k is an integer, at these points in the response. Therefore we can write this as a repeating function of ϕ since $\tan \phi = \tan(2\phi + \phi)$ implying that $\omega_d t = k \phi$, where k is even for the troughs and odd for the peaks, therefore:

$$\begin{aligned} t &= k \phi / \omega_d \quad (\text{where } t \text{ is an integer multiple of a half cycle of } \omega_d) \\ &= k \phi / [\omega_o(1 - \zeta^2)^{1/2}] \end{aligned}$$

Which is an expression that could probably have been guessed at intuitively. It allows us to find the time to each successive peak (or trough), for example the minimum peak overshoot occurs when $k = 1$ (all the transient responses have died away) and is usually the final steady state level. w_d is seen to be the reciprocal of the time between peaks or troughs of the oscillatory response. We find that:

$$t_{\text{peak } n} = \frac{(2n - 1)}{\omega_d (1 - \zeta^2)^{1/2}} \dots\dots\dots A(v) \qquad t_{\text{trough } n} = \frac{2n}{\omega_d (1 - \zeta^2)^{1/2}} \dots\dots\dots A(vi)$$

where n is the number of peaks or troughs we wish to calculate after the transient. These values can then be put back into $v_C(t)$ to find the value of the amplitude at that time. Using these values we can then derive the formula for the peak's "fractional overshoot", where we wish to know the relationship between the levels of $v_C(t)$ when $t = 0^-$ and $t = t_{\text{peak } 1}$. The level of peak 1 is then expressed as a fractional part of $v_C(t)$ and is represented by g (gamma). That is:

$$g_1 = \frac{v_C(t_{\text{peak } 1}) - v_C(0^-)}{v_C(0^-)} \qquad \text{where } g_1 \text{ is for peak 1, and } a = \text{infinity}$$

$$= v_C(t_{\text{peak } 1}) - 1 \qquad v_C(t) = 1 \text{ as } t \rightarrow \infty$$

Substituting Equation A(v) into A(iv), then using the identities $\cos \theta = \sin(\pi/2 - \theta)$ and $(1 - \zeta^2)^{1/2} = \sin \phi$, we have (with no loss of generality):

$$g_n = 1 - \frac{e^{-\zeta \omega_n t_{\text{peak } n}}}{(1 - \zeta^2)^{1/2}} \cdot \sin(\omega_d t_{\text{peak } n} + \phi) - 1$$

$$= - \left[\frac{e^{-\zeta \omega_n (2n - 1) / \omega_d (1 - \zeta^2)^{1/2}}}{(1 - \zeta^2)^{1/2}} \cdot \sin\left[\omega_d (1 - \zeta^2)^{1/2} \cdot \frac{(2n - 1)}{\omega_d (1 - \zeta^2)^{1/2}} + \phi\right] \right] \cdot \frac{1}{(1 - \zeta^2)^{1/2}}$$

$$= - \left[\frac{e^{-(2n - 1)\zeta}}{(1 - \zeta^2)^{1/2}} \right] \cdot \frac{\sin[(2n - 1)\phi + \phi]}{(1 - \zeta^2)^{1/2}}$$

$$= - \left[\frac{(2n - 1) \cos \phi}{\sin \phi} \right] \cdot \frac{\sin[(2n - 1)\phi + \phi]}{\sin \phi}$$

$$= - (2n - 1) \cot \phi \cdot \frac{\sin \phi}{\sin \phi} \qquad \text{(where } \sin[(2n - 1)\phi + \phi] = -\sin \phi)$$

$$= [- (2n - 1) \cot \phi] \qquad \text{(where } \cot \phi = \zeta / (1 - \zeta^2)^{1/2})$$

$$= \left[\frac{-(2n - 1)}{(1 - \zeta^2)^{1/2}} \right] \dots\dots\dots A(vii)$$

This last expression shows that the peak overshoot is determined entirely by the damping factor ζ . A similar equation could be derived for the troughs using simply $2n$ instead of $2n - 1$. Notice that the peak overshoot has a positive fractional value, whereas the trough overshoot will have a negative fractional value. For passive networks these values are always less than unity due to the conservation of energy. When we start to look at active networks it will be seen that ζ can be greater than unity (when $\zeta < 0$) and is in fact the requirement for an oscillator to initiate its oscillatory function.

AN-94

Damping

Once the response of a network can be predicted from a known value of ζ and ω_n , we can set about constructing the circuit. There is a good chance that we will wish to verify that it works as intended. Therefore it would be wise to arm ourselves with a formula for calculating ζ and ω_n from experimentally measured values for σ and τ ; this process is the reverse of that already described. Once σ and ω_n are known, the s-plane plot and time domain response (to the unit step function) for the practical unit can be generated then compared with that for the initial design procedure. Considering Equation A(vii), we can derive an expression for damping. This will be found to be of utility for dealing with active feedback devices as well as for passive networks. First we take Equation A(vii) and rearrange it so:

$$n = \left[\frac{-(2n - 1)}{(1 - \zeta^2)^{1/2}} \right]$$

$$\Rightarrow \ln n = \frac{-(2n - 1)}{(1 - \zeta^2)^{1/2}}$$

$$\Rightarrow (1 - \zeta^2)^{1/2} \cdot \ln n = -(2n - 1)$$

$$\Rightarrow \frac{(1 - \zeta^2)^{1/2}}{\ln n} = \frac{-(2n - 1)}{\ln n}$$

$$\Rightarrow \frac{1 - \zeta^2}{\ln^2 n} = \left[\frac{-(2n - 1)}{\ln n} \right]^2$$

$$\Rightarrow 1 - \zeta^2 = 2 \left[\frac{-(2n - 1)}{\ln n} \right]^2$$

$$\Rightarrow 1 = 2 \left\{ \left[\frac{-(2n - 1)}{\ln n} \right]^2 + 1 \right\}$$

$$\Rightarrow 2 = \left\{ \left[\frac{-(2n - 1)}{\ln n} \right]^2 + 1 \right\}^{-1}$$

therefore:
$$= \left\{ \left[\frac{-(2n - 1)}{\ln n} \right]^2 + 1 \right\}^{-1/2} \dots\dots\dots A(viii)$$

Where n is the number of the peaks after the transient that we are measuring, σ_n is the observed overshoot with respect to the value of $v_C(t)$ when $t \rightarrow \infty$, expressed as a fraction of that settled value. For example: from Figure A(iv) we can read off a value for $v_C(t)$ of 1.5266 for the first peak, giving a value of $\sigma_1 = 0.5266$ such that:

$$= \left\{ \left[\frac{-}{\ln 0.5266} \right]^2 + 1 \right\}^{-1/2} = 0.200$$

As would be expected! Practically it may be difficult to measure the absolute value of the first peak with respect to the $t = 0$ -value of $v_C(t)$ as the initial part of the step may be lost due to instrument (scope trigger) delays. To avoid this, we need a general expression to allow us to select any two peaks from later on in the response. These should not necessarily be consecutive peaks as it would be difficult to measure their amplitude difference for small damping factors.

If we consider the equation for the peak of the first overshoot to be true, then call the first peak of interest peak n and the second peak of interest peak m we can re-define Equation A(viii) as:

$$\frac{m}{n} = \left\{ \frac{-(2m - 1) - (2n - 1)}{(1 - 2)^{1/2}} \right\} \quad \text{(with working similar to the above)}$$

$$= \left[\frac{2(n - m)}{(1 - 2)^{1/2}} \right]$$

This last expression allows us to evolve a second equality for damping based upon the two peaks n and m (N.B: they occur in that order); from the above:

$$\Rightarrow \ln \frac{m}{n} = \frac{2(n - m)}{(1 - 2)^{1/2}}$$

therefore:

$$= \left\{ \left[\frac{2(n - m)}{\ln m/n} \right]^2 + 1 \right\}^{-1/2} \dots\dots\dots A(ix)$$

To demonstrate this last statement, take n = 1 and m = 3; that is, the first and third peaks. Using Equation A(vii) to calculate the third peak overshoot value as being $\zeta_3 = 0.0405$, we see:

$$= \left\{ \left[\frac{2(1 - 3)}{\ln (0.0405/0.5226)} \right]^2 + 1 \right\}^{-1/2} = 0.200 \text{ again, as expected.}$$

Settle Time

Occasionally, it is useful to know how quickly a transient response of a network will “settle” to within a certain error band (unit step + fractional error), that is, the envelope containing the oscillating response decays to a particular fraction of the initial step. The design effort required to select a particular transfer function frequently starts from a knowledge of the particular minimum settle time needed to settle to a specified fraction of a known step size. The following derivation does not necessarily follow on from the prior work, it is included here for the sake of completeness.

We know from the basic definition of the Laplace Transform that we multiply the function by a converging factor e^{-st} , which describes the transient part and the steady state part of the response of the function as determined when $s = -\sigma + j\omega$. That is:

$$e^{-st} = e^{-(\sigma + j\omega)t}$$

$$= e^{-\sigma t} \cdot e^{-j\omega t}$$

which describes the two axes of the s-plane. Here we are only interested in the $e^{-\sigma t}$ term which describes the transient “envelope” as determined by the vertical projection from a pole to the sigma axis. This is referred to as the damping term for the complete response since $\sigma = -\zeta\omega_n$. This is convenient as it allows us to find the time domain response of the exponential (envelope) decay directly: take t_s = settle time, to E (eta) = error band, as a ratio of the “unit” step. Therefore we can say that when:

$$e^{-\sigma t} = E$$

then: $\ln E = -\sigma t$

such that: $t_s = \frac{-\ln E}{\sigma} \dots\dots\dots A(x)$

AN-94

For example, from Figure A(iv) where $\zeta = 0.200$ and $\omega_n = 1$, the settle time to $\epsilon = 0.01$ (1%), will be 23.026 time constants, where the time constant is $1/\sigma$. Therefore the period of oscillation is $2\pi/\omega_d = 6.413 \cdot t$ ($= 6.413s$ for this example if $\omega_n = 1$ radian per second). The last peak at 22.445 Time Constants (the fourth peak) will just come into the error band on its falling edge. Notice that for some ratios, the error band will be achieved somewhat earlier by the previous peak (or trough) rather than when the decay envelope passes into the error band. The solution for an exact expression is complicated and beyond the scope of a note such as this. As a final point, we can rearrange this equation to give an expression for ω_n given that we need to meet a stipulated settle time. Nominally, we choose ζ to be 0.7071 leaving only ω_n to find:

$$\omega_n = \frac{-\ln \epsilon}{t_s} \dots\dots\dots A(xi)$$

These formulae will be of practical utility since we can usually approximate a high order transfer function by the quadratic function (across a small range of their roots) provided we scale them appropriately. By doing so we can make a quick empirical guess at the correct solution.

Magnitude, Phase and Delay.

These parameters are studied in the “Frequency Domain” rather than the Time Domain, using the steady state sinusoidal response of a network. This involves investigating the effect upon the network’s response when using an excitation that only has poles and zeros on the $j\omega$ axis. To find this type of Driving point function, we shall look at a sine wave which has poles at $\pm j \omega_1$:

$$L \{ \sin \omega_1 t \} = \frac{1}{s^2 + \omega_1^2}$$

$$= \frac{1}{(s + j \omega_1)(s - j \omega_1)}$$

Showing that the poles are on the j - axis since $\zeta = 0$ and $j = j \omega_1$. Now if we find the time domain form of this last statement we see the complex exponential form of the original sine wave function:

$$L^{-1} \left\{ \frac{1}{(s + j \omega_1)(s - j \omega_1)} \right\} = L^{-1} \left\{ \frac{A}{(s + j \omega_1)} + \frac{B}{(s - j \omega_1)} \right\}$$

where the coefficients are: $A = \frac{1}{-2j \omega_1}$ when $s = -j \omega_1$

and: $B = \frac{1}{2j \omega_1}$ when $s = j \omega_1$, by the “cover up” rule.

by substituting for A and B we can now write:

$$\sin \omega_1 t = L^{-1} \left\{ \frac{1}{2j(s - j \omega_1)} \right\} - L^{-1} \left\{ \frac{1}{2j(s + j \omega_1)} \right\}$$

$$= 1/2j \{ e^{j \omega_1 t} - e^{-j \omega_1 t} \}$$

Proving by manipulation that the original poles were on the j axis, i.e. $\omega = 0$, in the process the steps used to perform the Laplace Transform and its inverse. A similar procedure is used to illustrate the poles of the cosine wave:

$$\begin{aligned} L\{\cos \omega t\} &= \frac{s}{s^2 + \omega^2} \\ &= \frac{s}{(s + j\omega)(s - j\omega)} \end{aligned}$$

such that: $L^{-1}\left\{\frac{s}{(s + j\omega)(s - j\omega)}\right\} = L^{-1}\left\{\frac{C}{(s + j\omega)} + \frac{D}{(s - j\omega)}\right\}$

where: $C = \frac{-j\omega}{-2j\omega}$ when $s = -j\omega$ and $D = \frac{j\omega}{2j\omega}$ when $s = j\omega$ by the "cover up" rule.

We can now write:

$$\begin{aligned} \cos \omega t &= L^{-1}\left\{\frac{1}{2(s - j\omega)}\right\} - L^{-1}\left\{\frac{1}{2(s + j\omega)}\right\} \\ &= 1/2\{e^{j\omega t} + e^{-j\omega t}\} \end{aligned}$$

which also has a zero at the origin due to the s term in the numerator of the function. Both of these excitations fulfil our requirement for poles and zeros on the $j\omega$ axis only. The s -plane plots of these driving point functions are shown in Figure A(v).

TITLE: BM Document

CREATOR: BM

CR DATE:

If we multiply these driving point functions by a network transfer function we see the complex frequency domain response, similarly we can add the poles and zeros of both functions to the s -plane plot to see the complete response of that network to the chosen excitation. Consider the plot for a cosine excitation, $F(s) = L\{\cos \omega t\}$ and that for an integrator, $H(s) = L\{1\} = 1/s$; which will produce the response, $R(s) = L\{r(t)\}$. The pole and zero locations are shown in the LHS of Figure A(vi) and the pole / zero cancellation at the origin is shown in the RHS of Figure A(vi).

TITLE: BM Document

CREATOR: BM

CR DATE:

We know mathematically that the integral of a cosine wave is a sine wave of the same period with a scale factor of $1/\omega_1$ which only effects the amplitude, so the result seems correct and makes a powerful design tool. To investigate this further, we can extrapolate this method to that of a series R C low pass filter as in Figure A(vii).

TITLE: BM Document

CREATOR: BM

CR DATE:

Using this, we see how a steady state excitation such as $\cos \omega_1 t$ will undergo a magnitude and phase transformation, thus:

$$r(t) = L^{-1} \{ (s) \cdot H(s) \}$$

$$= L^{-1} \left\{ \frac{s}{s^2 + \omega_1^2} \cdot \frac{\omega_0}{s + \omega_0} \right\} \quad \text{where } \omega_0 = 1/RC$$

$$= L^{-1} \left\{ \frac{Fs + G}{s + \omega_0} + \frac{1}{s^2 + \omega_1^2} \right\} \quad \text{To enable us to form Partial Fractions.}$$

The coefficients E,F and G are:

$$E = \frac{-\omega_0^2}{\omega_0^2 + \omega_1^2} \quad \text{when } s = -\omega_0 \text{ by the cover up method.}$$

$$F = \frac{\omega_0^2}{\omega_0^2 + \omega_1^2} \quad \text{and} \quad G = \frac{\omega_0^2}{\omega_0^2 + \omega_1^2} \cdot \frac{\omega_1^2}{\omega_0} \quad \text{with working.}$$

Using these coefficients, we can state:

$$r(t) = \frac{\omega_0^2}{\omega_0^2 + \omega_1^2} - L^{-1} \left\{ \frac{-1}{s + \omega_0} + \frac{s}{s^2 + \omega_1^2} + \frac{1}{\omega_0} \cdot \frac{1}{s^2 + \omega_1^2} \right\}$$

$$= \frac{\omega_0^2}{\omega_0^2 + \omega_1^2} \left[-e^{-\omega_0 t} + \cos \omega_1 t + \frac{1}{\omega_0} \sin \omega_1 t \right]$$

which can be seen to be an amplitude scaling term $\omega_0^2 / (\omega_0^2 + \omega_1^2)$, an exponential which decays away and a steady state term which displays a constant peak magnitude once the transient has expired. This sinusoidal term has an arbitrary delay to its peak with respect to the excitation as determined by the ratio of ω_1 / ω_0 , where ω_1 is related to the excitation and ω_0 related to the network as would be expected. By trigonometric compound angle identities, we can re-write the cosine and sine terms as:

$$\cos \omega_1 t + \frac{1}{\omega_0} \sin \omega_1 t = r \cos(\omega_1 t - \phi) \quad \text{where } r = [1^2 + (\omega_1 / \omega_0)^2]^{1/2} \text{ and } \phi = \text{atan}(\omega_1 / \omega_0)$$

such that:

$$\text{LHS} = \left(\frac{\omega_0^2 + \omega_1^2}{\omega_0^2} \right)^{1/2} \cdot \cos\{\omega_1 t - \text{atan}(\omega_1 / \omega_0)\}$$

which if substituted into r(t) from above results in a complete time domain result of:

$$r(t) = \frac{\omega_0^2}{\omega_0^2 + \omega_1^2} \cdot [e^{-\omega_0 t} + \left\{ \frac{\omega_0^2 + \omega_1^2}{\omega_0^2} \right\}^{1/2} \cdot \cos\{\omega_1 t - \text{atan}(\omega_1 / \omega_0)\}]$$

and when $\omega_1 = \omega_0 = 1/RC$

$$\begin{aligned} r(t) &= 1/2 [e^{-t/RC} + 2^{1/2} \cdot \cos\{t/RC - \text{atan}(1)\}] \\ &= 1/2 [0 + 1.414 \cdot \cos(\omega_1 t - \phi/4)] \quad \text{where } e^{-t/RC} \rightarrow 0, \text{ as } t \rightarrow \infty \\ &= 0.7071 \cos(\omega_1 t - \phi/4) \end{aligned}$$

after the exponential has died away. This shows that the response of the network (when the excitation frequency is equal to ω_0) has a magnitude of 0.7071 and a phase angle of $-\phi/4$.

The magnitude and phase terms are considered to be on the ω -axis of a three dimensional plot, where the ϕ -axis is at right angles but "out of the page" to the x and y axes. They (Magnitude and Phase) are plotted on planes that intersect the s-plane and each other at the j axis (x axis) only. These form the Bode plots so commonly seen in Data Sheets. To view the Bode Plots we rotate the three dimensional plot about the x-axis until the y axis is out of the page; we then interchange the x and z axes to produce a pair of plots with frequency as the domain and the Magnitude or Phase as the range. Consider the pole-zero plot for the response R(s) as in figure A(viii):

TITLE: BM Document

CREATOR: BM

CR DATE:

If we draw a line from the pole due to H(s) (at $-\omega_0$ on the s axis) to the pole due to the excitation, ω_1 (s), which occurs at on the j axis, we see that the length of the line is:

$$(\omega_0^2 + \omega_1^2)^{1/2} = 1.414 \quad \text{if we normalise } \omega_0 = \omega_1 = 1.$$

This is the reciprocal of the magnitude term described earlier; we could have stated:

$$M(\omega_1) = \frac{1}{(\omega_1^2 + \omega_0^2)^{1/2}} \quad \text{where: } s = j\omega_1, s = 0$$

AN-94

The proof of this graphical interpretation of the s-plane to provide the frequency response can be found in the transfer function of a single pole's response in terms of its steady state conditions. Given that:

$$H(s) = \frac{O}{s + \sigma}$$

We set $s = j\omega$ and $s = 0$: $H(j\omega) = \frac{O}{j\omega + \sigma}$

We now wish to find the Inverse Phasor Transform of $H(j\omega)$, to obtain the time domain response at the frequency of excitation (ω). See reference 1, page 257 for Phasor Transforms. The transformation of $H(j\omega)$ is;

$$h(\omega) = M(\omega) e^{-j(\omega t + \phi)}$$

where: $M(\omega) = O \cdot \{[\text{Im}\{H(j\omega)\}]^2 + [\text{Re}\{H(j\omega)\}]^2\}^{-1/2}$ which is a vector magnitude,

and: $\phi(\omega) = \text{atan} [\text{Im}\{H(j\omega)\} / \text{Re}\{H(j\omega)\}]$ which is a phase angle.

This is then written in an abbreviated form: $h(\omega) = \text{Re}\{M(\omega) e^{-j\omega t}\}$ where the $j\omega t$ term in the exponential is considered to be implicit in the definition. Examination of reference 5, page 215 reveals the following formulae for multiple poles and zeroes:

$$M(\omega) = \frac{\prod_{i=0}^n \text{vector magnitude from the zeros to excitation frequency on the } j \text{ axis}}{\prod_{j=0}^m \text{P vector magnitude from the poles to excitation frequency on the } j \text{ axis}} \dots\dots\dots A(xii)$$

and: $\phi(\omega) = \sum_{i=0}^n \text{angles of the vectors from the zeros to a perpendicular to the } j \text{ axis}$
 $\quad \quad \quad - \sum_{j=0}^m \text{angles of the vectors from the poles to a perpendicular to the } j \text{ axis} \dots\dots\dots A(xiii)$

where \prod means "the product of" and \sum means "the sum of". We can use these equations to determine the magnitude and phase of the steady state frequency response for our Quadratic network. It will be found that the Magnitude Bode plot will be of interest whereas the phase plot will be of limited use when dealing with Phase-locked Loops.

To calculate the steady state response of G(s) for all excitation frequencies in general, we make $s = j\omega$ for $0 < \omega < \infty$, then refer to Equation A(iii) with its roots for $\omega < 1$ and to Equation A(xii), then write:

$$\begin{aligned}
 M(j\omega) &= \frac{\omega^2}{(j\omega - [-\omega_0 + j\omega_0(1 - \zeta^2)^{1/2}]) \cdot (j\omega - [-\omega_0 - j\omega_0(1 - \zeta^2)^{1/2}])} \\
 &= \frac{\omega^2}{(j\omega - \omega_0)^2 + \omega_0^2(1 - \zeta^2)} \\
 &= \frac{\omega^2}{-\omega^2 - 2j\omega\omega_0\zeta + \omega_0^2 + \omega_0^2 - 2j\omega_0^2\zeta} \\
 &= \frac{\omega^2}{\omega_0^2 - 2j\omega\omega_0\zeta - \omega^2}
 \end{aligned}$$

Which is normalised by dividing through by ω_0^2 then rearranged:

$$= \frac{1}{[1 - (\omega/\omega_0)^2] - 2j(\omega/\omega_0)\zeta}$$

Now, $M(\omega)$ is the absolute value of the vector magnitude of the complex and real parts of the networks steady state response when $s = j\omega$, so we square both, add them, then take the root to remove the operator j , so finding the vector's magnitude:

$$M(\omega) = \{ [1 - (\omega/\omega_0)^2]^2 + [2(\omega/\omega_0)\zeta]^2 \}^{-1/2} \dots\dots\dots A(xiv)$$

Which is plotted (on logarithmic axes) in Figure A(ix). Returning to R(s) in Figure A(viii) the RC pole-zero plot, we see that the line imposed from the pole of H(s) to that of E(s), makes an angle of $\pi/4$ to the s axis. This angle can be arrived at by taking the argument of the Imaginary projection of the line and the real projection of the line when the first is divided by the second:

$$\begin{aligned}
 &= \tan^{-1} \left[\frac{\text{Imaginary projection}}{\text{Real projection}} \right] \\
 &= \tan^{-1} [-1] \\
 &= -\pi/4
 \end{aligned}$$

such that a similarity to the equation given for Phase, Equation A(xiii), can be seen since the above relationship expresses the phase angle for a single pole (ω_0) to the excitation ($\cos \omega t$). Equation A(xiii) shows us that the poles cause a phase lag and the zeros a phase lead. Using Equation A(xiii), we can now express the Phase of our Quadratic response with respect to the input (sinewave) excitation by summing the angle of each pole, since there are no zeros in this response:

$$\phi(\omega) = 0 - \tan^{-1} \left[\frac{-\omega_0(1 - \zeta^2)^{1/2}}{\omega} \right] - \tan^{-1} \left[\frac{+\omega_0(1 - \zeta^2)^{1/2}}{\omega} \right] \quad A(xv)$$

The result of Equation A(xv) is plotted in Figure A(ix) in degrees; $\phi(\omega) \cdot (180/\pi)$. The top trace is for $M(\omega)$ whereas the bottom trace is for $\phi(\omega)$.

TITLE: BM Document

CREATOR: BM

CR DATE:

Notice that these relationships are for one point - they must be re-evaluated across the range of , to produce the set of Bode Plots in Figure A(ix).

One further parameter is associated with a network response. That of delay; two terms are generally used. First phase delay, where the delay of the output waveform's peak is delayed in time with respect to the input waveform at one particular frequency. The delay is specified as a fraction of one cycle of the excitation frequency. Therefore if a delay is more than one cycle, the concept of phase lead can be introduced.

The other delay term used is a time delay; where the response takes time to appear. This can be due to either energy storage or propagation; i.e: through a cable. This is termed group delay, being defined as the derivative of phase with respect to incremental frequency:

$$t_{gd} = d/d [()] \dots\dots\dots A(xvi)$$

This can be of importance when studying the Time Domain pulse response of a network since a change in group delay results in a change in phase for the same (quadrature) frequency. The network will alter the shape of the original pulse; consider the reconstruction of the Fourier series representing the input pulse, once operated upon by the network. The phase of each quadrature component will be altered differently for each discrete frequency in the output spectra. The addition of these will result in a distorted pulse shape at the output.

An evaluation of Equation (xvi) will show that the zeros give a negative group delay, whilst the poles give a positive group delay. Delay information is not normally considered when designing PLLs, so this will not be dealt with here, reference 5 page 245 picks up the subject.

Conclusion

The preceding work may seem excessive in terms of the result which is obtained, but it sets the scene for a conveniently simple graphical technique for determining Magnitude and Phase from the s-plane plot of the poles and zeros of a transfer function. In the light of more complex ideas to be expressed when analysing and confirming practical results from bench measurements, it is necessary to be mathematically rigorous in the proofs used. Once the interpretation process is understood, the relevant information may be derived by simple trigonometry from the plots rather than having to be calculated directly. Similarly, the poles and zeros can be confirmed from real measurements of the steady state excitation's response, by subtracting the excitation from that response to find the transfer function. This function can also be extrapolated from the transient measurements via function fitting a polynomial to these measurements in the time domain, then using the Laplace transform of that polynomial to find the complex frequency domain response. The graphical technique using the s-plane plots will prove to be an extremely powerful design and analysis tool, minimising the need for guess work.

Appendix B: Implementing the Root Finding Procedure for the Characteristic Equation

The root finding procedure for the cubic polynomial is as follows: express the polynomial (Equation B8) in its standard form:

$$s^3 + a_2 s^2 + a_1 s + a_0 = 0$$

where $a_2 = 1/T_1$ $a_1 = K/(N C_1)$ $a_0 = a_1/T_2$ (or those from the transfer function of the device under consideration). Next we take two variables to condition the coefficients for manipulation:

$$q = \frac{a_1}{3} - \left(\frac{a_2}{3}\right)^2$$

$$r = \frac{a_1}{2} \cdot \frac{a_2}{3} - \frac{a_0}{2} - \left(\frac{a_2}{3}\right)^3$$

From these two variables we can derive the discriminant and two more dummy variables which will allow us to express the roots of the polynomial. The discriminant ($\text{disc} = q^3 + r^2$) reveals the type of root available:

- If $\text{disc} > 0$ then the roots consist of one real root and two complex conjugate roots; the most useful result, since it gives an expression for ω_0 and ϕ directly; the optimum settle time for a control system results in a polynomial with roots in this area.
- If $\text{disc} = 0$ then all roots are real with at least two equal; it is seldom encountered practically due to component drift; it usually slips to the above or below condition.
- If $\text{disc} < 0$ then all roots are real, a slightly more common situation than the above since this condition represents the over damped case and is used when optimising phase noise; it results in a poor settle time.

Reference to standard texts on the subject of finding the roots for any general cubic equation, will encounter an area for the real roots where an incorrect result occurs. The following routines will allow a programmable calculator or computer to express the results for the roots s_1 , s_2 and s_3 correctly. To complete the procedure we express a second set of variables: z_1 and z_2 . However, we need to consider the below two conditional branches of the variables z_1 and z_2 , otherwise the real pole will take on a complex value (when the discriminant is greater than zero) when the real pole is of a lower value than the complex conjugate poles. To resolve this, the following procedure is found to work: take $z_1 = (r + \text{disc}^{0.5})^{1/3}$ and $z_2 = (r - \text{disc}^{0.5})^{1/3}$, which are generally available from the literature, then add the following conditional branches to alter the definition of z_1 and z_2 as follows:

IF $r < 0$ AND $q < 0$	THEN $z_1 = -[-r - \text{disc}^{0.5}]^{1/3}$	ELSE $z_1 = [r + \text{disc}^{0.5}]^{1/3}$
IF $r \geq 0$ AND $q < 0$	THEN $z_2 = [r - \text{disc}^{0.5}]^{1/3}$	ELSE $z_2 = -[-r + \text{disc}^{0.5}]^{1/3}$

AN-94

These allow us to write the final statements for the roots:

$$s_1 = (z_1 + z_2) - a_2/3$$

$$s_2 = -(z_1 + z_2)/2 - a_2/3 + (-3)^{0.5} (z_1 - z_2)/2$$

$$s_3 = -(z_1 + z_2)/2 - a_2/3 - (-3)^{0.5} (z_1 - z_2)/2$$

where s_1 , s_2 and s_3 are the roots of the polynomial. Notice that the right hand part of s_2 and s_3 would give the incorrect value if either z_1 or z_2 became complex; ergo, the conditional branches prevent this from happening. Now that we can find s_1 , s_2 and s_3 they will appear in the form of:

$$s_1 = p_1 \quad \text{where } p_1 \text{ is the real pole.}$$

$$s_2 = a + jb \quad \text{where } a \text{ is the real part of the positive conjugate pole and } b \text{ is the imaginary part of the positive conjugate pole when } \text{disc} > 0. \text{ When } \text{disc} < 0, a \text{ is the second real pole with } jb \text{ disappearing.}$$

$$s_3 = a - jb \quad \text{where } a \text{ is the real part of the negative conjugate pole and } b \text{ is the imaginary part of the negative conjugate pole when } \text{disc} > 0. \text{ When } \text{disc} < 0, a \text{ is the third real pole; here } a \text{ will be numerically different to } a \text{ for } s_2 \text{ above, so we equate } b \text{ to it and then remove the } j \text{ operator to discriminate between the real roots for } p_2 \text{ and } p_3.$$

Notice that the real part of the roots of s_2 and s_3 are equal when the discriminant is greater than zero, as is the absolute magnitude of the imaginary parts. The characteristic equation is now expressed as:

$$\text{C.E.} = (s + p_1) [s + (a + jb)] [s + (a - jb)] \quad \text{when } \text{disc} > 0$$

$$\text{or} \quad \text{C.E.} = (s + p_1) (s + a) (s + b) \quad \text{when } \text{disc} < 0$$

In the last statement we have assumed that $a = p_2$ and $b = p_3$, where p_2 and p_3 are the second and third real poles .

A more general method for finding the polynomials roots can be found in reference 7 dealing with extracting multiple real and complex roots via "Moore's Root Finder". The Algorithm as given is written in BASIC and will find up to the 35th root, but has some difficulty with multiple roots of equal value or roots of widely different magnitudes; fortunately neither of these situations are encountered commonly in practice.

References

Anyone interested in expanding the background to this Application Note may wish to refer to the following references; with the exception of number 6, all are cheap and readily available in the UK.

- 1/ "Applied Circuit Analysis" - Shlomo Karni, John Wiley and Sons, 1988. A good basic text with a concise introduction to each subject. Deals with the basics in network analysis in both the time and frequency domains. Well worth reading.
- 2/ "University Physics" - Sears, Zemansky and Young, Addison - Wesley Publishing Company, 5th Edition 1977. A companion volume to the above, providing some of the fundamental arguments to support reference 1's text; a good general reference work.
- 3/a "Engineering Maths", b "Further Engineering Maths" - Ken Stroud, Macmillan Education, Ltd, 1987. Designed for self tutorial purposes. Clear and easy to read texts covering the math required for studying network analysis. A couple of weeks spent on his Laplace Transform chapters will pay excellent dividends.
- 4/ "Automatic Control Systems" - Benjamin Kuo, Prentice - Hall International Inc. 5th Edition 1987. An excellent work dealing with analysis in the s plane; a must for anyone contemplating doing serious design work with linear networks. Very readable.
- 5/ "Network Analysis and Synthesis" - Franklin F. Kuo, John Wiley and Sons, 2nd Edition, 1966. A more advanced text than reference 4, abstract in parts, but gives body to network analysis. Requires plenty of concentration to fully understand.
- 6/ "Laplace Transforms for Electronic Engineers" - James G. Holbrook, Pergamon Press Ltd, 2nd Edition, 1969. An advanced text with an excellent Transform Table.
- 7/ "Moore's Root Finder"; a listing is to found in the Appendix of: "Circuit Design Using Personal Computers" - Thomas R Cuthbert Jr, John Wiley and Sons, 1983.

Note well: most of these texts miss many of the intermediate steps in formula development making them difficult to follow. It is recommended that a pencil and paper are kept at hand when reading them to allow for manipulation of the results to see the connecting thread. Some intuition will be required!



<http://www.mitelsemi.com>

World Headquarters - Canada

Tel: +1 (613) 592 2122
Fax: +1 (613) 592 6909

North America

Tel: +1 (770) 486 0194
Fax: +1 (770) 631 8213

Asia/Pacific

Tel: +65 333 6193
Fax: +65 333 6192

**Europe, Middle East,
and Africa (EMEA)**

Tel: +44 (0) 1793 518528
Fax: +44 (0) 1793 518581

Information relating to products and services furnished herein by Mitel Corporation or its subsidiaries (collectively "Mitel") is believed to be reliable. However, Mitel assumes no liability for errors that may appear in this publication, or for liability otherwise arising from the application or use of any such information, product or service or for any infringement of patents or other intellectual property rights owned by third parties which may result from such application or use. Neither the supply of such information or purchase of product or service conveys any license, either express or implied, under patents or other intellectual property rights owned by Mitel or licensed from third parties by Mitel, whatsoever. Purchasers of products are also hereby notified that the use of product in certain ways or in combination with Mitel, or non-Mitel furnished goods or services may infringe patents or other intellectual property rights owned by Mitel.

This publication is issued to provide information only and (unless agreed by Mitel in writing) may not be used, applied or reproduced for any purpose nor form part of any order or contract nor to be regarded as a representation relating to the products or services concerned. The products, their specifications, services and other information appearing in this publication are subject to change by Mitel without notice. No warranty or guarantee express or implied is made regarding the capability, performance or suitability of any product or service. Information concerning possible methods of use is provided as a guide only and does not constitute any guarantee that such methods of use will be satisfactory in a specific piece of equipment. It is the user's responsibility to fully determine the performance and suitability of any equipment using such information and to ensure that any publication or data used is up to date and has not been superseded. Manufacturing does not necessarily include testing of all functions or parameters. These products are not suitable for use in any medical products whose failure to perform may result in significant injury or death to the user. All products and materials are sold and services provided subject to Mitel's conditions of sale which are available on request.

M Mitel (design) and ST-BUS are registered trademarks of MITEL Corporation
Mitel Semiconductor is an ISO 9001 Registered Company
Copyright 1999 MITEL Corporation
All Rights Reserved
Printed in CANADA

TECHNICAL DOCUMENTATION - NOT FOR RESALE



**For more information about all Zarlink products
visit our Web Site at
www.zarlink.com**

Information relating to products and services furnished herein by Zarlink Semiconductor Inc. trading as Zarlink Semiconductor or its subsidiaries (collectively "Zarlink") is believed to be reliable. However, Zarlink assumes no liability for errors that may appear in this publication, or for liability otherwise arising from the application or use of any such information, product or service or for any infringement of patents or other intellectual property rights owned by third parties which may result from such application or use. Neither the supply of such information or purchase of product or service conveys any license, either express or implied, under patents or other intellectual property rights owned by Zarlink or licensed from third parties by Zarlink, whatsoever. Purchasers of products are also hereby notified that the use of product in certain ways or in combination with Zarlink, or non-Zarlink furnished goods or services may infringe patents or other intellectual property rights owned by Zarlink.

This publication is issued to provide information only and (unless agreed by Zarlink in writing) may not be used, applied or reproduced for any purpose nor form part of any order or contract nor to be regarded as a representation relating to the products or services concerned. The products, their specifications, services and other information appearing in this publication are subject to change by Zarlink without notice. No warranty or guarantee express or implied is made regarding the capability, performance or suitability of any product or service. Information concerning possible methods of use is provided as a guide only and does not constitute any guarantee that such methods of use will be satisfactory in a specific piece of equipment. It is the user's responsibility to fully determine the performance and suitability of any equipment using such information and to ensure that any publication or data used is up to date and has not been superseded. Manufacturing does not necessarily include testing of all functions or parameters. These products are not suitable for use in any medical products whose failure to perform may result in significant injury or death to the user. All products and materials are sold and services provided subject to Zarlink's conditions of sale which are available on request.

Purchase of Zarlink's I²C components conveys a licence under the Philips I²C Patent rights to use these components in an I²C System, provided that the system conforms to the I²C Standard Specification as defined by Philips.

Zarlink and the Zarlink Semiconductor logo are trademarks of Zarlink Semiconductor Inc.

Copyright 2001, Zarlink Semiconductor Inc. All Rights Reserved.

TECHNICAL DOCUMENTATION - NOT FOR RESALE



**For more information about all Zarlink products
visit our Web Site at
www.zarlink.com**

Information relating to products and services furnished herein by Zarlink Semiconductor Inc. trading as Zarlink Semiconductor or its subsidiaries (collectively "Zarlink") is believed to be reliable. However, Zarlink assumes no liability for errors that may appear in this publication, or for liability otherwise arising from the application or use of any such information, product or service or for any infringement of patents or other intellectual property rights owned by third parties which may result from such application or use. Neither the supply of such information or purchase of product or service conveys any license, either express or implied, under patents or other intellectual property rights owned by Zarlink or licensed from third parties by Zarlink, whatsoever. Purchasers of products are also hereby notified that the use of product in certain ways or in combination with Zarlink, or non-Zarlink furnished goods or services may infringe patents or other intellectual property rights owned by Zarlink.

This publication is issued to provide information only and (unless agreed by Zarlink in writing) may not be used, applied or reproduced for any purpose nor form part of any order or contract nor to be regarded as a representation relating to the products or services concerned. The products, their specifications, services and other information appearing in this publication are subject to change by Zarlink without notice. No warranty or guarantee express or implied is made regarding the capability, performance or suitability of any product or service. Information concerning possible methods of use is provided as a guide only and does not constitute any guarantee that such methods of use will be satisfactory in a specific piece of equipment. It is the user's responsibility to fully determine the performance and suitability of any equipment using such information and to ensure that any publication or data used is up to date and has not been superseded. Manufacturing does not necessarily include testing of all functions or parameters. These products are not suitable for use in any medical products whose failure to perform may result in significant injury or death to the user. All products and materials are sold and services provided subject to Zarlink's conditions of sale which are available on request.

Purchase of Zarlink's I²C components conveys a licence under the Philips I²C Patent rights to use these components in an I²C System, provided that the system conforms to the I²C Standard Specification as defined by Philips.

Zarlink, ZL and the Zarlink Semiconductor logo are trademarks of Zarlink Semiconductor Inc.

Copyright 2003, Zarlink Semiconductor Inc. All Rights Reserved.

TECHNICAL DOCUMENTATION - NOT FOR RESALE
